CHAPTER THIRTY-EIGHT

MOLECULAR SPECTROSCOPY AND REACTIONS OF ACTINIDES IN THE GAS PHASE AND CRYOGENIC MATRICES

Michael C. Heaven, John K. Gibson,
and Joaquim Marçalo

38.1 INTRODUCTION

In this chapter we review the spectroscopic data for actinide molecules and the reaction dynamics for atomic and molecular actinides that have been examined in the gas phase or in inert cryogenic matrices. The motivation for this type of investigation is that physical properties and reactions can be studied in the absence of external perturbations (gas phase) or under minimally perturbing conditions (cryogenic matrices). This information can be compared directly with the results from high-level theoretical models.

The interplay between experiment and theory is critically important for advancing our understanding of actinide chemistry. For example, elucidation of the role of the 5*f* electrons in bonding and reactivity can only be achieved through the application of experimentally verified theoretical models. Theoretical calculations for the actinides are challenging due the large numbers of electrons that must be treated explicitly and the presence of strong relativistic effects. This topic has been reviewed in depth in Chapter 17 of this series (Kaltsoyannis *et al.*, 2006). One of the goals of the experimental work described in this chapter has been to provide benchmark data that can be used to evaluate both empirical and ab initio theoretical models.

While gas-phase data are the most suitable for comparison with theoretical calculations, there are technical difficulties entailed in generating workable densities of gas-phase actinide molecules that have limited the range of species that have been characterized. Many of the compounds of interest are refractory, and problems associated with the use of high temperature vapors have complicated measurements of spectra, ionization energies, and reactions. One approach that has proved to be especially valuable in overcoming this difficulty has been the use of pulsed laser ablation to generate plumes of vapor from refractory actinide-containing materials. The vapor is entrained in an inert gas, which can be used to cool the actinide species to room temperature or below. For many spectroscopic measurements, low temperatures have been achieved by co-condensing the actinide vapor in rare gas or inert molecule host matrices. Trapping the products from gas-phase reactions that occur when trace quantities of reactants are added to the inert host gas has resulted in the discovery of many new actinide species. Selected aspects of the matrix isolation data were discussed in Chapter 17 (Kaltsoyannis *et al.*, 2006). In the present chapter we review the spectroscopic matrix data in terms of its relationship to gas-phase measurements, and update the description of the new reaction products found in matrices to reflect the developments that have occurred during the past 2 years. Spectra recorded in matrix environments are usually considered to be minimally perturbed, and this expectation is borne out for many closed shell actinide molecules. However, there is growing evidence that significant perturbations can occur for open shell molecules, resulting in geometric distortions and/or electronic state reordering.

Studies of actinide reactions in the gas phase provide an opportunity to probe the relationship between electronic structure and reactivity. Much of this work has focused on the reactions of ionic species, as these may be selected and controlled using various forms of mass spectrometry. As an example of the type of insight derived from reaction studies, it has been established that the reaction barriers for An^+ ions are determined by the promotion energies required to achieve the $5f^n6d7s$ configuration. Gas-phase reaction studies also provide fundamental thermodynamic properties such as bond dissociation and ionization energies.

In recent years, an increased number of gas-phase ion chemistry studies of bare (atomic) and ligated (molecular) actinide ions have appeared, in which relevant contributions to fundamental actinide chemistry have been made. These studies were initiated in the 1970s and carried out in an uninterrupted way over the course of the past 3 decades. Initial studies unsurprisingly focused on naturally occurring U (and Th) and were later extended (starting 10 years ago) to Pa and several of the more abundant members of the transuranium series, Np through Es. The main purpose of the reaction dynamics section of this chapter is to summarize (up to late 2008) the work done in the gas phase involving ionic species, with an emphasis on the key accomplishments. This topic was recently reviewed in a comprehensive way (Gibson 2002a; Gibson and Marçalo 2006). The small number of studies reported for gas-phase reactions of neutral actinide species are also briefly summarized.

38.2 EXPERIMENTAL TECHNIQUES FOR GAS-PHASE AND MATRIX ISOLATION SPECTROSCOPY, AND MATRIX REACTIONS

Conventional absorption and emission spectroscopy techniques have yielded a considerable body of valuable data for actinide-containing molecules, but these approaches are often limited by the extreme spectral congestion encountered. For refractory species this congestion arises from the extensive thermal population of low-lying ro-vibronic states associated with the high temperatures needed to achieve workable vapor pressures. This problem is exacerbated by the circumstance that vaporization usually produces a range of molecular species. In recent years these problems have been overcome by using laser ablation combined with supersonic expansion cooling to obtain low-temperature gas-phase samples (with molecules cooled to internal temperatures as low as 20 K). Complications associated with the production of multiple species have been resolved by using mass selected detection methods. Typically this involves pulsed laser ionization combined with time-of-flight mass spectrometry. The laser-based photoionization techniques that have been utilized for actinide spectroscopy have been described in a recent review article (Heaven, 2006). The key features are briefly outlined here to define terms used in the following sections.

The technique of resonantly enhanced multi-photon ionization (REMPI) provides a powerful and sensitive means for the recording of mass selected spectra for neutral molecules. In the simplest variant, one photon promotes the molecule to an excited state and a second photon ionizes the excited molecule. This can be done using one-color excitation if the photon energy exceeds half the ionization energy (IE).

Two-photon excitation techniques that employ independently tunable laser sources provide a means for recording accurate ionization energies and spectroscopic data for molecular ions. Photoionization efficiency (PIE) curves are recorded by using fixed-frequency excitation of a neutral molecule transition. The frequency of the second photon is scanned to find the threshold energy at which ions are produced. In addition to defining the ionization energy, these scans often reveal rich features above the threshold that are associated with autoionizing resonances.

A more detailed look at the energy levels of the molecular cation can be obtained by using the pulsed field ionization–zero kinetic energy (PFI-ZEKE) technique. This resembles the PIE measurement, but there are two important differences. First, the photoelectrons are detected, rather than the molecular ions. Second, and most important, the final ionization step is accomplished using a pulsed electric field. The second photon is used to excite long-lived Rydberg states of the molecule that lie just below a specific ionization limit (i.e., a single ro-vibrational level of a molecular ion). A weak pulsed electric field is used to ionize the excited molecule. By delaying the application of this field it is possible to bias the detection to observe only the electrons that have come from the Rydberg states. A spectral resolution of about 1 cm^{-1} can be achieved using this approach.

The greater majority of spectroscopic studies of matrix isolated actinide molecules have relied on conventional IR absorption measurements. However, there have also been studies of IR inactive vibrational modes using Raman scattering and electronically excited states using absorption and laser induced fluorescence measurements. For the first generation of experiments, sample preparation for refractory materials involved vaporization in specialized furnaces such as Knudsen cells. Since the early 1990s most of the experimental work in this area has been carried out by Andrews and co-workers using pulsed laser ablation to obtain the species of interest. This group has examined a multitude of reactions of Th and U in solid noble gas (or reactive) matrices. Their matrix isolation infrared spectroscopy technique is described in detail in the cited references; only a brief synopsis of the methodology is included here. Thorium or uranium atoms were produced by focusing a pulsed Nd:YAG laser onto a pure metal target and were co-deposited at temperatures in the range of 4–12 K in a solid matrix comprised of a dilute mixture of one or more reactive gases in bulk neon, argon, krypton and/or xenon; for some studies the entire bulk matrix was the reactive species (e.g., H_2 or N_2). Reactions that did not spontaneously occur under the deposition conditions could be induced by annealing the matrix to temperatures ranging from 6 to 40 K, to promote aggregation of the actinide atoms and the reactive molecules. Alternatively, broadband UV photolysis was used to induce some reactions, and other reactions are attributed to excited-state laser ablated metal atoms, M*, or reaction intermediates, [ML]*.

38.3 SPECTROSCOPIC STUDIES OF ACTINIDE OXIDES

38.3.1 Spectra and theoretical calculations for ThO and ThO^+

ThO is one of the few actinide oxides for which there are extensive gas-phase spectroscopic data. As a consequence, this molecule has also been the focus of theoretical studies (Marian *et al.*, 1988; Kuchle *et al.*, 1994; Paulovic *et al.*, 2003). Many of the early electronic spectroscopy studies were carried out by Edvinsson, Lagerqvist and co-workers (Edvinsson and Lagerqvist, 1984, 1985a, b, 1987, 1988, 1990) using conventional absorption and emission techniques. They confirmed that the ground state is $X^1\Sigma^+$, which was consistent with the expected ground state configuration $Th^{2+}(7s^2)O^{2-}$.

Ground state vibrational constants have been derived from the gas-phase electronic spectra and the IR absorption spectrum of ThO isolated in solid Ar. These measurements yielded values for the harmonic vibrational constant ($Th^{16}O$) of ω_e = 895.77 cm^{-1} (gas phase, (Edvinsson and Lagerqvist, 1984)) and 883.8 cm^{-1} (matrix, (Gabelnick *et al.*, 1974)), the difference between these being indicative of a minor perturbation by the matrix environment. A pure rotation spectrum for ThO(X) was reported recently (Dewberry *et al.*, 2007a, b). This is the first example of the application of microwave spectroscopy to a gas-phase actinide molecule. The $J = 0 \rightarrow 1$ transition was observed for several vibrational levels of $Th^{16}O$, $Th^{17}O$, and $Th^{18}O$ (where J indicates the rotational angular momentum). Analysis of these results yielded highly accurate rotational constants and an isotope independent equilibrium bond length of r_e=1.840186 (2) Å. Additional insights concerning the electronic structure were obtained from the $Th^{17}O$ data. Due to the non-zero spin of the ^{17}O nucleus, line splittings were observed that were caused by spin-rotation and nuclear quadrupole coupling.

Twenty-two electronically excited states of ThO have been characterized by emission spectroscopy. A further three states have been identified in the REMPI spectrum recorded using expansion cooling (Goncharov *et al.*, 2005). Table 38.1 lists the states with Ω = 0 and 1 (where Ω is the projection of the electronic angular momentum along the bond axis) that have been observed to date. Both ab initio theory and ligand field theory (LFT) calculations indicate that the lowest energy excited states are derived from the $Th^{2+}(7s6d)O^{2-}$ configuration. Seven of the 12 states that belong to this configuration have been observed. Theoretical predictions for the energies of these states are also listed in Table 38.1. Note that the lowest energy excited state is formally $^3\Delta_2$. ThO($^3\Delta_2$) and the isoelectronic species $ThF^+(^3\Delta)$ have been identified as favorable systems for investigation of the electric dipole moment of the electron (Meyer and Bohn, 2008). The determination of this quantity (or refinement of its upper bound) can be used to test proposed Super-symmetry extensions of the Standard Model.

Assignments for the ThO states in the energy range 16,000–31,000 cm^{-1} are more difficult to establish. Kaledin *et al.* (1994) and Goncharov *et al.* (2005) used LFT calculations to assign fifteen of these states to the metal ion configurations $7s5f$, $7s7p$, and $6d^2$. However, ab initio calculations indicate that the states from $7s5f$ and $7s7p$ will not be found at energies below 32,200 cm^{-1}. If this is correct, all states in the 16,000–30,000 cm^{-1} range should be assigned to $6d^2$. This configuration gives rise to seven Ω = 1 states, but nine have been observed in the specified range. The first seven span the energy range 19,539–28,578 cm^{-1}, while the LFT predictions of Kaledin *et al.* (1994) for the Ω = 1 states span the range 20,397–36,551 cm^{-1}. Consequently, if these states do arise from $6d^2$, the LFT calculations have overestimated the ligand field interaction parameters

Table 38.1 Experimentally determined electronic term energies and comparison with the results of LFT calculations for the $\Omega = 1$ and $\Omega = 0$ states of ThO.

	$\Omega = 1$				$\Omega = 0$			
Conf.[a]	State	Calculated[b]	Observed[c]	Δ	State	Calculated[b]	Observed[c]	Δ
$7s^2$					X	0	0	0
$6d7s$	H	5,501	5,317	184		10,580[d]		
	B	10,937	11,129	192	A	10,814	10,601	213
	C	14,461	14,490	29		15,571[d]		
	D	15,794	15,946	152	E	16,476	16,320	156
$5f7s$	I	21,028	19,539	1,489		22,772[d]		
	K	23,169	22,636	533	P	23,162	23,156	6
	L	26,174	24,857	1,317		26,580[d]		
	N	27,185	27,719	534	A’	27,716	28,029	313
$7s7p$	M	21,734	21,734	0	R	19,028[d]	19,050[d]	22
		33,073				20,560		
		41,103				33,740[d]		
						44,617		
$6d^2$		20,398			F	18,337	18,337	0
	U	24,241	25,136	895		23,615[d]		
	C’	25,939	28,578	2,639		25,101		
	E’	30,037	29,073	964		26,469		
	B’	31,686	30,313	1,373	F’	28,876	30,718	1,902
		33,577				30,256[d]		
		36,581			G’	33,145	30,960	2,185
						36,153		
						40,903		

[a] Formal outer electronic configuration of the Th^{2+} ion.
[b] Calculated energies (cm^{-1}) from Kaledin et al. (1994). This table includes all of the Ω=0 and 1 states arising from the specified configurations.
[c] Energies (cm^{-1}) are from Von Bornstedt et al. (1979), Edvinsson and Lagerqvist (1984), 1985a, b, 1987, 1988, 1990), Goncharov et al. (2005)
[d] $\Omega = 0^-$ state.

$B_0^2(6d)$ and $B_0^4(6d)$. The two remaining $\Omega=1$ states must be derived from 7*s*5*f* and/or 7*s*7*p*, indicating that at least one of these configurations is at a lower energy than the existing ab initio calculations predict.

Six $\Omega = 0$ states have been observed at energies above 16,500 cm^{-1} (c.f., Table 38.1). Goncharov *et al.* (2005) had assigned three of these states to the $6d^2$ configuration. In light of the above discussion it now seems likely that all six states should be assigned to $6d^2$.

Spectroscopic determinations of the ionization energy for ThO have been made using PIE, MATI and PFI-ZEKE techniques (Goncharov *et al.*, 2005; Goncharov and Heaven, 2006). The data for all three measurements were in good agreement, with the PFI-ZEKE spectrum providing the most accurate result. The value obtained, IE=6.60268(2) eV, was 0.5 eV higher than that reported previously from electron impact ionization measurements (6.1(1) eV (Rauh and Ackerman, 1974)). The reason for this large discrepancy was easily identified. In the electron impact study, vapor phase ThO was obtained by heating a sample of solid thorium dioxide to 2,000 K. At this temperature many vibrational levels of ThO(X) would be populated, along with the low-lying states at 5,317 and 6,128 cm^{-1}. Hence the ThO^+ appearance potential most probably corresponded to the ionization of thermally excited ThO. This problem was avoided in the multi-photon ionization measurements. Note that jet-cooling alone would not be sufficient to ensure that ionization from the ground state was observed. The laser ablation process populates many excited levels, and metastable electronically excited states can survive the jet-cooling process. Consequently, single photon ionization threshold measurements with jet-cooled samples may also yield underestimated IE values. With resonantly enhanced two-color ionization the first laser is tuned to a transition that is known to originate from the electronic ground state. This ensures that the true IE is obtained, regardless of the presence of excited molecules.

When combined with the IE for atomic Th, the IE for ThO yields the difference between the dissociation energies of ThO and ThO^+ (IE(ThO)-IE (Th) = $\mathrm{D_0(ThO)}$–$\mathrm{D_0(ThO^+)}$). With the corrected IE for ThO it was apparent that the neutral molecule is 0.3 eV more tightly bound than the cation. This was a surprising result as ionization was expected to involve removal of one of the non-bonding 7*s* electrons, thereby reducing the screening of the Th^{3+} ion core. Spectroscopic studies of ThO^+ were initiated to further understand the effects of ionization on the bonding, and to establish methods for obtaining spectra for gas-phase actinide ions. ThO^+ was chosen as an ideal prototype for proof-of-principle experiments as the pattern of low-lying electronic states should be relatively simple. The ionic $\mathrm{Th^{3+}O^{2-}}$structure has a single unpaired electron associated with the closed shell Th^{4+} ion core. Formally, the lowest energy configuration is expected to be $\mathrm{Th^{3+}(7s)O^{2-}}$, giving rise to a $X^2\Sigma^+$ ground state. The low-lying electronically excited states should be $^2\Delta$, $^2\Pi$ and $^2\Sigma$ derived from the $\mathrm{Th^{3+}(6d)O^{2-}}$ configuration.

Rotationally-resolved spectra for ThO^+ were obtained using the PFI-ZEKE technique (Goncharov and Heaven, 2006). As an example, Fig. 38.1 shows the rotational structure of the $X\,^2\Sigma^+$, v=0 level. These data were obtained using two-color excitation, with the first laser set to excite a single rotational level of the intermediate electronically excited state. The "lines" in the PFI-ZEKE spectra actually correspond to unresolved groups of high-n Rydberg levels that converge on a specific rotational level of the ion. The vertical broken lines in Fig. 38.1 show the zero-field rotational energies that these series are converging to. Note that the range of rotational states observed in each trace increased with increasing angular momentum of the intermediate electronically excited state. Spectra such as those shown in Fig. 38.1 supply four valuable pieces of information. These are the term energy for the state, the rotational constant, the Ω value, and an indication of the angular momentum coupling case (Brown and Carrington, 2003). The latter is obtained by fitting energy level expressions to

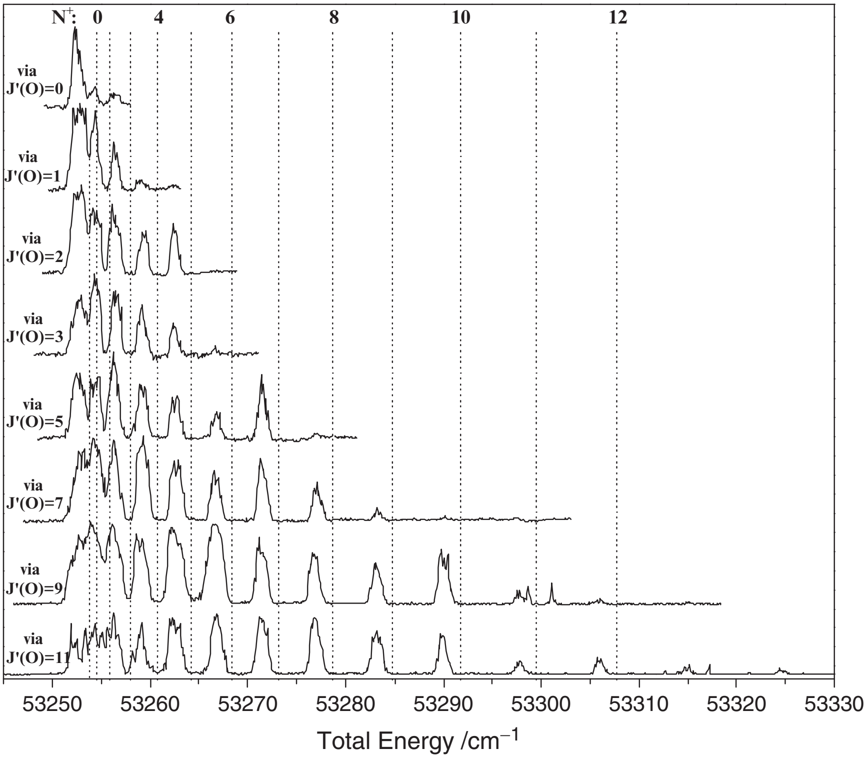

Fig. 38.1 *PFI-ZEKE spectra for* ThO^+ *recorded via specific rotational levels* (J' = 0, 1, 2, 3, 5, 7, 9, 11) *of the intermediate state O. The spectra are plotted against total energy of the transition from the ThO(X)* v = 0, J = 0 *state* (*reused with permission from Vasiliy Goncharov, Journal of Chemical Physics*, 124, 064312 (2006). *Copyright* 2006, *American Institute of Physics*).

the rotational term series. Levels characterized by integer quantum numbers correspond to Hund's case *b* coupling while half-integer quantum numbers indicate coupling cases *a* or *c* (intermediate coupling cases may also be recognized by identifying the appropriate energy level expression) (Brown and Carrington, 2003). The data shown in Fig. 38.1 confirmed that the ground state of ThO^+ is $X\,^2\Sigma^+$.

Vibrationally excited levels were readily observed. For example, ground state levels ranging from $v = 0$ to 7 have been characterized. The observation of highly excited vibrational levels of the ion in these spectra was unexpected, given the details of the excitation process. The intermediate electronically excited states used for these measurements had equilibrium bond lengths and vibrational frequencies that were similar to those of the ThO^+ states that were accessed. Although the Frank–Condon factors strongly favored the production of $v = 0$ ions, transitions to levels with $v = 5$ and 6 were observed. This indicated that the Franck–Condon factors play only a minor role in determining the relative intensities of the PFI-ZEKE bands. In total 16 vibronic states of ThO^+ have been analyzed. The electronically excited states $1^2\Delta(\Omega=3/2)$ (2,934 cm^{-1}), $1^2\Delta(\Omega=5/2)$ (5814 cm^{-1}) and $1^2\Pi(\Omega=1/2)$ (7,404 cm^{-1}) were characterized. A summary of the spectroscopic data obtained for ThO^+ is presented in Table 38.2.

Relativistic ab initio calculations for ThO^+ have been reported by Tyagi (2005). In this work the MCSCF method was used with a 68 electron core

Table 38.2 Molecular constants for the $X\,^2\Sigma^+$, $1^2\Delta_{3/2}$, $1^2\Delta_{5/2}$ and $1^2\Pi_{1/2}$ states of ThO^+.

State	v	T_o/cm^{-1}Theory[a]	T_o/cm^{-1}, Experiment[b]	B_v /cm^{-1}	ω_e/cm^{-1}	$\omega_e x_e/cm^{-1}$
$X\,^2\Sigma^+$	0	0,{IE=52,000}	0, {IE =53,253.8(2)}	0.3450(6)	954.97(6)	2.45(3)
	1	–	950.0(1)	0.3439(5)		
	2	–	1,895.3(1)	0.3434(5)		
	6	–	5,627.0(1)	0.3409(10)		
	7	–	6,547.2(5)	–		
$1^2\Delta_{3/2}$	0	2,602	2,933.7(1)	0.3374(7)	917.9(5)	2.55(10)
	1	–	3,846.2(1)	0.337(1)		
	3	–	5,656.8(1)	0.3379(13)		
	4	–	6,554(1)	–		
$1^2\Delta_{5/2}$	0	5,852	5,814.4(1)	0.3410(2)	915.5(2)[c]	–
	1	–	6,729.9(1)	0.340(1)		
$1^2\Pi_{1/2}$	0	9,167	7,404.1(1)	0.3365(11)	904.22(2)	2.339(3)
	1	–	8,303.6(1)	0.3354(10)		
	2	–	9,198.5(2)	0.3334(6)		
	3	–	10,088.7(2)	0.3330(7)		
	5	–	11,855.0(2)	0.333(2)		

[a] Tyagi 2005
[b] Goncharov and Heaven 2006
[c] $\Delta G_{1/2}$ value.

potential for Th. Both spin free and spin–orbit coupled results were obtained. These calculations supported the simple picture of the electronic structure presented above. The ground state wavefunction was found to have 90% 7*s* character. The theoretical energies for the two components of the $^2\Delta$ state were in good agreement with the measured values (errors of 332 and 38 cm^{-1}). The energy for $^2\Pi_{1/2}$ was greater than the measured value by 1,763 cm^{-1}, but the correlation between the observed and calculated energy level patterns was unambiguous. The wavefunctions for the $^2\Delta$ and $^2\Pi$ states all possessed greater than 85% 6*d* character.

Tyagi (2005) also calculated the IE for ThO. The results were very sensitive to the method used to treat dynamical correlation. The highest level method employed, multi-reference configuration interaction with single and double excitations (MRCISD), yielded a vertical IE of 6.45 eV, just 0.15 eV below the experimental value.

The IE measurements had shown that ThO is more strongly bound than ThO^+. In contrast, the molecular constants seemed to show the opposite trend. The bond length for $ThO^+(X)$ was shorter (R_e = 1.807 vs 1.840 Å) and the vibration frequency was higher (ω_e = 955 vs 896 cm^{-1}). Goncharov and Heaven (2006) explored this apparent paradox using density functional theory (DFT) calculations with relativistic core potentials. These were successful in reproducing the molecular constants for ThO and ThO^+. Spin-density calculations for ThO^+ were also consistent with the formal $Th^{3+}O^{2-}$ charge separation. Scans of the potential energy curves provided insights concerning the lower dissociation energy for ThO^+. While the structure near the equilibrium distance corresponds to tightly bound $Th^{3+}O^{2-}$, the ground state must correlate with the $Th^+(7s6d^2, {}^4F) + O({}^3P)$ dissociation asymptote. Therefore, adiabatic dissociation of the molecule must involve avoided crossings with states that correlate with the $Th^{2+} + O^-$ and $Th^+ + O$ dissociation asymptotes. Due to these avoided crossings the dissociation energy of ThO^+, relative to that of ThO, is influenced by the magnitude of the IE for Th^{2+}.

It has since been shown that HfO, which has the analogous $6s^2$ metal ion configuration, behaves similarly on ionization. PFI-ZEKE spectra for HfO were recently recorded by Merritt *et al.* (2009). The IE was found to be 7.91689(12) eV (0.37 eV greater than the electron impact value), showing that the $HfO^+(X)$ bond is weaker than that of HfO(*X*) by 1.1 eV. However, the molecular constants for the ion (ω_e = 1,020.8(2), B_0 = 0.403(5) cm^{-1}) indicate a shorter and stiffer bond. Hence the unusual differences between the ThO(*X*) and $ThO^+(X)$ bonds do not appear to be associated with relativistic effects.

38.3.2 Spectra and theoretical calculations for UO and UO^+

Studies of the electronic transitions of UO have been carried out using absorption and emission spectroscopy (Kaledin *et al.*, 1986, 1989), REMPI of jet-cooled samples (Heaven *et al.* 1985), and the application of wavelength selected fluorescence excitation techniques to UO that was vaporized in a high temperature furnace (T = 2,500 K) (Kaledin *et al.*, 1994; Kaledin and Heaven, 1997). Thirty-three electronic transitions have been examined at high-resolution. Energy linkages between all of the upper and lower states sampled by these transitions were established. A compilation of the observed states for $^{238}U^{16}O$ is presented in Table 38.3. The ground state of UO was found to be an $\Omega = 4$ component of the $U^{2+}(5f^{3}7s, {}^{5}I_{4})O^{2-}$ configuration. Seven other states belonging to this configuration were identified. The lowest energy excited state, also $\Omega = 4$, was located just 294.1 cm^{-1} above the ground state. This state did not fit

Table 38.3 Summary of constants for $^{238}U^{16}O$ derived from laser absorption, laser excitation and thermal emission spectra (cm^{-1})[a]

State	v	T_v	B_v	Method[b]
[21.079]5		21,079.493 (7)	0.344 1 (1)	LE
[20.807]5		20,807.445 (4)	0.325 3 (1)	LE
[20.726]5		20,726.226 (5)	0.330 8 (1)	LE
[20.491]6	0	20,491.39 (30)	0.334 47 (5)	LE
[19.950]4	0	19,950.005 (8)	0.328 55 (5)	FJ
[19.906]4		19,906.755 (3)	0.326 80 (4)	LE
[19.479]4	0	19,478.575 (15)	0.333 3 (3)	FJ
[19.470]3	0	19,469.994 (3)	0.324 65 (4)	FJ, LE
[19.453]3	0	19,452.967 (3)	0.339 97 (3)	FJ, LE
[19.217]5	2	19,217.415 (4)	0.327 70 (7)	LE
[18.430]5	1	18,430.067 (3)	0.332 58 (3)	LE
[18.404]5	0	18,404.167 (2)	0.339 11 (3)	LE
[18.403]5	0	18,403.841 (3)	0.330 96 (3)	LE
[17.653]5	1	17,653.710 (17)	0.332 6 (4)	LE
[17.613]5	0	17,613.965 (4)	0.332 38 (3)	FJ
[16 940]5	0	16,940.081 (11)	0.321 2 (1)	FJ
[16.845]5	0	16,845.129 (7)	0.331 6 (2)	FJ, LE
[16.563]5	0	16,563.827 (18)	0.333 4 (2)	FJ
[16.561]5	0	16,560.987 (16)	0.338 6 (2)	FJ
[14.016]4	0	14,016.591 (3)	0.340 957 (4)	TE
[?]5	0	z[c] + 15,423.375 (5)	0.338 76 (7)	TE
[?]5	0	z	0.334 89 (7)	TE
(1)6	0	4,469(5)	0.330(5)	TE
(2)2	0	2,118(10)		TE
(3)3	0	1,941.48	0.327	TE
(1)5	0	1,043.00(3)	0.3297(2)	TE
(1)2	0	958.664(5)	0.32452(4)	TE
(1)3	0	651.125(4)	0.327949(8)	TE
(2)4	0	294.119(2)	0.346188(36)	TE
X(1)4	0	0.0	0.333325(29)	TE, LE, FJ

[a] Data compiled from Kaledin et al. (1994), Kaledin and Heaven (1997). Error limits in parentheses are one standard deviation in the units of the last digit reported.

[b] Technique used to observe transition. LE – laser excitation; FJ – free-jet expansion; TE – thermal emission.

[c] z. The energy of this state relative to the ground state is unknown.

as a member of the $5f^37s$ group, and its molecular constants were consistent with the configuration $U^{2+}(5f^27s^2, {}^3H_4)O^{2-}$. The interactions between the three lowest energy $\Omega = 4$ states were large enough to cause a significant perturbation of the first vibrational interval for the ground state (Kaledin and Kulikov, 1989; Kaledin *et al.*, 1994). A deperturbation analysis was carried out for these states (separated by 294 and 1,280 cm^{-1}) (Kaledin *et al.*, 1994). The deperturbed ground state vibrational interval of $\Delta G_{1/2}$=841.9 was substantially smaller than the observed interval of 882.4 cm^{-1}.

UO provides an example of the complications encountered when comparing spectroscopic data with theoretical predictions. As calculated vibrational constants are usually derived from the second derivative of the potential energy curve, they do not include the effects of vibronic perturbations. Hence the calculated vibrational constant for UO reported by Krauss and Stevens (1983) (ω_e = 845 cm^{-1}) did not seem consistent with the measured gas-phase vibrational interval, but it was in good agreement with the deperturbed vibrational constant (ω_e = 846.5 cm^{-1}). UO also illustrates the complications for spectra recorded in cryogenic rare gas matrices that result from host-induced electronic state mixing. The fundamental vibrational transition was observed at 889.5 cm^{-1} in solid Ne (Zhou *et al.*, 2000) and 819.8 cm^{-1} in solid Ar (Gabelnick *et al.*, 1973a; Hunt and Andrews, 1993). These anomalously large matrix effects are probably caused by differences in the guest–host interactions that change the energy intervals between the $5f^37s$ and $5f^27s^2$ states.

Kaledin *et al.* (1994) performed LFT calculations for neutral UO in an attempt to provide configurational assignments for the electronic transitions they observed. The low-lying energy levels of UO were successfully fitted using a semi-empirical LFT method where selected interaction parameters were treated as variables. Tentative assignments for a sub-set of the observed states were proposed using the results from the LFT analysis. Eight states were assigned to $5f^37s$ and a further five were assigned to $5f^27s^2$.

The LFT model is very successful in describing the low-lying states of lanthanide oxides and halides. It works because the 4*f* orbitals are compact and do not participate in covalent bonding to a significant degree. As the 5*f* orbitals of the early actinides are less compact, LFT may not be as successful in representing the low-lying states of actinide oxides and halides. If this is the case, empirical fitting of energy levels to a LFT model may yield physically meaningless ligand field parameters that have little or no predictive capability. One indication of the validity of the LFT approach for diatomic actinide compounds can be obtained through measurements of the dipole moments. This can be used to see if the charge distributions in AnO molecules are comparable to those of their LnO analogs. Furthermore, properties such as the dipole moment and magnetic *g*-factor reflect the characteristics of the electronic wavefunction of a given state, and may be used to identify states that are associated with a common metal ion electronic configuration. In a study motivated by these considerations, Heaven *et al.* (2006) measured dipole moments and magnetic *g*-factors for

UO using the optical Stark and Zeeman effects. For the ground state they obtained a dipole moment of $\mu = 3.363(26)$ D and a *g*-factor of 2.562(12). The value for the dipole moment, which was the same as that of the isoelectronic lanthanide oxide (NdO(X, Ω=4), μ=3.369(13) D) (Linton *et al.*, 2008), supports the notion that the degree of charge separation in the early actinide oxides is suitable for the meaningful application of LFT models. Krauss and Stevens (2003) reached a similar conclusion based on their comparative theoretical study of NdO and UO.

To interpret the magnetic *g*-factor for UO, the mixing of low-lying states must be taken into account. The deperturbation analysis for the $\Omega = 4$ states of UO indicated that the ground state is 84.5% $5f^{3}7s$, $^{5}I_4$ with 15.4% $5f^{2}7s^{2}$, $^{3}H_4$ (Kaledin *et al.*, 1994). This combination yields a magnetic *g*-factor of 2.53, in reasonable agreement with the observed value.

The two electronically excited states examined by Heaven *et al.* (2006) were separated by less than 1 cm^{-1}, but exhibited markedly different constants ($\mu = 2.68$ D, $g = 3.51$ for [18,403]5 and $\mu = 3.11$ D, $g = 4.83$ for [18,404]5). This suggests that systematic measurements of excited state dipole moments and *g*-factors might be used to deduce the configurational assignments for the range of states that are accessed in the visible and near IR spectral ranges.

Electron impact measurements of the IE for UO provided a consistent value for the IE of 5.6(1) eV (Rauh and Ackerman, 1974; Capone *et al.*, 1999). Allen *et al.* (1988) obtained a low-resolution photoelectron spectrum for UO that exhibited a broad feature (corresponding to ionization energies of 5.8–7.6 eV) where the low-energy threshold appeared to be in agreement with the electron impact IE. Re-examination of the IE of UO using multi-photon ionization techniques yielded a significantly higher value of 6.03111(3) eV (Han *et al.*, 2003, 2004; Goncharov *et al.*, 2006). As for ThO, the low IE obtained in the earlier measurements was attributed to the ionization of thermally excited molecules. The difference between the IEs for UO and U shows that UO^{+} is 0.163 eV more tightly bound than neutral UO. Theoretical calculations of the IE for UO have predicted values of 6.17 (Malli, 1989), 5.71 (Boudreaux and Baxter, 2002), 6.05 (Paulovic *et al.*, 2005), and 5.59 eV (Tyagi, 2005). It is noteworthy that the complete active space state interaction – spin orbit coupling (CASSI-SOC) calculations of Paulovic *et al.* (2005) yielded reliable values for the IE's of both UO and U atoms (IE(U)=6.20 (calc) versus 6.194 (obs) eV).

UO^{+} is of theoretical interest as it is small enough to be amenable to high-level treatments, but challenging as it possesses a large number of low-lying excited states. Several high-level relativistic calculations had been carried out to predict the electronic structure and properties of UO^{+} (Krauss and Stevens, 1983; Allen *et al.*, 1988; Michels, 1989; Paulovic *et al.*, 2005; Tyagi, 2005). Krauss and Stevens (1983) published one of the earliest theoretical studies. They concluded that lowest energy configuration was U^{3+}($5f^{3}(^{4}I)$)O^{2-}, giving rise to an $\Omega = 4.5$ ground state. They also predicted the energies for all 26 states derived from the ^{4}I configuration (with Ω values ranging from 0.5 to 7.5).

Kaledin *et al.* (1994) used their empirically adjusted LFT model for UO to predict the states of UO^+ associated with the $U^{3+}(5f^3(^4I))$ ion core, and obtained results that were qualitatively in agreement with the calculations of Krauss and Stevens (1983).

UO^+ is also of practical interest as it can be formed by the associative ionization reaction $U+O \rightarrow UO^+ + e^-$ (Fite *et al.*, 1974; Paulovic *et al.*, 2005). Consequently, spectroscopic data for UO^+ have been sought for inclusion in atmospheric radiance models that are used to predict phenomena associated with nuclear explosions (Michels, 1989).

Gas-phase spectroscopic data for UO^+ were obtained by Goncharov *et al.* (2006), who recorded rotationally resolved PFI-ZEKE spectra for 33 vibronic bands of UO^+. Transitions to the ground state and nine electronically excited states were characterized within the energy range from 0 to 5,200 cm^{-1} (relative to $UO^+(X, v = 0)$). These results are summarized in Table 38.4. In accordance with theoretical predictions, the ground state was $\Omega = 4.5$. Figure 38.2 shows the rotational structure for the zero-point level. As for ThO^+, the PFI-ZEKE spectra for UO^+ showed extensive vibrational progressions for each electronic state. An advantage of PFI-ZEKE spectroscopy is that it is not constrained by the usual optical selection rules (e.g., $\Delta\Omega = 0, \pm 1$ for a single photon transition). The UO^+ spectra included transitions to states with all Ω values in the range from $\Omega = 0.5$–5.5, using just the $[19,453]\Omega = 3$ intermediate state of UO. Molecular constants for the ground state of UO^+ ($\omega_e = 911.9(2)$, $B_0 = 0.3467$ (7) cm^{-1}) were larger than those of neutral UO, consistent with ionization by

Table 38.4 Experimental and theoretical term energies (cm^{-1}) for the low energy states of UO^+.

State (Config.)	Measured term energy	MCSCF /VCI, 1983[a]	MCSCF /CI, 2005[b]	LFT, 1994[c]	LFT, 2006[d]
X(1)4.5 ($5f^3$)	0	0	0	0	0/0
(1)3.5 ($5f^3$)	764.93(20)	1,319	582	633	767
(1)2.5 ($5f^3$)	1,132.42(20)	1,895	856	696	1,131
(1)1.5 ($5f^3$)	1,284.5(3)	2,094	1,076	580	1,270
(1)0.5 ($5f^3$)	1,324.9(3)	3,296	–	695	1,309
(1)5.5 ($5f^3$)	4,177.83(20)	2,563	3,744	3,991	4,150
(2)4.5 ($5f^3$)	4,758.46(20)	3,599	4,180	4,601	4,767
(2)3.5 ($5f^3$)	5,161.96(20)	4,045	–	4,770	5,110
(3)2.5 ($5f^3$)	5,219.37(20)	–	–	4,744	5,293
(3)3.5 ($5f^27s$)	4,982.44(20)	–	4,287	–	–

[a] Krauss and Stevens 1983
[b] Tyagi 2005
[c] Kaledin et al., 1994
[d] Goncharov et al., 2006. The interaction parameters were treated as variables and fit to the experimental data in this semi-empirical LFT model.

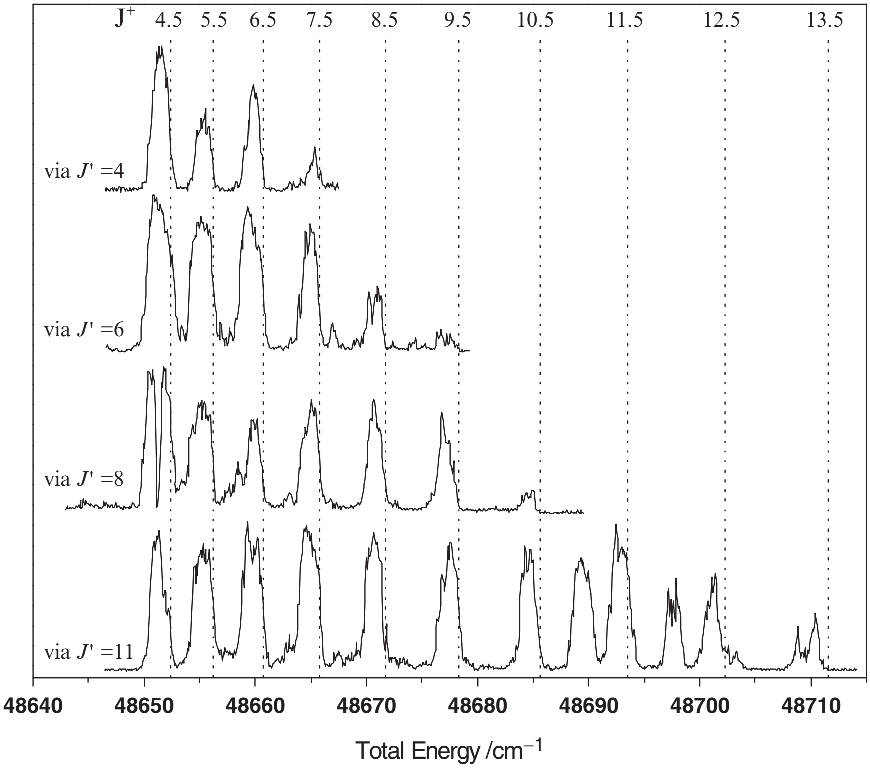

Fig. 38.2 *PFI-ZEKE spectra for* UO^+ *recorded via specific rotational levels* (J' = 4, 6, 8, 11) *of the intermediate state* [19.453]3. *The spectra show the rotational structure for the* UO^+ $X(1)4.5$ $v^+ = 0$ *level. The spectra are plotted against total energy of the transition from the UO* $X(1)4$ $v = 0$, $J = 0$ *state* (*reused with permission from Vasiliy Goncharov*, *Journal of Chemical Physics*, 125, 133202 (2006). *Copyright* 2006, *American Institute of Physics*).

removal of the non-bonding 7*s* electron. The calculations of Krauss and Stevens (1983) yielded reasonably good estimates for the ground state constants (ω_e = 925(30) cm^{-1}, R_e=1.842 Å (R_e(exp)=1.801(5) Å)), while the CASSI-SOC calculations of Paulovic *et al.* (2005) predicted constants that were within the experimental error limits (ω_e = 912 cm^{-1}, R_e = 1.802 Å).

The pattern of electronic states observed for UO^+ was readily understood using LFT. The low-lying states correlate with the $^4I_{4.5}$ and $^4I_{5.5}$ spin–orbit levels of the $U^{3+}(5f^3)$ ion. The atomic ion spin–orbit coupling strength was preserved in UO^+ to the extent that the atomic spin–orbit interval was recurrent in the energy level structure. For a given value of the atomic ion core angular momentum vector (J_a) the lowest energy state corresponds to the maximum projection of J_a on the diatomic axis for the first and third quarters of the nf^Nshell (Kaledin *et al.*, 1992) (e.g., $X(1)4.5$ from $5f^3$ ($^4I_{4.5}$)). The energies of

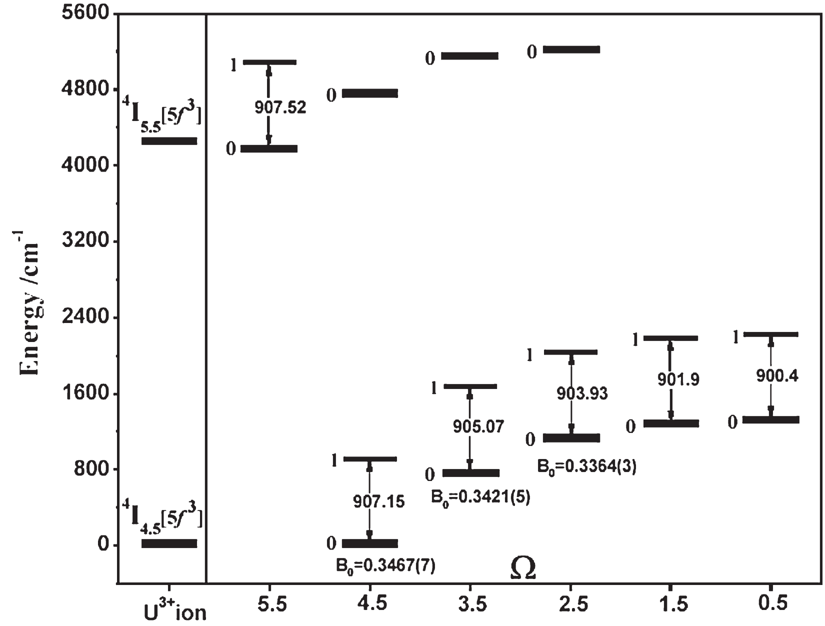

Fig. 38.3 *Observed low-lying electronic states* (v = 0 *and* 1 *only*) *for the* $U^{3+}(5f^3)O^{2-}$ *configuration of* UO^+, *arranged according to energy and* Ω. *For comparison, the spin–orbit splitting for* $U^{3+}(5f^3, {}^4I)$ *is shown on the left hand side of the diagram* (*reused with permission from Vasiliy Goncharov, Journal of Chemical Physics*, 125, 133202 (2006). *Copyright* 2006, *American Institute of Physics*).

the states increase as the vector is tipped away from the molecular axis. Hence, the atomic ion $^4I_{4.5}$ core gives rise to states with Ω = 4.5, 3.5, 2.5, 1.5, and 0.5 in ascending energy order. Similarly, $^4I_{5.5}$ gives rise to states with Ω from 5.5 to 0.5. These patterns were apparent in the spectrum of UO^+. All five of the states from $^4I_{4.5}$ were observed, along with the four lowest energy states of $^4I_{5.5}$. The right hand side of Fig. 38.3 shows the energy levels of UO^+, arranged in stacks that belong to a specific Ω value. The spin–orbit interval for the free $U^{3+}(5f^3)$ ion is indicated on the left. The $^4I_{5.5}-{}^4I_{4.5}$ interval for $U^{3+}(5f^3)$ is estimated to be 4,265 cm^{-1} (Carnall and Crosswhite, 1985), while the corresponding Ω = 5.5–4.5 interval for UO^+ is 4,178 cm^{-1}. To a first approximation it is expected that the states arising from a particular atomic ion configuration will have very similar vibrational and rotational constants (Field, 1982). The vibrational intervals indicated in Fig. 38.3 fit this expectation, as did the rotational constants. For the $^4I_{4.5}$ states it can be seen that there was a slight, systematic decrease in the vibrational frequency as the projection of J_a along the diatomic axis decreased. This trend is reasonable as the rotation of J_a away from the bond axis rotates the orbitals in a way that increases the repulsive interaction between the 5*f* electrons and the O^{2-} ligand (the same effect that results in the observed energy ordering of the states). Note that the $\Omega = 3.5$ state at 4,982.4 cm^{-1} did not belong to the ^{4}I group. This particular state was identified as the lowest energy state of the $U^{3+}(5f^27s, {}^4H_{3.5})O^{2-}$ group (Goncharov *et al.*, 2006).

Table 38.4 lists the results from LFT and ab initio calculations for the excited states of UO^+. The third and fourth columns list the energies of Krauss and Stevens (1983) and Tyagi (2005), respectively. In comparing with the experimental data, it can be seen that the calculations of Krauss and Stevens (1983) correctly predicted the energy ordering of the $^4I_{4.5}$ states, but the energy intervals between the states were overestimated by a factor of almost 2. This suggests that the electrostatic perturbation of the U^{3+} ion had been overestimated. In contrast, the interval between the $\Omega = 4.5$ and 5.5 states was underestimated, which suggests that the spin–orbit coupling of the ion core was partially quenched. This may also be a consequence of the overestimation of the strength of the ligand field. The more recent calculations of Tyagi (2005) were in better quantitative agreement with the experimental data, but there were a few puzzling discrepancies. States corresponding to (1)0.5, (2)3.5 and (3)2.5 were not predicted in the 0–8,800 cm^{-1} energy range. With the experimental data now available for UO^+ it is anticipated that there will be further theoretical studies in the near future.

38.3.3 Spectra and theoretical calculations for UO_2 and UO_2^+

UO_2 and the cations UO_2^+ and $UO_2^{2+}$are species of considerable importance in the chemistry of uranium, and these species have been the subjects of numerous theoretical studies. A detailed account of the theoretical studies of UO_2^{2+} up to the year 2005 is presented in Chapter 17 (Kaltsoyannis *et al.*, 2006). From the perspective of the densities of low-lying electronic states, their complexity increases in the order $UO_2^{2+} < UO_2^+ < UO_2$. However, the difficulties encountered in gas phase experimental studies of this series increase rather steeply in the reverse order.

Gas-phase spectroscopic data have been obtained for UO_2 and UO_2^+. The bare UO_2^{2+} ion has been detected in a mass spectrometer (Cornehl *et al.*, 1996; Gibson *et al.*, 2005b), but spectra have not been reported to date. However, there have been recent reports of IR spectra for UO_2^{2+} complexed with anionic ligands and solvent molecules (Groenewold *et al.*, 2006b; 2008a, b, c) that are discussed in Section 38.6.4.

One of the first investigations of gas-phase UO_2 involved electric field deflection measurements, which provide information concerning the permanent electric dipole moment of the molecule. Kaufman *et al.* (1967) noted only a weak deflection of UO_2 from a molecular beam, and concluded that the molecule was linear and centrosymmetric (the slight defection was attributed to the presence of molecules with bending mode excitation). This result was in agreement with theory, which has consistently predicted linear symmetric equilibrium structures for UO_2, UO_2^+ and UO_2^{2+}. In contrast, both electric deflection measurements

(Kaufman *et al.*, 1967) and IR spectra for matrix isolated ThO_2 (Gabelnick *et al.*, 1974) indicate a bent equilibrium structure. As UO_2^{2+} and ThO_2 are isoelectronic, this surprising difference has also been a point of theoretical interest (Dyall, 1999).

One of the first objectives in the spectroscopic study of gas-phase UO_2 was to determine the electronic assignment for the ground state. Ab initio calculations carried out in the 1980s predicted that the metal-centered 5*f* orbitals were the highest occupied molecular orbitals (HOMO's) (Wood *et al.*, 1981; Michels and Hobbs, 1983; Allen *et al.*, 1988; Pepper and Bursten, 1991). Calculated energies for the $5f\phi_u$ and $5f\delta_u$ orbitals were close enough to complicate the task of identifying the ground state configuration. Wood *et al.* (1981) and Michels and Hobbs (1983) found that $(5f\phi_u)^2$ gave the lowest energy, which would produce a ${}^3\Sigma_g{}^-$ ground state. Alternatively, the calculations of Allen *et al.* (1988) indicated that either $(5f\phi_u)(5f\delta_u)$ or $(5f\delta_u)^2$ would be lowest in energy, yielding either a ${}^3H_g$ or ${}^3\Sigma_g{}^-$ ground state. More recent investigations (ab initio and DFT) yielded a ${}^3\Phi_u$ ground state derived from the $(5f\phi_u)(7s\sigma_g)$ configuration (Zhou *et al.*, 2000; Gagliardi *et al.*, 2001, 2005; Chang, 2002; Tyagi, 2005; Fleig *et al.*, 2006; Infante *et al.*, 2007a). All of the published studies predicted partially occupied 5*f* orbitals that give rise to manifolds of low-lying electronic states, which is consistent with the large heat capacity of vapor phase UO_2.

The first electronic spectra for gas-phase UO_2 were reported by Han *et al.* (2003, 2004). These data were obtained using two-color REMPI excitation with mass selected ion detection. Supersonic jet cooling was used to reduce the spectral congestion. Twenty-two vibronic bands of neutral UO_2 were observed in the range from 17,400 to 32,000 cm^{-1}. The vibronic selection rules deduced from these spectra indicated that the molecule was linear and centrosymmetric for the ground state and for most of the excited states (progressions indicative of a bent excited state were not seen). Ionization threshold measurements were used to determine the absolute energies of the lower levels for these transitions. The electronic states of UO_2 that have been observed to date are listed in Table 38.5.

Deviations from thermal equilibrium distributions are often encountered with jet cooling, and this permitted the detection of a few transitions that originated from low-lying excited states. Due to the low frequency of the ground state bending vibration (120 cm^{-1}) levels with v_b=0–2 were significantly populated. In addition, transitions were observed that originated from an electronically excited state that was approximately 360 cm^{-1} above the ground state. The presence of this low-lying state provided the key to determining the lowest energy electronic configuration. The ab initio calculations of Chang (2002), Tyagi (2005), Gagliardi *et al.* (2001) and Infante *et al.* (2007a) all indicated that the angular momentum coupling for the low-lying states of UO_2 is intermediate between *LS* and *Jj*. Viewed from the latter perspective, the states of U $(5f\phi_u 7s\sigma_g)O_2$ are built on the ${}^2F$ term arising from the 5*f* electron. The J_f=5/2 and 7/2 components of this term are widely separated by the spin–orbit

Table 38.5 Electronic transition and ionization energies for UO_2.[a]

Transition energy (cm^{-1})[b]	Lower state	v_b''	Upper state	v_b'	IE[c]
17,406	3u	2	4g	2	48,825
17,447	3u	1	4g	1	48,940
17,499	3u	0	4g	0	49,070
17,621	3u	1	4g	3	–
17,664	3u	0	4g	2	–
18,096	2u	1	1g	1	–
18,159	2u	0	1g	0	49,425
18,227	3u	0	–	0	49,080
18,423	2u	0	1g	0	–
27,259	2u	0	2g	0	–
28,667	–	–	–	–	–
28695	–	–	–	–	–
28,722	–	–	–	–	–
28,745	–	–	–	–	–
28,782	–	–	–	–	–
28,805	–	–	–	–	–
29,654	2u	1	–	1	–
29,700	2u	0	–	0	49,430
31,419	3u	1	2g	1	48,935
31,478	3u	0	2g	0	49,070
31,788	2u	1	2g	1	49,300
31,838[c]	2u	0	2g	0	49,420

[a] Han et al. 2003

[b] Band centers. The error limits are ±5 cm^{-1}. v_b is the bending vibrational quantum number.

[c] Ionization energy for the lower level of the transition. The error limits are ±20 cm^{-1}.

interaction. The lower energy $J_f = 5/2$ component is split into $J_a = 3_u$ and 2_u terms by the much weaker interaction between J_f and the spin of the 7*s* electron. The two lowest energy states of UO_2 are produced when the electronic angular momentum vectors have their maximum projections along the molecular axis. The $J_a = 3_u$, $\Omega = 3_u$ and $J_a = 2_u$, $\Omega = 2_u$ components correlate with the *LS* term symbols $^3\Phi(3_u)$ and $^3\Phi(2_u)$. Theoretical calculations (Gagliardi *et al.*, 2001, 2005; Chang, 2002; Tyagi, 2005; Fleig *et al.*, 2006; Infante *et al.*, 2007a) predict that these states are separated by energies in the range of 378–439 cm^{-1}. The next pair of states correspond to $\Omega = J_a - 1$ (2_u and 1_u) and they are approximately 2,000 cm^{-1} above the ground state ($\tilde{X}^3\Phi(2_u)$). The pattern of low-lying states originating from $U(5f\phi_u 5f\delta_u)O_2$ is markedly different. The two lowest energy states for this configuration are $^3H(4_g)$ and $^3H(5_g)$, and they are separated by a relatively strong spin–orbit interaction (Fleig *et al.*, 2006). Hence, the observation of a low-lying electronic state of UO_2 confirmed that the ground state is derived from the $5f\phi_u 7s\sigma_g$ configuration. In this context it is of interest to note that the ground state predicted for the isoelectronic PuO_2^{2+} ion is $^3H(4_g)$, arising from the $5f\phi_u 5f\delta_u$ configuration (Maron *et al.*, 1999; Clavaguera-Sarrio *et al.*, 2004; Infante *et al.*, 2006).

Excited states of UO_2, along with oscillator strengths for transitions originating from $\tilde{X}^3\Phi(2_u)$ were calculated by Chang (2002). Han *et al.* (2004) used these data to propose assignments for states in the 17,800–31,900 cm^{-1} energy range. As the oscillator strengths were not available for transitions from $^3\Phi(3_u)$, assignments for the bands associated with these states were advanced based on the application of the $\Delta\Omega = 0, \pm 1$ selection rule. It was proposed that the stronger bands in this energy range were formally metal-centered $5f7p \leftarrow 5f7s$ transitions. A pair of transitions was identified that appeared to originate from the$\tilde{X}^3\Phi(2_u)$ and $^3\Phi(3_u)$ states, and terminate on a common upper level. The interval between these bands was used to refine the estimate for the $\tilde{X}^3\Phi(2_u)$ - $^3\Phi(3_u)$ energy difference. Subsequent high-level calculations have shown that revisions of the proposed assignments are needed (Gagliardi *et al.*, 2005; Tyagi, 2005; Infante *et al.*, 2007a). Calculations of the oscillator strengths for transitions from both $\tilde{X}^3\Phi(2_u)$ and $^3\Phi(3_u)$ revealed an unexpected pattern. There were no occurrences of excited state levels that had good oscillator strengths for transitions from both lower states. This implied that the transitions ascribed to a common upper state actually terminated on two nearby states. Recent PFI-ZEKE measurements for UO_2 (Merritt *et al.*, 2008) have shown that, if two upper states are involved, they cannot be separated by more than 2 cm^{-1}.

Electronic states in the 600–17,000 cm^{-1} range were not probed in the gas-phase experiments, but low-lying states have been observed in dispersed fluorescence spectra for UO_2 isolated in solid Ar (Lue *et al.*, 2004). Interpretation of these data is complicated by the unusual interaction between UO_2 and the host matrix. This issue is discussed at some length in Chapter 17 (Kaltsoyannis *et al.*, 2006). To summarize briefly, IR absorption spectra for matrix isolated UO_2 show the asymmetric stretch fundamental at 914 and 776 cm^{-1} for Ne and Ar hosts, respectively (Hunt and Andrews, 1993; Zhou *et al.*, 2000). Andrews, Bursten and co-workers (Zhou *et al.*, 2000; Li *et al.*, 2004) have proposed that this exceptionally large matrix effect indicates that the low-lying electronic states are reordered by the interaction with the Ar host. The ground state changes from $5f7s$ $^3\Phi(2_u)$ in Ne to $5f^2$ $^3H(4_g)$ in Ar. These states were predicted to have significantly different vibrational constants for the asymmetric stretch (919 and 824 cm^{-1} in the gas phase) (Li *et al.*, 2004). Electronic excitation spectra for UO_2 in an Ar matrix are difficult to reconcile with this model. If the proposed state re-ordering occurred, the ground state would change from *u* to *g* inversion symmetry. Excitation spectra for UO_2 in Ar would then access states of *u* symmetry, while the gas-phase REMPI spectra would show excited states of *g* symmetry. Under these circumstances the electronic spectra for Ar matrix isolated and gas-phase UO_2 would be expected to be markedly different, reflecting transitions to mutually exclusive manifolds of excited states. However, Lue *et al.* (2004) found that there was a good correlation between the two.

Another important issue for the state reordering model is the separation between the $X^3\Phi(2_u)$ and the $^3H(4_g)$ states for the unperturbed molecule. Calculations prior to 2007 had yielded an interval of 3,000–4,000 cm^{-1} (Chang, 2002; Li *et al.*, 2004; Gagliardi *et al.*, 2005; Fleig *et al.*, 2006). A large differential matrix shift is needed to reorder states that are this far apart, but the calculations of Li *et al.* (2004) indicate that it is feasible. However, the most recent theoretical study (Infante *et al.*, 2007a) finds an interval of 10,914 cm^{-1} and a relatively high value of 911 cm^{-1} for the asymmetric stretch frequency of 4_g state. They also found low energy states associated with the 5*f*6*d* configuration, and speculate that it may be the lowest energy state of this group that becomes the ground state in Ar and the heavier rare gas matrices. This interpretation has the advantage that it preserves the inversion symmetry for the ground state.

Lue *et al.* (2004) used the theoretical predictions of Chang (2002) to assign the dispersed fluorescence spectrum for UO_2 isolated in an Ar matrix. Subsequent theoretical work suggests that these assignments should be revised, even under the assumption that there is no state reordering in the matrix. Lue *et al.*(2004) correlated energy levels at 1,094 and 1,401 cm^{-1} with the 5*f*7*s* $^3\Delta(1_u)$ and $^3\Delta(2_u)$ states. Calculations by Gagliardi *et al.* (2005), Fleig *et al.* (2006), and Infante *et al.* (2007a) all find that the term energy for $^3\Delta(2_u)$ exceeds 2,000 cm^{-1}, and two of these studies also find $^3\Delta(1_u)$ above this energy. It is evident from this range of discrepancies that a study of the dispersed fluorescence spectrum of gas-phase UO_2 is needed to make further meaningful progress.

The IE for UO_2 was determined from multiphoton ionization measurements. The most accurate result was 6.127(1) eV from the PFI-ZEKE spectrum (Merritt *et al.* 2008). The spectroscopic IE was 0.7 eV higher than the previously accepted value from electron impact measurements (Rauh and Ackerman, 1974; Capone *et al.*, 1999), but in excellent agreement with theoretical predictions of Zhou *et al.* (2000) and Gagliardi *et al.* (2001). The fact that theory arrived at the correct IE in advance of the experimental results seemed to provide a strong endorsement for the current generation of relativistic electronic structure calculations. Unfortunately, calculations by Tyagi (2005) have raised new concerns. Gagliardi *et al.* (2001) obtained their results using spin-free CASSCF or CASPT2 calculations with subsequent treatment of the spin–orbit operator (a two-step approach). Tyagi (2005) carried out MCSCF calculations with explicit treatment of the spin–orbit operator from the outset (one-step approach). The basis sets for uranium were of double zeta or triple zeta quality, with relativistic core potentials that included 60 or 68 electrons in the core. Tyagi (2005) examined the dependence of the predicted IE on the core size and basis set size. Calculations were performed for vertical and adiabatic ionization, with or without inclusion of the spin–orbit interaction. IE values close to 5.7 eV were obtained, with very little dependence on the factors examined. It was surprising to find that such high-level calculations yielded results that differed from the measured value by about 0.4 eV. The relativistic coupled cluster calculations of Infante *et al.* (2007a) yielded an adiabatic IE of 5.92 eV. They speculated that coupled cluster methods might systematically underestimate the IE of UO_2 as an earlier coupled cluster study (Majumdar *et al.*, 2002) yielded IE value of 6.01 eV.

The photoionization kinetics of UO_2^+ proved to be of interest in their own right. At the energetic threshold the electrons were ejected from the molecule with a characteristic decay time of 189 ns (Merritt *et al.*, 2008). This value decreased with increasing energy above the ionization limit. Delayed ionization of this kind has been observed for metal clusters, but the case of UO_2 is the first example of this phenomenon for a triatomic molecule. It occurs because the IE for UO_2 is approximately 1 eV lower than the OU–O bond dissociation energy. Due to this circumstance, the zero-point level of UO_2^+ is immersed in a dense manifold of the ro-vibronic levels of UO_2. The slow ionization kinetics is a consequence of mixing of the ion and neutral molecule states. In essence, gas-phase UO_2 exhibits thermionic emission of electrons at the ionization threshold.

The electronic ground state of the UO_2^+ cation has been examined in the gas phase using PFI-ZEKE spectroscopy (Merritt *et al.*, 2008). These measurements were carried out at the level of vibrational resolution. Fig. 38.4 shows the low-energy region of this spectrum. In this trace a very harmonic progression with a spacing of approximately 145 cm^{-1} is easily recognized. A second progression with a spacing of 145 cm^{-1} begins at 919 cm^{-1} above the origin of the first progression. Spectra recorded for the $U^{16}O_2^+$ and $U^{18}O_2^+$ isotopes confirmed assignment of the low frequency vibrational progression to the bending mode, and the high frequency interval to the symmetric stretch. Data were obtained for levels of UO_2^+ that were up to 4,700 cm^{-1} above the ground state zero-point level. The congestion of the spectrum increased dramatically with increasing energy. Fortunately, the underlying structure of the spectrum was straightforward. The greater majority of the levels could be assigned as excited bending vibrations, built on symmetric stretch levels with the vibrational quantum numbers $v_s = 0, 1, 2, 3$, and 4. The first electronically excited state was found at 2,678 cm^{-1}. Progressions in the bending and symmetric stretch levels of this state were also observed.

The only other spectroscopic data for UO_2^+ have been obtained from matrix isolation studies. Zhou *et al.* (2000) observed the asymmetric stretch fundamental at 980.1 cm^{-1} for UO_2^+ isolated in solid Ne. The same transition was reported for Ar, Kr and Xe matrices at 952.3, 941.6, and 930.6 cm^{-1} respectively (Wang *et al.*, 2004). In keeping with the prediction of a linear symmetric structure for UO_2^+, the symmetric stretch was not observed in the IR spectra. Although the bending mode is IR active, it was outside the spectral range examined. Hence a direct comparison of the gas phase and matrix data is not possible.

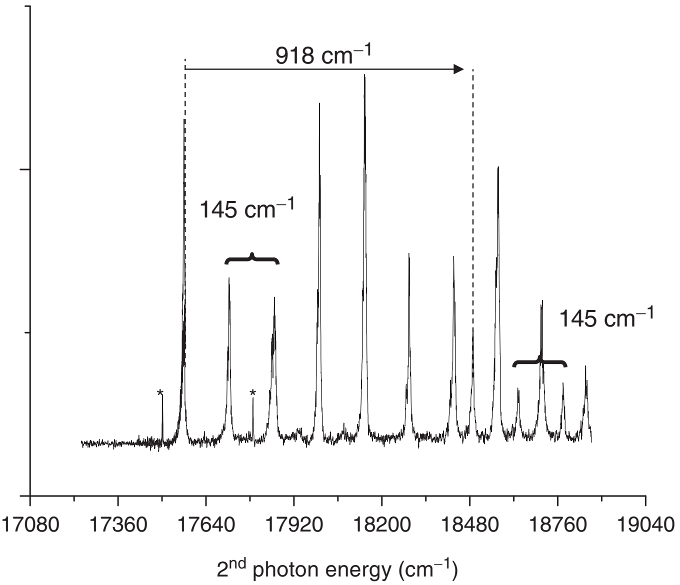

Fig. 38.4 *PFI-ZEKE spectrum of* $U^{16}O_2^+$ *recorded up to* ~1,100 *cm*$^{-1}$ *above the ground state of the cation. The regularly spaced peaks are assigned to the bending progression of* UO_2^+. *At 918 cm*$^{-1}$ *above the ground state, a second series of peaks was observed that are assigned to a bending progression built upon the excitation of one quanta of symmetric stretch. The peaks marked with an asterisk correspond to atomic uranium PFI-ZEKE transitions.*

Theoretical calculations for UO_2^+ have consistently converged to a $U(5f\phi_u)O_2^+\ \tilde{X}^2\Phi$ ground state. For the symmetric stretch, vibrational frequencies in the range of 858–971 cm^{-1} have been predicted, with bending frequencies of 101–191 cm^{-1}. The results were scattered around the experimental values and the DFT calculations appeared to be marginally more accurate that the ab initio treatments for the levels of approximation that have been employed so far. The spin-free DFT calculations of Zhou *et al.* (2000) predicted that the first electronically excited state is $U(5f\delta_u)O_2^+\ {}^2\Delta$ at 1,760 cm^{-1}. The ab initio calculations of Infante *et al.* (2007a), which included explicit treatment of spin–orbit interactions, yielded a $U(5f\phi_u)O_2^+\ \tilde{X}^2\Phi(5/2_u)$ ground state with the first excited state, $U(5f\delta_u)O_2^+\ {}^2\Delta(3/2_u)$ at 2,736 cm^{-1}. The latter is in good agreement with the experimental result, which finds the electronically excited state near 2,678 cm^{-1}. Note that the symmetric stretch and bend frequencies of the excited state were close to those of the ground state, as would be expected if the configurations differed by just the details of the occupation of the non-bonding *f*-orbitals.

UO_2^+ is isoelectronic with NpO_2^{2+}, so it is of interest to compare the patterns of low-lying states for the two ions. The ground and first excited states of

NpO_2^{2+} are also predicted to be $5f\phi_u\ \tilde{X}^2\Phi(5/2_u)$ and $5f\delta_u\ ^2\Delta(3/2_u)$ (Matsika and Pitzer, 2000). The primary difference is the stronger ligand field of NpO_2^{2+}. The relativistic calculations of Matsika and Pitzer (2000) predict a much smaller energy separation between these states (447 cm^{-1}) than that seen in UO_2^+, despite the larger internal field. However, subsequent calculations by Infante *et al.* (2006) yielded results that are in accord with ligand field theory expectations. They obtained energy spacings between the $5f\phi_u\ \tilde{X}^2\Phi(5/2_u)$ and $5f\delta_u\ ^2\Delta(3/2_u)$ states of 2,376 cm^{-1} for UO_2^+ and 3544 cm^{-1} for NpO_2^{2+}.

38.3.4 Matrix isolation spectroscopy of UO_3, $UO_2(O_2)$, $UO_3(O_2)$ and plutonium oxides

Gabelnick and co-workers used thermal vaporization of uranium dioxide to trap UO_3 in solid Ar (Gabelnick *et al.*, 1973a, b, c; Green *et al.*, 1980). Samples with ^{18}O enrichment yielded spectroscopic data for all $^{16}O/^{18}O$ combinations. From these data they were able to show that the molecule has a T-shaped geometry with a near linear OUO sub-unit (C_{2v} symmetry for four of the six possible isotopomers). Fundamental vibrational frequencies were measured for five modes for each C_{2v} isotopomers, and for all six modes for the C_s isotopomers.

Laser ablation of uranium in the presence of O_2 has also been used to produce samples of UO_3 trapped in Ar and Ne matrices. Hunt and Andrews (1993) obtained results for UO_3 in Ar that were in excellent agreement with the study by Gabelnick *et al.* (1973b). Spectra for the high-frequency modes of UO_3 in a Ne matrix were recorded by Zhou *et al.* (2000). They noted a slight blue shift of the bands, relative to the Ar matrix results (12.8 and 14.8 cm^{-1}). Density functional theory calculations yielded a C_{2v} equilibrium structure with bond angles of 158.8° and 100.6°.

Oxide complexes were also formed in the laser ablation – matrix isolation experiments. Hunt and Andrews (1993) tentatively assigned features in the Ar matrix spectra to $(UO_2^+)(O_2^-)$ and UO_3–O_2. These assignments were deduced from isotopic substitution, photolysis and matrix annealing experiments. In the Ne matrix, Zhou *et al.* (2000) identified bands of $(UO_2^+)(O_2^-)$ and the anionic complex O_2-UO_2^-.

The IR absorption spectra for matrix isolated PuO and PuO_2 were investigated by Green and Reedy (1978). Vapor phase samples for deposition were generated by sputtering Pu metal from a hollow cathode. Ar and Kr were used as the host materials, with a trace of O_2 present to form the oxides. ^{18}O substitution was used to facilitate assignment. Prior to annealing, several lines were observed for PuO due to the presence of multiple trapping sites. On annealing, one of these sites proved to be the most stable, yielding a vibrational frequency for $Pu^{16}O$ of 822.2 cm^{-1}. This frequency exhibited a modest red shift to 817.3 cm^{-1} when the host material was changed to Kr.

The antisymmetric stretch of PuO_2 was observed in both Ar and Kr matrices (794.2 and 786.8 cm^{-1} respectively for $Pu^{16}O_2$). As for PuO, the shift was consistent with the physical change of the guest–host interaction resulting from the change in the polarizability of the host. The symmetric stretch was only detected for the $^{16}OPu^{18}O$ isotopomer. These data clearly indicated that PuO_2 has a linear symmetric equilibrium structure. Green and Reedy (1978) searched for bands of PuO_3 in their data, but could not find evidence for the presence of this species in their samples.

38.4 SPECTROSCOPIC STUDIES OF ACTINIDE HALIDES

38.4.1 Vibrational spectroscopy of UF_6, NpF_6 and PuF_6

The actinide hexafluorides are particularly suitable for gas-phase spectroscopic investigation as they have significant vapor pressures at ambient temperatures (Frlec and Claassen, 1967). IR spectra have been reported for UF_6, NpF_6 and PuF_6. In addition, Raman spectroscopy has been used to study the IR inactive bands of UF_6. From these data it has been established that these molecules have octahedral equilibrium structures. The patterns of vibrational energy levels of the molecules are similar, which is a consequence of having the heavy metal atom at the center of the structure (Kim and Mulford, 1990). This causes the An–F bonds to act somewhat like local mode oscillators (Person *et al.*, 1986). For AnF_6 molecules there are three stretch vibrational modes ($\nu_1(A_{1g})$, $\nu_2(E_g)$ and $\nu_3(T_{1u})$) and three bending modes ($\nu_4(T_{1u})$, $\nu_5(T_{2g})$ and $\nu_6(T_{2u})$). The stretch and bend frequencies cluster into two groups. For example, for UF_6 the stretches are in the range 606 ± 51 cm^{-1} and the bending frequencies span 174 ± 23 cm^{-1} (Kim and Mulford, 1990). The frequency spread within the two groups decrease with increasing mass of the central atom. Only the ν_3 and ν_4 modes are IR active, but all six fundamentals for the three molecules have been derived from observations of overtone and combination bands. Rotational analyses have been carried out for the stronger IR bands, yielding rotational constants, Coriolis constants and higher order rotation–vibration interaction parameters. There have been many theoretical studies of actinide hexafluorides and these have been discussed in Chapter 17 (Kaltsoyannis *et al.*, 2006).

As UF_6 is of technological importance (and relatively easy to handle) it has received the most attention. In part, this work has been motivated by the hope of developing efficient laser-based isotope separation schemes that rely on selective excitation (Takeuchi *et al.*, 1989; Okada *et al.*, 1995; Baranov *et al.*, 1999). IR multiphoton dissociation of UF_6 has been observed in several studies and selective excitation has been used to demonstrate $^{235}U/^{238}U$ isotope enrichment via dissociation or vibrationally mediated enhancement of reactivity (Rabinowitz *et al.*, 1978; Tiee and Wittig, 1978; Koren *et al.*, 1982; Averin *et al.*, 1983; Oyama *et al.*, 1986; Takeuchi *et al.*, 1989; Okada *et al.*, 1995). Challenges in devising selective excitation schemes are associated with the thermal population of vibrationally excited levels and the small isotope shifts resulting from the central position of the U atom.

To put the thermal congestion problem into perspective, it is estimated that 99.6% of UF_6 molecules populate vibrationally excited levels at a temperature of 300 K (Aldridge *et al.*, 1985; Kim and Mulford, 1990). Consequently, each vibrational band in the room temperature spectrum of UF_6 is the result of multiple overlapping transitions. To mitigate this problem, many of the earlier spectroscopic studies utilized low temperature cells. Due to the concomitant drop in the equilibrium vapor pressure, long-path absorption techniques were required to achieve measurable absorbances, and this resulted in a practical lower limit for the cell temperature of about 160 K. A particularly notable example of this kind of study is that of McDowell *et al.* (1974), where 44 vibrational bands were characterized using a combination of IR and Raman measurements. Isotope shifts were measured, and a quadratic harmonic force field was derived from the full data set. The isotope shift for the ν_3 fundamental, which is the most intense absorption feature, was just 0.65 cm^{-1}. A much larger isotope shift of 18 cm^{-1} has been reported by Zhang *et al.* (1996) for the $3\nu_3$ overtone.

Further progress with UF_6 was enabled by applying the technique of isentropic expansion cooling (Baronov *et al.*, 1981; Aldridge *et al.*, 1985; Yato and Yamaguchi, 1992). Gas-phase samples with internal temperatures as low as 40 K were obtained by this method, permitting the observation of spectra where transitions from the zero-point vibrational level dominated. High-resolution spectra for both thermally and expansion cooled UF_6 have been recorded using tunable diode lasers. To date, rotationally resolved spectra have been recorded for the ν_3 fundamental (^{238}U(Aldridge *et al.*, 1985), ^{235}U(Aldridge *et al.*, 1985), and ^{236}U(Yato and Yamaguchi, 1992) isotopes), $\nu_1+\nu_3$ (McDowell *et al.*, 1985), and 3v_3 (Krohn *et al.*, 1988). An extensive set of rotation-vibration molecular constants have been developed for UF_6, and can be found in the references given here.

IR and Raman spectra for matrix isolated UF_6 have been reported (Paine *et al.*, 1976; Holland and Maier, 1983). For UF_6 in Ar, Paine *et al.* (1976) observed five fundamentals and six combination bands. The frequency shifts caused by the matrix were less than 1%. In situ photolysis, which produced UF_5, was also investigated.

Moderate resolution IR spectra for NpF_6 and PuF_6 were very similar to the results for UF_6. Band contour analyses were used to derive band origins and Coriolis constants from these data (Frlec and Claassen, 1967; Person *et al.*, 1986; Kim and Mulford, 1990). In their analysis of the systematic trends for the series An=U, Np, Pu, (Person *et al.*, 1986) noted that the IR transition intensities decrease with increasing atomic number for the metal.

High-resolution gas-phase IR spectra for NpF_6 and PuF_6 have been recorded using thermal cooling to reduce the spectral congestion problems. As compared to UF_6, the rotational structures for the bands of NpF_6 and PuF_6 are complicated by the partially occupied 5*f* orbitals of the metal atom. The ground state configurations are 5*f* and $5f^2$ for the Np and Pu hexafluorides, respectively. This complication is most significant for NpF_6, as the single unpaired electron results in half-integer total angular momentum states. Mulford and Kim (1996) have analyzed partially resolved rotational structures for the ν_3 and $\nu_1+\nu_3$ bands of NpF_6. Scalar molecular properties were derived from these data, but they did not attempt to extract tensor properties. Spectra and analyses for the $\nu_1 + \nu_3$, $\nu_2 + \nu_3$ and $3\nu_3$ bands have also been reported (Kim and Mulford, 1989).

Resolved rotational structure has been analyzed for the ν_3 fundamental of PuF_6. In this study it was found that the P and R branches followed the expected rotational energy level pattern for an octahedral molecule excited to a triply degenerate vibrational state. However, the Q-branch lines deviated from this model, indicating mixing of the ν_3 level with excited bending level (Kim *et al.*, 1988).

38.4.2 Electronic spectroscopy of actinide hexahalides

Electronic spectra have been recorded for UF_6, NpF_6 and PuF_6 in the gas phase and for samples isolated in cryogenic rare gas matrices. As noted above, UF_6 is unique in this group as the U^{6+} ion is closed shell. Consequently, the lowest energy transitions of UF_6 are formally ligand-to-metal charge transfer bands, while those of NpF_6 and PuF_6 are metal-centered *f–f* transitions.

The absorption spectrum of gas-phase UF_6 shows a series of broad bands (Steindler and Gunther, 1964; Lewis *et al.*, 1976; McDiarmid, 1976; Buecher, 1977; Oldenborg *et al.*, 1978), starting at a transition energy of 3.03 eV. Local absorption maxima are seen in the regions of 3.2–3.4, 3.8–4.6, and 5.4–5.8 eV. The absorption cross-section increases with increasing excitation energy, and the features above 4 eV are far stronger than the lower energy bands. Theoretical calculations (Koelling *et al.*, 1976; Boring and Hecht, 1978; Boring and Wood, 1979; Hay, 1983) indicate that the lower energy bands belong to $g \leftarrow g$ type transitions that are electric dipole forbidden (e.g., promotion of an electron from the fluorine $12\gamma_{8u}$ orbital to the $4\gamma_{7u}$, $13\gamma_{8u}$ or $5\gamma_{7u}$ *f*-orbitals). They are either magnetic dipole allowed or the transition is facilitated by vibronic interactions. The bands at energies above 4.0 eV range are attributed to electric dipole allowed transitions where the electron is promoted from the highest energy *g*-symmetry MO of the F atoms ($11\gamma_{8g}$) to the metal 5*f* orbitals. Vibronic structure could not be resolved in the gas phase, but highly structured spectra were obtained from UF_6 isolated in solid Ar at temperatures below 15 K. Lewis *et al.* (1976) used the results from theoretical calculations to assign their matrix spectra. Five separate electronic transitions were identified in the 3–4 eV range. Similar results were reported by Miller *et al.* (1979), who achieved slightly better resolution by using a higher Ar/UF_6 dilution ratio. The vibrational frequency changes resulting from $p \rightarrow f$ electronic excitation show a systematic decrease in the stretching frequencies. Due to these changes, each electronic band system exhibits long progressions of overtone and combination bands.

Electronic states of UF_6 at energies up to 28.5 eV were probed by Srivastava *et al.* (1976) using inelastic electron scattering. Their low-resolution spectrum was in good agreement with the optical absorption data at energies below 6.3 eV, and revealed numerous high-energy states that have large optical cross sections. At energies above the ionization limit (14.14 eV), the features in the inelastic scattering spectrum correspond to auto-ionizing resonances. A particularly intense band in the 12–14 eV range observed by Srivastava *et al.* (1976) has been used to interpret the unusual visible wavelength multiphoton processes that result in the ejection of U^+ and U^{2+} from UF_6.

Photoelectron spectra for gas-phase UF_6 have been examined for removal of both valence and core electrons (Maartensson *et al.*, 1984; Beach *et al.*, 1986). The lower energy region of this spectrum (electron binding energies of 14.14–17.5 eV) consists of five features when recorded at a resolution of 0.7 eV. These bands are assigned to removal of electrons from orbitals that are primarily F 2*p*, with some admixture of U 6*p* and 5*f*. Detailed discussions of this region of the photoelectron spectrum have been presented (Onoe *et al.*, 1994; de Jong and Nieuwpoort, 1996; Peralta *et al.*, 2005; Kaltsoyannis *et al.*, 2006). In agreement with earlier theoretical analyses, these studies find that the HOMO for UF_6 is $4\gamma_{8u}$ t_{1u}. However, in the analyses of their data, both Beach *et al.* (1986) and Maartensson *et al.* (1984) conclude that the HOMO is of t_{1g} symmetry. The question of the correct assignment remains unresolved. Clearly, reassignment to an orbital of *g* symmetry has implications for interpretation of the intensity patterns seen in the visible and near UV absorption spectra.

Higher energy photoelectron spectra show features corresponding to removal of the U 4*d*, 4*f*, 5*p*, 5*d*, and F 1*s* electrons. Shifts in the energies of the metal orbitals, relative to those of uranium metal, have been discussed in terms of configuration interaction models (Maartensson *et al.*, 1984).

Miller *et al.* (1979) and Grzybowski and Andrews (1978) examined the emission spectra resulting from pulsed laser excitation of UF_6/Ar matrices. Vibronic relaxation was found to be rapid and the emission spectra were (for a given matrix site) independent of the excitation wavelength. A fluorescence decay lifetime of 600 μs was observed, indicative of an electric dipole forbidden transition.

The fluorescence decay kinetics of UF_6 in the gas phase has also been examined using pulsed laser excitation (Oldenborg *et al.*, 1978; Wampler *et al.*, 1978d, 1979c; Rice *et al.*, 1980; Baranov *et al.*, 1999). Oldenborg *et al.* (1978) found that the relative fluorescence quantum yield decreased with increasing excitation energy over the range 3.0–3.3 eV. For excitation at 3.15 eV they observed non-linear self quenching kinetics that extrapolated to a collision-free fluorescence decay lifetime of 40 μs. Taken with the radiative lifetime from the matrix study, this was consistent with an estimate for the fluorescence quantum yield of 0.07. Oldenborg *et al.* (1978) proposed a two state collision-induced electronic energy transfer model to account for these observations. Quenching of electronically excited UF_6 by foreign gas collision partners has also been explored (Wampler *et al.*, 1978a, b, c; 1979a, b).

The dissociation energy for the process $UF_6 \rightarrow UF_5 + F$ is estimated to be 3.0 eV, so all of the electronically excited states have the possibility of undergoing predissociation (Armstrong *et al.*, 1994). Vibronic structure has not been reported for the states above 4.0 eV, and this may be a consequence of rapid predissociation and/or excitation to states that undergo direct dissociation. It has been shown that photolysis occurs at all absorption wavelengths below 407 nm (3.0 eV) (Baranov *et al.*, 1999). The photodissociation dynamics associated with 4.66 eV excitation have been characterized by measuring the recoil velocity of the ejected F atoms under collision free conditions (Kroger *et al.*, 1978). The fragments were produced with a non-isotropic angular distribution, indicative of rapid dissociation from a state with lowered symmetry (e.g., Jahn–Teller distortion). The F atom velocity distribution was bimodal, which suggests that two dissociation channels were operative.

There have been relatively few studies of the electronic spectrum of gas-phase or matrix isolated NpF_6. Gas-phase spectra covering the range from 0.5 to 6.2 eV were reported by Steindler and Gerding (1966). Two groups of structured bands were observed near 0.94 and 1.18 eV. Both had small absorption cross-sections. At energies above these features the spectrum did not show resolved vibronic structures. A broad, weak absorption in the 2.1–3.0 eV range was followed by a steady climb in the absorption strength from 3.0 eV onward. Intense absorption maxima were located at 4.8 and 5.6 eV. This pattern reflects electric dipole forbidden *f–f* transitions at low energies followed by allowed ligand to metal charge transfer bands at higher energies.

Beitz *et al.* (1982) used pulsed laser excitation at 1.16 eV to examine the fluorescence decay lifetime and quantum yield for the lowest excited states in the gas phase. They reported a lower limit of 3.5 ms for the lifetime and estimated that the quantum yield was near unity.

Mulford *et al.* (1991) subsequently investigated the low energy structured transitions of NpF_6 isolated in solid Ar. The band systems were characterized using both absorption and laser induced fluorescence techniques. The lowest energy transition was assigned to the $4\gamma_{7u} \rightarrow 13\gamma_{8u}$ electron promotion. In addition to the origin band, all fundamentals with the exception of ν_5 were active in the spectrum. The changes in vibrational frequencies that accompanied electronic excitation were small, as would be expected for an *f–f* transition. The fluorescence decay lifetime of the Γ_{8u} state was 4.6 ms. The second electronic band system, ascribed to the $4\gamma_{7u} \rightarrow 5\gamma_{7u}$ promotion, consisted of the origin band and the ν_4 and ν_6 fundamentals. All of these transitions were doubled by a matrix site effect that produced a splitting of approximately 20 cm^{-1}. Mulford *et al.* (1991) noted that it was surprising that only the higher energy transition was subject to a site splitting, but the cause for the selectivity effect could not be determined.

Survey absorption spectra for PuF_6 were reported by Steindler and Gunther (1964), and Walters and Briesmeister (1984). Several weak vibronic band systems were found in the 0.5–2.3 eV range, corresponding to a series of *f–f* transitions. Above 3.0 eV the absorption strength increases dramatically as the allowed charge transfer bands become accessible. These higher energy bands do not show structure, but have broad local maximum at 3.93, 4.96, 5.51, and 5.93 eV. As for NpF_6, most of the subsequent spectroscopic work has been focused on the structured *f–f* band systems.

In the near IR and visible spectral ranges, vibrational resolved spectra for gas-phase and matrix isolated PuF_6 are quite similar, but there are some intriguing differences in detail for the lowest energy band systems. Theoretical calculations show that transitions in the 0.5–0.7 eV range (often denoted as the 2.3 μm band) are associated with the $4\gamma_{7u}\rightarrow 13\gamma_{8u}$ electron promotion (Koelling *et al.* 1976; Boring and Hecht 1978). The $(4\gamma_{7u})^2$ configuration gives rise to a $(1)\Gamma_{1g}$ ground state while $(4\gamma_{7u})^1(13\gamma_{8u})^1$ yields states of $(1)\Gamma_{3g}$, $(1)\Gamma_{4g}$, and $(1)\Gamma_{5g}$ symmetry (the numbers in parentheses indicate the energy ordering for states of a given symmetry). The transition from Γ_{1g} to Γ_{4g} is magnetic dipole allowed, but transitions to the Γ_{3g} and Γ_{5g} states are both electric and magnetic dipole forbidden. Vibrationally excited levels of the latter can be observed due to vibronic mixing. In their analysis of the gas-phase spectrum, David and Kim (1988) concluded that $(1)\Gamma_{4g}$ is lowest in energy, separated from $(1)\Gamma_{3g}$ and $(1)\Gamma_{5g}$ by intervals of 0.03 and 0.15 eV, respectively. Transitions to $(1)\Gamma_{3g}$ and $(1)\Gamma_{5g}$ were enabled by the ν_3 and ν_6 modes. For PuF_6 isolated in solid Ar, Dewey *et al.* (1986) proposed an assignment scheme where $(1)\Gamma_{3g}$ lies below $(1)\Gamma_{4g}$, and the bands of the $(1)\Gamma_{5g} \leftarrow (1)\Gamma_{1g}$ transition are red-shifted relative to those of the gas phase by approximately 690 cm^{-1}. In light of the anomalous matrix shifts that have since been encountered for UO_2 and CUO (Zhou et al. 2000), these differences suggest that the $(1)\Gamma_{3g}$, $(1)\Gamma_{4g}$, and $(1)\Gamma_{5g}$ states are perturbed and possibly re-ordered by the Ar matrix host.

The second group, known as the 1.0 μm bands, is associated with the $4\gamma_{7u} \rightarrow 5\gamma_{7u}$ electron promotion. This excited configuration produces states of $(2)\Gamma_{4g}$ and $(2)\Gamma_{1g}$ symmetry, with the $(2)\Gamma_{4g}$ state lower in energy. The gas-phase (David and Kim 1988) and matrix (Dewey *et al.*, 1986) data for these transitions are in reasonably good agreement and confirm the theoretical predictions. The matrix bands show red-shifts of just 10–15 cm^{-1}. In the gas phase the $(2)\Gamma_{1g} \leftarrow (1)\Gamma_{1g}$ transition is enabled by the ν_4 vibrational mode.

The third group of bands (0.8 μm) has been assigned to as $(2)\Gamma_{5g} \leftarrow (1)\Gamma_{1g}$ and $(2)\Gamma_{3g} \leftarrow (1)\Gamma_{1g}$ transitions, both enabled by the ν_3 and ν_6 vibrational modes. Again there was good agreement between the gas-phase and matrix spectra for this spectral range. Based on the calculations of Boring and Hecht (1978), the upper states are assigned to the two-electron excited $(5\gamma_{7u})^2$ configuration. The 0.8 μm bands were found to be the only features that exhibited clearly discernable $^{239}Pu/^{242}Pu$ isotope shifts (0.3–1.2 cm^{-1}) in spectra recorded at a resolution of 0.05 cm^{-1} (Kugel *et al.*, 1976). Doppler limited, rotationally resolved spectra have been recorded for the $(2)\Gamma_{3g}+\nu_3 \leftarrow (1)\Gamma_{1g}$ band (Kim *et al.*, 1987). A partial assignment of these data was achieved and it appeared that the excited state structure was consistent with conservation of the octahedral equilibrium geometry.

Moving to still higher energies, the matrix spectra show well-resolved vibronic band systems at 2.0–2.3 eV (Dewey *et al.*, 1986). The first few bands in this range have been attributed to the $(3)\Gamma_{4g} \leftarrow (1)\Gamma_{1g}$ transition, and the remaining features are unassigned.

The fluorescence decay kinetics of electronically excited PuF_6 are complex, and have been the subject of several studies (Beitz *et al.*, 1982; Barefield *et al.*, 1983; Rice and Barefield, 1985a, b; Pack *et al.*, 1986). The radiative decay rates have been estimated from the absorption cross sections obtained for matrix isolated PuF_6. Lifetimes of 190, 6.4 and 4 ms were calculated for the upper states of the 2.3, 1.0, and 0.8 μm bands, respectively (Dewey *et al.*, 1986). The measured fluorescence decay lifetimes were much shorter, indicative of both spontaneous and collision induced electronic energy transfer. In the gas phase, the low-pressure lifetime for the 2.3 μm emission was 0.218 ms (Beitz *et al.*, 1982), corresponding to a fluorescence quantum yield of 10^{-3}. Excitation of PuF_6 in the 0.8 μm region results in short-lived emissions from bands at 1.0, and 1.9 μm, along with much slower emission from the 2.3 μm band. The kinetics of these processes have been examined in detail by Pack *et al.* (1986), who were able to show that electronic relaxation occurs by direct parallel processes rather than sequential cascade. In addition to work on the self-deactivation kinetics, there have been a few studies of fluorescence quenching induced by collisions with HF, H_2, D_2, rare gases and a range of other small molecules (Barefield *et al.*, 1985; Rice *et al.*, 1985, 1986). Quenching of the 2.3 μm fluorescence was found to be mediated by physical processes, rather than reactive removal.

UCl_6 is the only other actinide hexahalide for which gas-phase spectra have been published. The visible and UV absorption bands were investigated at a temperature of 380 K to achieve an adequate vapor pressure (Hurst and Wilson, 1971). The spectrum consists of a broad, weak feature in the 2.4–2.7 eV range. Above 2.9 eV a much stronger absorption begins, and this has not reach a maximum by 3.1 eV, where the reported spectrum ends. Apart from being shifted down in energy by about 0.75 eV, the spectrum of UCl_6 strongly resembles that of UF_6. Photoelectron spectra for the valence electrons of UCl_6 (Thornton *et al.*, 1979) also have a marked qualitative similarity to the results for UF_6. The ionization energy for the hexachloride is 11.28 eV and there are five bands in the 11–14 eV range. Thornton *et al.* (1979) used scattered wave $X\alpha$ calculations to guide their interpretation of the spectrum. As expected, the valence orbitals are primarily constructed from the Cl 3*p* orbitals. The HOMO was identified as γ_{8g} t_{1g}. This assignment has been supported by more recent density functional calculations, but, as is the case for UF_6, it poses a problem for the interpretation of the absorption spectrum. The weakness of the lowest energy ligand to metal transfer band is difficult to explain if the transition is not symmetry forbidden.

38.4.3 Vibrational and electronic spectra of actinide tetrahalides

The tetrahalides are model systems for studies of actinides in the +4 oxidation state. Experimental studies have focused on the MX_4 compounds with M = Th and U and X = F, Cl, and Br. One of the interesting differences between these compounds is that Th^{4+} is closed shell while U^{4+} has two electrons in the 5*f* orbital. Gas-phase electron diffraction measurements, IR spectra and theoretical calculations all support the conclusion that the ThX_4 compounds have tetrahedral equilibrium structures (Konings and Hildenbrand, 1998). For UX_4 the open shell ground state may be subject to a significant Jahn–Teller distortion, and there has been some disagreement concerning the equilibrium structures. The earlier studies seemed to support structures with symmetries lower than T_d. Evidence of distortion was derived from electron diffraction measurements, matrix IR spectra and calculations of standard entropies using estimated spectroscopic constants. For example, it was predicted that the entropies for UF_4 and UCl_4 were too low when calculated under the assumption of T_d geometry (which has a symmetry number of 12), but this discrepancy could be removed assuming a C_{2v} symmetry, which has a symmetry number of 2. Subsequent investigations have concluded that deviations from T_d symmetry for the UX_4 compounds are very slight or non-existent. Re-analyses of the electron diffraction data for both UF_4 and UCl_4 are consistent with the T_d geometry, details of the matrix IR spectra that indicated symmetry lowering have been shown to be site splitting effects and the entropy calculations have been corrected by the use of more accurate vibrational frequencies (Haaland *et al.*, 1995; Konings and Hildenbrand, 1998).

Systematic studies of the photoelectron spectra for the M = Th and U and X = F, Cl, and Br tetrahalides have been carried out by Dyke and co-workers (Dyke *et al.*, 1980, 1981; Boerrigter *et al.*, 1988; Beeching *et al.*, 2001). The results show that the spectra for all of these molecules are closely similar, and that the general features of these spectra can be understood in terms of a fairly simple molecular orbital model. Spectra for all six molecules are shown in Fig. 38.5, which is adapted from Beeching *et al.* (2001). The most obvious difference between the ThX_4 and UX_4 spectra is the occurrence of a low energy peak for the latter, which corresponds to the removal of a 5*f* electron. This peak appears at 10.32, 9.97, and 9.65 eV for F, Cl, and Br, respectively. The next group of features, which is common to both the ThX_4 and UX_4 spectra, is assigned to removal of electrons from orbitals that are primarily constructed from X n*p* (n = 2, 3, and 4 for F, Cl and Br). These atomic orbitals combined to produce molecular orbitals that transform as a_1 and t_2 (radial orbitals) and e, t_1 and t_2 (tangential orbitals) in the T_d point group. These are partially mixed with the metal 6*p* and 5*f* orbitals, which transform as t_2 and $a_1 + t_1 + t_2$. Taking this

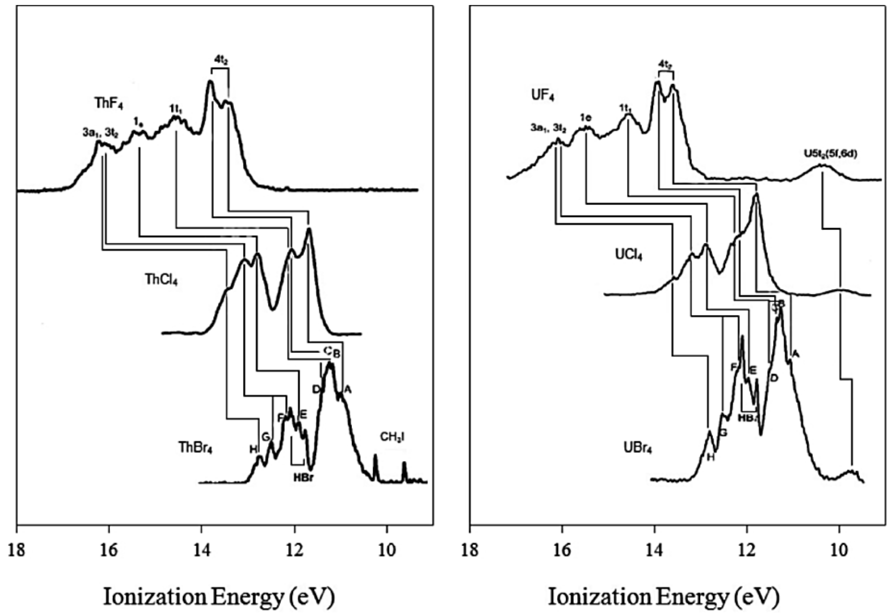

Fig. 38.5 *Photoelectron spectra for AnX_4 species (reused with permission from L. J. Beeching, Journal of Chemical Physics, 114, 9832 (2001). Copyright 2001, American Institute of Physics).*

mixing into account, Beeching *et al.* (2001) predicted that these X n*p* valence orbitals have the energy ordering $3a_1 < 3t_2 < 1e < 1t_1 < 4t_2$. As indicated in Fig. 38.5, the first five features of ThX_4 and those above the 5*f* peak for UX_4 have been assigned accordingly.

All of the theoretical studies carried out in recent years have yielded T_d equilibrium structures for the MX_4 species (Dyke *et al.*, 1980; Boerrigter *et al.*, 1988; Pierloot *et al.*, 1991; Gagliardi *et al.*, 2000; Beeching *et al.*, 2001; Peralta *et al.*, 2005). Studies aimed at interpretation of the photoelecton spectra have noted two important details that must be taken into account in order to achieve satisfactory agreement with the experimental data. First, although the metal 6*p* orbital is quite deeply bound, it mixes with the valence orbitals and must be included in the active space (mixing with 5*d* is also significant, but to a lesser degree). Secondly, spin–orbit coupling is important in determining the orbitals. One manifestation of the role of spin–orbit coupling is the evolution of structure in the X_4 valance bands seen in going from MF_4, which shows five resolvable peaks, to MBr_4 where eight peaks are observed. This is ascribed to the increasing magnitude of the spin–orbit coupling constant with increasing atomic number of the halogen (Beeching *et al.*, 2001). The spin–orbit interaction for the 5*f* electrons yields $u_{3/2}$ and $e_{1/2}$ spinors from $5t_1$ and $5t_2$. For t_1, $u_{3/2}$ is lower in energy, while the reverse is true for t_2. Based on this ordering, and the fact that UX_4 species have open-shell ground states, Boerrigter *et al.* (1988) assign the 5*f* HOMO as $5t_1\ u_{3/2}$.

Additional spectroscopic data for the ThX_4 species are rather limited in scope. IR absorption spectra have been observed for matrix isolated ThF_4 (Bukhmarina *et al.* 1992), $ThCl_4$ (Beattie *et al.* 1988), and $ThBr_4$ (Beeching *et al.*, 2001). Gas-phase data have been obtained for the fluoride and chloride (Buchler *et al.*, 1961; Konings, 1996). In T_d symmetry MX_4 molecules have vibrations of $a_1(\nu_1)$, $e(\nu_2)$, and two modes of t_2 symmetry. The t_2 modes are IR active and correspond to stretch (ν_3) and bending (ν_4) modes. Lowering the symmetry breaks the degeneracies and results in the presence of more IR active modes. Spectra for ThF_4 isolated in rare gas solids (Bukhmarina *et al.*, 1992) and in the gas phase obeyed the selection rules expected for T_d symmetry. Gas-phase vibrational frequencies of ν_3=520 (Buchler *et al.*, 1961) and ν_4 = 116 cm^{-1} (Konings, 1996) were reported.

Data for the ν_3 fundamental $ThCl_4$ isolated in solid Ne are also consistent with a tetrahedral geometry, but Beattie *et al.* (1988) found that the symmetry was lowered when Ar, or Kr was used as the matrix host. The symmetry information was derived by using $^{35}Cl/^{37}Cl$ isotope substitution to create distinguishable isotopomers. For $ThCl_4$ in Kr, Beattie *et al.* (1988) speculate that two Kr atoms may coordinate to the metal, producing a highly distorted octahedral-like structure. The gas-phase frequency for the ν_3 fundamental is 335 cm^{-1} (Buchler *et al.*, 1961), while ν_4 has not yet been characterized. The only IR data available for $ThBr_4$ is a measurement of the ν_3 fundamental (229.8 cm^{-1}) in an Ar matrix by Beeching *et al.* (2001).

Gas-phase IR spectra and electron diffraction data for UF_4 were recorded and analyzed by Konings *et al.* (1996). Rotational band contours were obtained for both the ν_3 (539 cm^{-1}) and ν_4 (114 cm^{-1}) modes, with the former showing a clear P/Q/R type envelope. The electron diffraction data, which had previously been used as evidence for a distorted equilibrium structure, were shown to be consistent with a T_d structure. Matrix spectra for UF_4 show complex splitting patterns that were interpreted by Bukhmarina *et al.* (1987, 1990) as evidence for a significant Jahn–Teller effect, while Kunze *et al.* (1977) ascribed the same splittings to matrix site effects. The gas-phase data clearly favor the latter interpretation.

UCl_4 is the most extensively studied molecule in this series. Gas-phase IR spectra yielded bands at 338 cm^{-1} (ν_3) and 72 cm^{-1} (ν_4). No other IR active modes were detected. Haaland *et al.* (1995), who obtained these results, also extended the electron diffraction characterization and were the first to show that the latter indicates a T_d equilibrium geometry for UCl_4. This work inspired the reanalysis of the UF_4 diffraction data mentioned above. The electronic transitions of UCl_4 were observed throughout the near IR and visible spectral ranges (Morrey *et al.*, 1967). Well-resolved spectra for UCl_4 isolated in solid nitrogen at 4 K were obtained by Clifton *et al.* (1969). More than 30 sharp bands were observed in the 0.5–3.1 eV (4,000–25,000 cm^{-1}) range, and these were all attributed to transitions between the states arising from the $5f^2$ metal ion configuration. A LFT model was constructed for these states and the interaction parameters were refined by fitting to the observed energy levels. Surprisingly, this assignment scheme did not identify any vibronically excited levels. Spectra for the 3.7–5.7 eV were considerably less structured. These bands were tentatively assigned to metal $f \rightarrow d$ and ligand to metal charge transfer transitions. Following this study, Gruber and Hecht (1973) obtained gas-phase spectra for UCl_4 at the level of vibronic resolution. They identified the first electronic state just 710 cm^{-1} above the ground state, and all bands below 3.1 eV were again ascribed to *f–f* bands. Gruber and Hecht (1973) also used a LFT model to interpret their data. Some discrepancies between their model and that of Clifton *et al.* (1969) were noted, but the overall level of agreement was acceptable.

Apart from the photoelectron data, spectroscopic data for UBr_4 consist of a gas-phase measurement of the ν_3 fundamental (233 cm^{-1}) (Ezhov *et al.*, 1989), an Ar matrix observation of the same band (239.4 cm^{-1}) (Beeching *et al.*, 2001), and a nitrogen matrix isolation study of the electronic absorption bands in the 0.5–6.2 eV range. Clifton *et al.* (1969) found that the spectra for UBr_4 and UCl_4 were quite similar in both the visible and near UV spectral ranges. As for UCl_4, bands in the 0.5–3.1 eV range were assigned as *f-f* transitions and analyzed using a LFT model for the $5f^2$ configuration. The LFT parameters obtained were reasonably close to the values predicted from a simple point charge model. The success of this approach confirms that the 5*f* orbitals retain much of their atomic character in UCl_4 and UBr_4.

38.5 MATRIX STABILIZED REACTION PRODUCTS

Matrix reactions of actinide atoms and molecules that were studied through 2005, many of which were discussed recently in Chapter 17 (Kaltsoyannis *et al.*, 2006), are summarized in Table 38.6. The observation of bonding interactions between actinide complexes and noble gas matrix atoms (Ng = Ne, Ar, Kr, and/or Xe), are not included in Table 38.6 as they are not necessarily considered to represent conventional “reactions”. Major developments in matrix reactions reported since the review of Chapter 17 (Kaltsoyannis *et al.*, 2006) are described below. The new compounds observed can be broadly classified as hydroxides, hydrides, organometallics, and species with actinide–nitrogen or actinide–phosphorus bonds. The experimental techniques are as described in Section 38.2. Unless noted otherwise, the products from the reactions discussed below were trapped in solid argon matrices.

38.5.1 Thorium and uranium hydroxides

In view of the importance of thorium hydroxide species in aqueous chemistry, and the nonexistence of solid crystalline $Th(OH)_4$, the synthesis and characterization of the $Th(OH)_4$ molecule by Wang and Andrews (2005) is a particularly

Table 38.6 Summary of actinide reactions in cryogenic matrices[a]

Initial reactants	Reactions and products	References
U, O_2	$U + O_2 \rightarrow UO + O$ $U + O_2 \rightarrow UO_2$ $UO_2 + O_2 \rightarrow UO_3 + O$ $UO_3 + O_2 \rightarrow UO_3–O_2$ $UO_2 + O_2 \rightarrow (UO_2^{+})(O_2^{-})$ $U + 2O_2 \rightarrow (UO_2^{2+})(O_2^{2-})$ $(UO_2^{2+})(O_2^{2-}) \rightarrow UO_3 + O$	Hunt and Andrews, 1993; Hunt et al., 1994a
U, O_2	$U^* + O_2 \rightarrow [OUO]^* \rightarrow UO + O$ $U + O_2 \rightarrow UO_2$ $UO + O_2 \rightarrow UO_3$ $UO_2 + O_2 \rightarrow (O_2)UO_2$ $U^+ + O_2 \rightarrow UO_2^+$ $UO_2 + e^- \rightarrow UO_2^-$	Zhou et al., 2000
U, N_2	$U + N_2 \rightarrow UN + N$ $UN + xN_2 \rightarrow (N_2)_xUN$ $U + N_2 \rightarrow NUN$ $NUN + xN_2 \rightarrow (N_2)_x(NUN)$ $UN_2 + N_2 \rightarrow UN_2–N_2$ $UN_2 + 2N_2 \rightarrow UN_2–(N_2)_2$ $UO_2 + N_2 \rightarrow (UO_2^{+})(N_2^{-})$ $U + N_2 \rightarrow UN + N$ $UN_2 + U \rightarrow U(\mu - N)_2U$ $UN + UN_2 \rightarrow NU(\mu - N)_2U$ $NU(\mu - N)_2U + xN_2 \rightarrow (N_2)_x(NU(\mu - N)_2U)$ $U + N_2 \rightarrow U - \eta^2 - N_2$ $U- \eta^2 - N_2 + xN_2 \rightarrow (N_2)_x (U - \eta^2 - N_2)$	Hunt et al., 1993, 1994a; Kushto et al., 1998
Th, N_2	$Th + N_2 \rightarrow ThN + N$ $ThN + xN_2 \rightarrow (N_2)_xThN$ $Th + N_2 \rightarrow NThN$ $NThN + xN_2 \rightarrow (N_2)_x(NThN)$ $ThN_2 + Th \rightarrow Th(\mu - N)_2Th$ $Th + N_2 \rightarrow Th–N–N$ $ThN_2 + N_2 \rightarrow N–N–Th–N–N$ $Th + N_2 \rightarrow Th–\eta^2–N_2$	Kushto et al., 1998
U, H_2	$U + H_2 \rightarrow UH + H$ $U + H_2 \rightarrow UH_2$ $UH + H_2 \rightarrow UH_3$ $UH_2 + H_2 \rightarrow UH_4$ $2(UH) \rightarrow U_2H_2$ $2(UH_2) \rightarrow U_2H_4$	Souter et al., 1996, 1997a
Th, H_2	$Th + H_2 \rightarrow ThH + H$ $Th + H_2 \rightarrow ThH_2$ $ThH + H_2 \rightarrow ThH_3$ $ThH_2 + H_2 \rightarrow ThH_4$	Souter et al., 1997b
U, H_2O	$U + H_2O \rightarrow UO + H_2$ $U + H_2O \rightarrow H_2UO$ $UO + H_2O \rightarrow UO_2 + H_2$ $UO + H_2O \rightarrow HUO(OH) + H_2UO_2$ $H_2UO_2 + H_2O \rightarrow H_2UO(OH)_2$	Liang et al., 2005

Table 38.6 (*Contd.*)

Initial reactants	Reactions and products	References
Th, H_2O	$Th + H_2O \rightarrow ThO + H_2$	Liang et al., 2002
	$Th + H_2O \rightarrow HThOH$	
	$Th + H_2O \rightarrow H_2ThO$	
	$Th + H_2O \rightarrow HThO + H$	
	$ThO + H_2O \rightarrow ThO_2 + H_2$	
	$ThO + H_2O \rightarrow HThO(OH)$	
	$ThO_2 + H_2O \rightarrow OTh(OH)_2$	
	$HTHO(OH) + H_2O \rightarrow HTh(OH)_3$	
U, NO_2	$U + NO_2 \rightarrow UN + O_2$	Green and Reedy, 1976
	$UN + NO_2 \rightarrow UN_2 + O_2$	
U, NO, NO_2, N_2O	$U + NO \rightarrow NUO$	Kushto et al., 1997; Zhou and Andrews 1999
	$U + NO \rightarrow UNO$	
	$U^+ + NO \rightarrow NUO^+$	
	$NUO + NO \rightarrow (NUO^+)(NO^-)$	
	$U + N_2O \rightarrow NUN + O$	
	$NUO + NO \rightarrow NUO_2 + N$	
	$2(NUO) \rightarrow (NUO)_2$	
	$U + N_2O \rightarrow UO + N_2$	
	$UO + N_2O \rightarrow UO_2 + N_2$	
	$UO_2 + N_2O \rightarrow UO_3 + N_2$	
Th, NO	$Th + NO \rightarrow NThO$	Kushto and Andrews, 1999; Zhou and Andrews, 1999
	$NThO + NO \rightarrow (N_2)ThO_2$	
	$Th + NO \rightarrow ThO + N$	
	$ThO + NO \rightarrow ThO_2 + N$	
	$Th + (NO)_2 \rightarrow OTh\text{–}N,N\text{–}\eta^2\text{–}N_2O$	
UO, UO_2, NO, NO_2	$UO_2 + NO_2 \rightarrow (UO_2{}^+)(NO_2{}^-)$	Green et al., 1976
	$UO + NO_2 \rightarrow (UO_2{}^+)(NO^-)$	
	$UO + NO_2 \rightarrow UO_2 + NO$	
	$UO_2 + NO \rightarrow (UO_2{}^+)(NO^-)$	
U, CO	$U + CO \rightarrow UCO$	Tague et al., 1993; Zhou et al., 1999b
	$UCO + (x\text{-}1)CO \rightarrow U(CO)_x$ $(x = 2\text{–}6)$	
	$U^* + CO \rightarrow CUO$	
	$CUO + CO \rightarrow OUCCO$	
	$U(CO)_2 \rightarrow OUCCO$	
	$U(CO)_x \rightarrow (CO)_{x\text{-}2}OUCCO$	
	$OUCCO \rightarrow (\eta^2\text{-}C_2)UO_2$	
	$CUO + e^- \rightarrow CUO^-$	
	$U(CO)_x + e^- \rightarrow U(CO)_x{}^-$ $(x = 1\text{–}5)$	
Th, CO	$Th + CO \rightarrow ThCO$	Zhou et al., 1999a; Li et al., 2001
	$ThCO + (x\text{-}1)CO \rightarrow Th(CO)_x$ $(x = 2\text{–}6)$	
	$Th^* + CO \rightarrow CThO$	
	$ThCO^* \rightarrow CThO$	
	$CThO + CO \rightarrow OThCCO$	
	$Th(CO)_2 \rightarrow OThCCO$	
	$OThCCO \rightarrow OTh(\eta^3\text{–}CCO)$	
	$CThO + e^- \rightarrow CThO^-$	
	$Th(CO)_2 + e^- \rightarrow Th(CO)_2{}^-$	

Table 38.6 (*Contd.*)

Initial reactants	Reactions and products	References
U, CO_2	$U + CO_2 \rightarrow OUCO$ $OUCO + CO_2 \rightarrow O_2U(CO)_2$ $OUCO + CO_2 \rightarrow O_2UCO + CO$ $O_2U(CO)_2 + e^- \rightarrow O_2U(CO)_2^-$ $O_2U(CO)_2^- \rightarrow O_2U(CO)_2 + e^-$ $U^+ + CO_2 \rightarrow OUCO^+$	Tague et al., 1993; Andrews et al., 2000
Th, CO_2	$Th + CO_2 \rightarrow OThCO$ $OThCO + CO_2 \rightarrow O_2Th(CO)_2$ $O_2Th(CO)_2 + e^- \rightarrow O_2Th(CO)_2^-$ $Th^+ + CO_2 \rightarrow OThCO^+$	Andrews et al., 2000
UF_6	$UF_6 \rightarrow UF_5 + F$	Paine et al., 1976
UF_6	$UF_6 \rightarrow UF_5 + F$ $UF_5 + F \rightarrow UF_6$	Jones and Ekberg, 1977
UF_4, F_2	$UF_4 + F_2 \rightarrow UF_5 + F$ $UF_5 + F_2 \rightarrow UF_6 + F$	Kunze et al., 1976; 1977
U, F_2	$U + F_2 \rightarrow UF + F$ $UF + F \rightarrow UF_2$ $UF_2 + F \rightarrow UF_3$ $UF_3 + F \rightarrow UF_4$ $UF_4 + F \rightarrow UF_5$ $UF_5 + F \rightarrow UF_6$	Hunt et al., 1994b
U, Cl_2	$U + Cl_2 \rightarrow UCl_2$ $UCl_2 + Cl_2 \rightarrow UCl_4$	Hunt et al., 1994b
U, O_2, F_2 [b]	$? \rightarrow UO_2F_2$ $? \rightarrow UO_2F$ $? \rightarrow UOF_4$	Souter and Andrews, 1997
UF_6, H_2O	$UF_6 + H_2O \rightarrow UF_6—OH_2$ $UF_6 + H_2O \rightarrow UOF_4 + 2HF$ $UOF_4 + H_2O \rightarrow UO_2F_2 + 2HF$	Sherrow and Hunt, 1992
UF_x, M, MF M = alkali metal	$M + UF_4 \rightarrow MUF_4$ $M + UF_6 \rightarrow MUF_6$ $MF + UF_4 \rightarrow MUF_5$ $2MF + UF_4 \rightarrow M_2UF_6$ $MF + UF_6 \rightarrow MUF_7$	Kunze et al., 1978

[a] Recently reported reactions are not included here, but rather discussed in the text. The identified reactions proceed under varying conditions of excitation or photolysis, and are not necessarily intrinsically energetically or kinetically favorable.

[b] The mechanisms for these reactions are indeterminate.

significant accomplishment; $Th(OH)_2$ was also identified there as a minor species. The relevant reactions are as follows:

$$Th + H_2O_2 \rightarrow Th(OH)_2 \tag{38.1}$$

$$Th(OH)_2 + H_2O_2 \rightarrow Th(OH)_4 \tag{38.2}$$

Both of these reactions are highly exothermic. The $Th(OH)_2$ molecule is somewhat distorted from linear and $Th(OH)_4$ is nearly tetrahedral. The evident instability of crystalline $Th(OH)_4$ is attributed to the extraordinary stability of $ThO_2(s)$.

By reacting U atoms with H_2O_2, Wang *et al.* (2006) synthesized and characterized three uranium hydroxide molecules: $U(OH)_2$, $UO_2(OH)$, and $UO_2(OH)_2$. The assigned reaction mechanisms are as follows:

$$U + H_2O_2 \rightarrow U(OH)_2 \tag{38.3}$$

$$U(OH)_2 + H_2O_2 \rightarrow \left[U(OH)_4\right]^* \rightarrow UO_2(OH)_2 + H_2 \tag{38.4a}$$

$$\rightarrow UO_2(OH) + OH + H_2 \tag{38.4b}$$

The decomposition of excited state transient uranium tetrahydroxide (equations 38.4a and 38.4b) contrasts with the stability of $Th(OH)_4$ and is attributed to the accessibility of the higher U(V) and U(VI) oxidation states. The calculated structures are linear C_{2v} for $U(OH)_2$; C_2 for $UO_2(OH)_2$, in which the uranyl moiety is nearly linear and the HO–U–OH bond angle is 108.4°; and C_s for $UO_2(OH)$, an approximately T-shaped uranyl derivative. It was also found that (divalent) $U(OH)_2$ rearranges to the hexavalent uranyl dihydride, H_2UO_2, which was previously found in the reaction of U with H_2O (Liang *et al.*, 2005).

38.5.2 Uranium and thorium polyhydrides

The several uranium hydrides previously produced in matrices by the reactions of uranium atoms with H_2 ((Souter *et al.*, 1996, 1997a) – Table 38.6) were recently reproduced by Raab *et al.* (2007). Among the most important of these hydrides first identified in the earlier work are U_2H_2 and U_2H_4 in solid neon, which were considered to represent the first examples of an actinide–actinide bond. A striking new result of the recent study was evidence in solid hydrogen matrices for new uranium polyhydrides, $UH_4(H_2)_x$ with $x \leq 6$. The report of the large $UH_4(H_2)_6$ complex is particularly significant due to the extraordinary number of hydrogen atoms bound to the uranium metal center. The calculated binding energy of each of the six H_2 molecules to UH_4 is $\sim$10 kJ/mol.

The ThH_2 and ThH_4 molecules previously reported by Souter *et al.* (1997b) (Table 38.6) were again produced by reactions of Th atoms with H_2 in solid neon, and characterized in greater detail, both spectroscopically and theoretically (Wang *et al.*, 2008a). In addition to the ThH_x molecules, in this recent work H_2 adducts with ThH_4 in solid hydrogen were also identified, $ThH_4(H_2)_{1,2,3,4}$. Whereas UH_4 coordinates up to six H_2 molecules, the largest polyhydride of ThH_4 has four H_2 molecules, each with a calculated binding energy of $\sim$16 kJ/mol, which is significantly greater than that for each of the six H_2 molecules in $UH_4(H_2)_6$. Bonding analysis revealed somewhat different bonding in the uranium and thorium tetrahydride ployhydrides, with ThH_4 being highly polarized. In view of the previous report of HUUH, in which there is U–U bonding (Souter *et al.*, 1996; 1997a), the HThThH dimer was sought by Wang *et al.* (2008a), but to no avail.

38.5.3 Thorium and uranium organometallic complexes

The several recent matrix isolation studies of Th and U organometallics are significant extensions of these types of studies to the actinides, and have resulted in important advances in fundamental organoactinide chemistry. Many matrix organometallic studies of *d*-block transition metal atoms have been reported and these new actinide results shed important light on the similarities and, more so, the differences between the *d*- and *f*-elements. Such comparisons are presented in most of the referenced studies, and often point to a (surprisingly) significant role for the 5*f* orbitals, even in the case of Th, which is often considered as a group 4 *d*-block element but quite clearly is not such.

Thorium and uranium methylidene complexes have been prepared and characterized. The elementary $H_2C{=}ThH_2$ and $H_2C{=}UH_2$ methylidene metal dihydrides were prepared by Andrews and Cho (2005) and Lyon *et al.* (2007a), respectively. These complexes were synthesized by reacting the metal atoms with methane to form the $H_3C{-}MH$ insertion product, which then rearranges by α–H transfer to give the $H_2C{=}MH_2$ product, equation 38.5 (M = Th, U); for M = U, the $H_3C{-}UH$ intermediate insertion product was also identified.

$$M + CH_4 \rightarrow H_3C - MH \rightarrow H_2C = MH_2 \tag{38.5}$$

U is less efficient than Th at such methane activation. An intriguing aspect of these species is the agostic interaction between one of the CH_2 hydrogen atoms and the actinide metal center, as indicated by structural distortions and particularly the reduced so-called agostic $H'{-}C{-}M$ angle which results from the $H'{-}M$ agostic bonding interaction. In the case of $H_2Th{=}CH_2$, this angle is similar to that in $H_2Hf{=}CH_2$; for $H_2U{=}CH_2$ the $H'{-}C{-}U$ angle is significantly smaller. Lyon *et al.* (2007a) calculated the structures for both $H_2C{=}ThH_2$ and $H_2C{=}UH_2$ using different levels of theory and consistently found a significantly greater agostic interaction in the uranium methylidene. Based on bonding analysis, these authors attributed the greater agostic interaction to a more favorable interaction with the U(5*f*) versus Th(6*d*) orbitals. Roos *et al.* (2007) theoretically analyzed the agostic interaction in several $H_2M{=}CH_2$ complexes (M = Y, Zr, Nb, Mo, Ru, Th, U) and similarly concluded that the particularly strong interaction in the case of M = U is due to the distinctive character of the singly occupied 5*f* orbitals. Andrews and Cho (2006) have reviewed the methylidene results, and compared the actinide and *d*-block transition metal methylidenes.

Lyon and Andrews (2005, 2006) synthesized the methylidene metal hydride halides, $H_2C{=}ThHX$ and $H_2C{=}UHX$ (X = F, Cl, Br). These were formed by insertion of the metal into the C–X bond, followed by α-H transfer to the metal center as in equation 38.6 (M = Th, U; X = F, Cl, Br).

$$M + CH_3X \rightarrow H_3C - MX \rightarrow H_2C = MHX \tag{38.6}$$

The $H_3C{-}UF$ intermediate was also observed; the presumed $H_3C{-}UCl$ and $H_3C{-}UBr$ intermediates would not be seen in these studies as the U–Cl and

U–Br stretching modes should be below the low-energy cutoff of the spectrometer. As with the corresponding $H_2C{=}MH_2$ complexes (M = Th, U), these monohalogenated methylidene complexes exhibit significant agostic interactions.

Lyon *et al.* (2008) employed the reaction scheme analogous to that in equation 38.6 (M = U), but using as the reactant molecules methylene dihalides, CH_2F_2, CH_2FCl and CH_2Cl_2. The expected three new uranium methylidene complexes were synthesized, $H_2C{=}UF_2$, $H_2C{=}UFCl$ and $H_2C{=}UCl_2$. For all three complexes the agostic distortion was substantial; structural comparisons were made with non-agostic $H_2C{=}WF_2$ and other $H_2C{=}MX_2$. The bonding analysis reveals the particular importance of the 5*f* orbitals in the chemistry of uranium complexes. Using CH_2FCl as the reagent molecule, Li *et al.* (2007) prepared the methylidenes $H_2C{=}ThFCl$ and $H_2C{=}UFCl$. A significant agostic interaction was identified for both complexes, with the effect again somewhat greater for the uranium complex. A particularly intriguing and potentially significant result is that the C_1 symmetry of these $H_2C{=}MFCl$ molecules renders them chiral, with the two optical isomers at equal energy.

Reactions of Th atoms with several di-, tri-, and tetra-fluoro, -chloro, and -flurorochloro methanes were studied by Lyon and Andrews (2008), with the results summarized in equations 38.7 through 38.16.

$$\mathrm{Th + CH_2F_2 \rightarrow H_2C = ThF_2} \tag{38.7}$$

$$\mathrm{Th + CH_2Cl_2 \rightarrow H_2C = ThCl_2} \tag{38.8}$$

$$\mathrm{Th + CH_2FCl \rightarrow H_2C = ThFCl} \tag{38.9}$$

$$\mathrm{Th + CHF_3 \rightarrow HC \equiv ThF_3} \tag{38.10}$$

$$\mathrm{Th + CHCl_3 \rightarrow HC \equiv ThCl_3} \tag{38.11}$$

$$\mathrm{Th + CHF_2Cl \rightarrow HC \equiv ThF_2Cl} \tag{38.12}$$

$$\mathrm{Th + CHFCl_2 \rightarrow HC \equiv ThFCl_2} \tag{38.13}$$

$$\mathrm{Th + CF_4 \rightarrow FC \equiv ThF_3} \tag{38.14}$$

$$\mathrm{Th + CF_3Cl \rightarrow ClC \equiv ThF_3 + FC \equiv ThF_2Cl} \tag{38.15}$$

$$\mathrm{Th + CF_2Cl_2 \rightarrow ClC \equiv ThF_2Cl + FC \equiv ThFCl_2} \tag{38.16}$$

With the dihalomethane reagents, the most stable products are the singlet methylidenes (equations 38.7 through 38.9). With tri- and tetrahalomethane reactants (equations 38.10 through 38.16), the very strong bonding between thorium and the halogen atoms renders the observed triplet methylidynes, designated as $HC{\equiv}ThX_3$ or $XC{\equiv}ThX_3$ (X = F or Cl), more stable. For reactions 38.15 and 38.16, the first of the indicated two observed products, which corresponds to the maximum the number of Th–F bonds, is the more stable and is accordingly dominant. The bonding analysis for the methylidynes indicates electron transfer from the carbon atom to the metal center, which augments the weak π bonding in these electron deficient species. This electron transfer is enhanced by replacing F with Cl on the metal and/or carbon atoms(s). There is evidently significant participation of the Th 5*f* orbitals in the π-bonding orbitals.

The reactions of Th and U atoms with ethylene were studied in argon matrices (Andrews *et al.* 2006). The thorium reaction is given by

$$\mathrm{Th}\left({}^{3}\mathrm{F}\right) + \mathrm{C_2H_2} \rightarrow \mathrm{Th(C_2H_2)}\,{}^{3}\mathrm{A_2} \qquad (38.17)$$

The conclusion that the Th–η^2–(C_2H_2) thorium cyclopropene product is a triplet contrasts with the theoretical prediction that the ground state of the gas-phase species is almost certainly singlet, and the discrepancy is attributed to stabilization of the triplet state by the argon matrix. Additional thorium molecules thought to have been formed include Th–η^2–$(C_2H_2)_2$ (C_{2v}, $^1A_1$), Th–η^2–$(C_2H_2)^+$, and Th–C≡CH, thorium ethynyl. Uranium cyclopropene, U–η^2–(C_2H_2) $^5A_1$, was produced in the association reaction analogous to 38.17. Also reported were the corresponding U–η^2–$(C_2H_2)_2$, U–η^2–$(C_2H_2)^+$, and U–C≡CH, uranium ethynyl. In the case of uranium, the insertion product, HUCCH, was also reported. In a comparison with other M–η^2–(C_2H_2), Andrews *et al.* (2006) concluded that the interaction between U and acetylene is the strongest of those so far studied, and that this interaction is almost as strong in the Th–acetylene complex. For these species, the greater bonding interaction for U and Th, as compared with Pd and Pt, for example, is not attributed to significant participation of their 5*f* orbitals but rather to the suitability of their 6*d* orbitals for this bonding.

The reactions of excited state Th* and U* atoms with ethane Cho *et al.* (2008) produced new organometallic complexes according to equations 38.18 through 38.20.

$$\begin{aligned}\mathrm{Th^*} + \mathrm{C_2H_6} \rightarrow \mathrm{CH_3CH_2 - ThH}\ (\mathbf{i}) &\rightarrow \mathrm{CH_3(H)C = ThH_2}\ (\mathbf{e}) \\ &\rightarrow \mathrm{CH_2 = CH - ThH_3}\ (\mathbf{t})\end{aligned} \qquad (38.18)$$

$$\mathrm{Th^*} + \mathrm{C_2H_6} \rightarrow \mathrm{CH_3CH_2 - ThH}\ (\mathbf{i}) \rightarrow \mathrm{(CH_2)_2 - ThH_2}\ (\mathbf{d}) \qquad (38.19)$$

$$\mathrm{U^*} + \mathrm{C_2H_6} \rightarrow \mathrm{CH_3CH_2 - UH}\ (\mathbf{i}) \rightarrow \mathrm{CH_3(H)C = UH_2}\ (\mathbf{e}) \qquad (38.20)$$

Th was more reactive with ethane than U, as was the case for methane. For U, only the ethylidene dihydride (**e**) was produced, whereas for Th the vinyl methyl trihydride (**t**) and metallocyclopropane dihydride (**d**) were produced. From the intermediate insertion complex (**i**), only α–H transfer occurs for U, while β-H transfer additionally occurs for Th; this is consistent with the calculated energetics. The agostic interactions in the actinide ethylidene dihydrides were greater than previously found for the corresponding methylidene dihdrides, and the distortion was again greater for U than Th.

Lyon *et al.* (2007b) took advantage of the high affinity of uranium for halogen atoms to prepare uranium methylidynes which comprise the elusive U≡C triple bond, which had previously been reported by Zhou *et al.* (1999b) in the CUO molecule The five observed reactions, which proceed by halogen transfer from carbon to uranium, are summarized by equations 38.21 through 38.23.

$$U + CHX_3 \rightarrow [XU - CHX_2]^* \rightarrow [X_2U = CHX]^* \rightarrow X_3U \equiv CH \quad (38.21)$$

$$U + CF_4 \rightarrow [FU - CF_3]^* \rightarrow [F_2U = CF_2]^* \rightarrow F_3U \equiv CF \quad (38.22)$$

$$U + CHClF_2 \rightarrow [FU - CHClF]^* \rightarrow [F_2U = CHCl]^* \rightarrow ClF_2U \equiv CH \quad (38.23)$$

The three $X_3U{\equiv}CH$ (X = F, Cl, Br) and $F_3U{\equiv}CF$ are all stable hexavalent uranium singlet species with C_{3v} symmetry. DFT calculations confirmed that the U–C bond lengths and orders accord with a triple bond. The bonding analysis indicates that the U≡C triple bond is comprised of one σ-bond between U *dfσ* and C *spσ* hybrid orbitals, and two π-bonds between U *dfπ* and C *pπ* orbitals; the uranium 5*f* orbitals are clearly substantially involved in the bonding.

The two actinide benzene complexes, $U(C_6H_6)$ and $Th(C_6H_6)$, were prepared by the reactions of U and Th atoms with benzene (Infante *et al.* 2007b). The bonding in these species was examined in detail by theory. The calculated U-benzene binding energy is 167 kJ/mol, with transfer of 0.17 electrons from U to C_6H_6; the bonding energy in Th-benzene is larger and the charge transfer is smaller, this latter effect attributed to the reduced availability of valence electrons for back-donation to the benzene ring. It was predicted by theory that $U(C_6H_6)$, $(C_6H_6)U(C_6H_6)$, $(C_6H_6)U_2(C_6H_6)$, $Th(C_6H_6)$, $(C_6H_6)Th(C_6H_6)$, and $(C_6H_6)Th_2(C_6H_6)$ should also all be formed exothermically by the reactions of the metal atoms with benzene. The observation of only the elementary $M(C_6H_6)$ (M = Th, U) complexes was attributed to limitations in reagent concentrations which precludes aggregation to form the larger complexes.

38.5.4 Species with actinide–nitrogen or actinide–phosphorus bonds

The strong inductive effect of the fluorine employed to stabilize the first uranium methylidyne complex, $FC{\equiv}UF_3$ (see Section 38.5.3) was employed by Andrews *et al.* (2008) to produce the $N{\equiv}UF_3$ and $P{\equiv}UF_3$ molecules, these being examples of N≡U and P≡U triple bonds not accessible in condensed phase complexes. The reaction mechanisms by which these new species were produced are given by equations 38.24 and 38.25.

$$U + NF_3 \rightarrow F_2N - UF \rightarrow FN = UF_2 \rightarrow N \equiv UF_3 \quad (38.24)$$

$$U + PF_3 \rightarrow F_2P - UF \rightarrow FP = UF_2 \rightarrow P \equiv UF_3 \quad (38.25)$$

These reactions are enabled by the formation of extremely strong U–F bonds at the expense of the weaker N–F and P–F bonds. The calculated bond orders are 2.78 for N≡U and 2.4 for P≡U, which are consistent with the respective calculated bond lengths, 1.76 and 2.40 , and energies, 460 and 176 kJ/mol. The enhanced ability of N to form a much stronger triple bond than P with U is attributed partly to the greater ability of the smaller nitrogen atom to bond with the 5*f* orbitals of uranium.

Wang *et al.* (2007) reported that Th atoms readily activate ammonia according to the highly exothermic reaction pathway

$$\mathrm{Th} + \mathrm{NH_3} \rightarrow \mathrm{Th{:}NH_3} \rightarrow \mathrm{H_2N - ThH} \rightarrow \mathrm{HN = ThH_2} \qquad (38.26)$$

The N=Th bond in the thorimine product is very short and strong, exhibiting some triple bond character. The calculated electron configuration for Th is $[\mathrm{core}]7s^{0.42}5f^{\,0.28}6d^{\,0.73}7p^{0.02}$. When the 5*f* orbitals were removed from the Th basis set, the Th=N bond was elongated by 0.110 Å and weakened by 181 kJ/mol. It is thus apparent that the 5*f* orbitals of Th substantially participate in the strong Th=N bond.

The reaction of U with NH_3 was also studied by Wang *et al.* (2008b). In close analogy with Th, the reaction sequence in equation 38.27 was identified.

$$\mathrm{U} + \mathrm{NH_3} \rightarrow \mathrm{U : NH_3} \rightarrow \mathrm{H_2N - UH} \rightarrow \mathrm{HN = UH_2} \qquad (38.27)$$

The high-energy $N{\equiv}UH_3$ isomeric nitride complex comprising hexavalent uranium was absent. Of the four possible UNH_3 isomers, calculations indicate that $H_2N–UH$ and $HN{=}UH_2$ are of approximately comparable stability, and are significantly more stable than the $U{:}NH_3$ adduct and the $N{\equiv}UH_3$ nitride. Bonding analysis of the uranium and thorium amines and imines indicates that the 5*f* orbitals substantially enhance the π-bonding, more so in the case of U than Th. In addition to the two intermediates and the ultimate uranimine complex, the bis-ammonia complex, $U(NH_3)_2$, was also observed.

38.6 REACTIONS OF ACTINIDE ATOMIC AND MOLECULAR IONS AND NEUTRALS IN THE GAS PHASE

38.6.1 Background and experimental methodologies

Studies of gas-phase reactions are greatly facilitated by the ability to exert control over a sub-set of the reactants and products. Consequently the presence of charged species is of great advantage and, therefore, most of the research has involved ionic species and the use of a variety of mass spectrometry (MS) techniques, either with commercial or specially designed instruments.

Three main types of instruments have been employed for ion chemistry studies: flow/drift tubes, ion traps, and ion beams. Flow/drift techniques, e.g.

flowing afterglow (FA) or selected-ion flow tubes (SIFT), and ion traps, e.g. ion cyclotron resonance (ICR) and its more recent form Fourier transform ion cyclotron resonance (FTICR) or quadrupole ion traps (QIT), are best suited for studies of ion/molecule reactions at room temperature, including kinetics measurements, while ion beam or guided ion beam (GIB) techniques permit studies of ion/molecule reactions over a broad range of collision energies, due to a refined control over the kinetic energy of the reactant ions. The two groups of techniques are essentially complementary and in conjunction they provide detailed kinetic, mechanistic, and thermochemical information. At the fundamental level, reactivity correlates directly with the electronic structures of the reactants and with the energetics of the reaction processes.

The underlying principles, experimental techniques and methodologies for the study of gas-phase ion/molecule reactions have been fully described in the literature: theory of gas-phase processes (Armentrout, 2003b, 2004); instrumentation – mass analyzers (McLuckey and Wells, 2001; Armentrout, 2003b), ion sources (Vestal, 2001; Armentrout, 2003b); ion activation and dissociation (Armentrout, 2003a; McLuckey and Goeringer, 1997; Sleno and Volmer, 2004); ion thermochemistry (Ervin, 2001; Armentrout, 2003b). Theoretical methods play an important role in the elucidation of gas-phase reactions and a comprehensive review of theoretical methods as related to gas-phase ion chemistry studies has recently appeared (Mercero *et al.*, 2005). Experimental studies of the gas-phase chemistry of bare and ligated metal ions have been the subject of several excellent reviews (Russell, 1989; Eller and Schwarz, 1991; Roth and Freiser, 1991; Weisshaar, 1993; Schröder and Schwarz, 1995, 1999; Freiser, 1996a, b; Schröder *et al.*, 2000; Stace, 2002; Armentrout, 2003a; Operti and Rabezzana, 2003; Schwarz, 2003; Nibbering, 2004; Bohme and Schwarz, 2005; Operti and Rabezzana, 2006; Roithová and Schröder, 2007; Bohme, 2008).

In gas-phase actinide ion chemistry studies, the methods indicated above have all been employed during almost 4 decades of research, with an emphasis in the last decade, when the studies were extended to the more radioactive members of the series, using a special MS technique designated laser ablation with prompt reaction and detection (LAPRD (Gibson, 2002a)) and FTICR/MS. The work has encompassed a large number of reactivity studies that have increased our knowledge of the chemical properties of the actinides from Th to Es, and have produced significant data for the thermodynamic properties of actinide species, particularly oxides.

38.6.2 Reactivity of neutral actinide species and ion chemistry of volatile actinide compounds

Many of the initial gas-phase chemistry studies involving the actinides dealt with volatile uranium compounds, particularly uranium hexafluoride. The purpose of this research was of a fundamental nature, but with implications for contemporary research on uranium enrichment processes. The ionization of neutral UF_6 was studied in detail, as well as the reactions of some the ionic products formed with neutral UF_6 itself.

Negative ion formation in UF_6 molecules was studied by Stockdale *et al.* (1970), who observed the formation of UF_6^- by charge exchange with SF_6^- and UF_5^- produced directly from electron attachment to UF_6.

McAskill (1975) studied the clustering reactions of UF_6 in a medium-pressure ion source coupled to a MS, and identified the formation of $U_2F_{11}^+$ from UF_5^+, $U_2F_{10}^+$ from UF_4^+ and $U_3F_{16}^+$ from $U_2F_{10}^+$.

ICR was used by Beauchamp (1976a) to investigate the formation and reactions of both positive and negative ions derived from UF_6. The processes observed included clustering of UF_n^+ (n = 3–5) with UF_6, formation of UF_6^- by electron attachment and by electron transfer from UF_5^-, SF_6^-, and Cl^-, and detection of UF_7^-. This work was followed (Beauchamp, 1976b) by a study of the endothermic reactions of UF_6^-, generated by surface ionization, with UF_6, BF_3, and SF_6, in which values for the electron affinity (EA) of UF_6 and the first U–F bond dissociation energy (D) in UF_6^- and UF_7^- were deduced.

Compton (1977) performed a detailed study of positive and negative ion formation in UF_6. Cross sections were determined for positive ion formation by electron impact ionization, and for negative ion formation by electron attachment and by reaction with alkali atoms in crossed beams. From these last experiments, a lower limit for EA[UF_6] and values for EA[UF_5] and D[F_5U–F] were obtained.

Crossed beams were also used by Mathur *et al.* (1977) to study the ionization reactions of UF_6 with alkali atoms and dimers. Lower limits for EA[UF_6] and EA[UF_5] were reported.

The FA technique was used by Streit and Newton (1980) to examine the process of electron transfer from negative ions (halides and SF_6^-) to UF_6. This work included measurements for the rate coefficients.

The same technique was later employed by Streit and Babcock (1987) to study the reactions of UF_6 with a variety of positive ions (rare gases, atomic and molecular nitrogen and oxygen) that produced ions of the type UF_n^+ with n = 3–5; these ions subsequently reacted with UF_6 to produce cluster ions $U_2F_n^+$. The authors also reported the first gas-phase hetero-ligand uranium ion UOF_3^+, formed in the reactions of H_2O^+ and H_3O^+ with UF_6. Oxo-fluoride uranium anions, UOF_5^- and UOF_4^-, were observed as products of the reactions of O^- and O_2^- with UF_6.

Another volatile uranium compound, uranium tetrahydroborate, was also examined. Armentrout and Beauchamp (1979) used ICR to study some of the thermodynamic properties of $U(BH_4)_4$ that included the determination of its IE and enthalpy of formation, as well as several bond dissociation energies for the parent neutral and its positive fragment ions. The formation of the molecular anion by thermal electron attachment was observed. An upper limit for EA[$U(BH_4)_4$] was inferred from the absence of reactivity of neutral $U(BH_4)_4$ with F^- and NO_2^-. The reactions of both positive and negative ions in $U(BH_4)_4$

alone were studied and several clustering reactions were identified. Based on the thermodynamics results, the authors noted that the use of $U(BH_4)_4$ as a source of atomic uranium was justified when compared with UF_6.

Babcock *et al.* (1984a) studied the ionization-fragmentation of $U(BH_4)_4$ in a FA apparatus and identified the positive ions formed by reactions with He^+ and N^+/N_2^+, and the negative ions formed by attachment of thermal electrons. Fluoride transfer with SF_6^-, BF_4^-, and UF_n^- (n = 5–7) and reactions with other small ions (O^-, O_2^-, NO_2^-, F^-, Cl^-, O_2^+) were described.

The same authors (Babcock *et al.*, 1984b) used the FA technique to study the ionization-fragmentation of the archetypal actinide organometallic molecule bis-cyclooctatetraene uranium(IV), $U(C_8H_8)_2$, or uranocene. The reaction with He^+ produced $U(C_8H_8)^+$ and $U(C_6H_6)^+$ as the most intense ions, while with N^+/N_2^+ the only uranium containing ions observed were $U(C_8H_8)_2^+$ and $U(C_8H_8)^+$. As for the negative ions, non-dissociative electron attachment was observed, but no reactions were detected with O^-, O_2^-, F^-, Cl^-, SF_6^-, or UF_6^-.

Finally, a few experimental studies of the reactions of atomic uranium have been described involving oxidants. Lang *et al.* (1980) used crossed molecular-beams to examine UO production in the reactions of U with O_2, NO, NO_2, N_2O, CO_2, and SO_2, and measured the respective cross sections. Johnsen and Biondi (1972) reported the chemi-ionization of uranium by the association reaction with O_2 to form UO_2^+ in a drift mobility-tube MS apparatus. The same type of process was described by this group for the case of thorium (Johnsen *et al.*, 1974). The chemi-ionization reactions of U with O_2 and N_2O were also studied by Dyke *et al.* (1988) using electron spectroscopy.

38.6.3 Reactivity of atomic and molecular actinide ions in the gas phase

(a) Reactions with hydrocarbons

Hydrocarbons, alkanes and alkenes in particular, are convenient substrates to establish correlations between the electronic configurations of the reactant ions and the reaction products and mechanisms, as extensively demonstrated in the past 2 decades (Eller and Schwarz, 1991; Schröder and Schwarz, 1995; Operti and Rabezzana, 2006). Hydrocarbon activation by metal ions generally proceeds by oxidative insertion into a C–H or C–C bond, which requires two chemically active valence electrons at the metal center, such as in $\{C–M^+–H\}$ or $\{C–M^+–C\}$ intermediates. Early examinations of reactions of lanthanide ions (Ln^+) with hydrocarbons in the gas phase, by the groups of Freiser (Huang *et al.*, 1987), Beauchamp (Schilling and Beauchamp, 1988), Sunderlin and Armentrout (1989), and Cornehl *et al.* (1995), have demonstrated the utility of this type of chemical reactivity in elucidating the role of electronic structures of 4*f*-element ions in inducing bond activation. Therefore, product distributions and efficiencies of the reactions of actinide ions with alkanes and alkenes were also studied and interpreted in the context of the electronic configurations of the ground state and low-lying excited states of the ions, in order to elucidate the role of the 5*f* electrons at the actinide metal center.

The first studies of actinide ion/hydrocarbon reactivity in the gas phase, by Armentrout *et al.* (1977a, b), examined in an ion beam instrument the reaction of translationally excited U^+ ions with CD_4 to produce UD^+, which was characterized thermodynamically.

Subsequent studies of actinide ion/hydrocarbon reactions focused on reactions under low-energy conditions, where only inherently thermoneutral or exothermic reactions are observed. The initial low-energy studies employed FTICR/MS to characterize reactions of U^+, Th^+, and the corresponding oxides with hydrocarbons. In the first report of this type of experiment (Liang *et al.*, 1990), preliminary results for the activation of 1,3,5-tri-*t*-butylbenzene by U^+ were described. Another preliminary account from the same group (Leal *et al.*, 1993) described the reactions of U^+ and Th^+ with benzene and substituted benzenes.

Heinemann *et al.* (1995) carried out the first detailed study of the reactions of U^+ with alkanes and alkenes. A variety of C–H and C–C bond activation processes were identified, which occurred at higher kinetic efficiencies compared with Nd^+, the congener from the Ln series. The cyclotrimerization of ethylene mediated by U^+ to form the uranium–benzene ion was also described.

That U^+ does not react with methane or ethane, in concurrence with the observations of Heinemann *et al.* (1995), was reported by Marçalo *et al.* (1995) who also described the activation of the same alkanes by Th^+, indicating an increased reactivity of this ion as compared to U^+. The same authors (Marçalo *et al.* 1996) later extended the work with Th^+ to larger alkanes and to alkenes, confirming the high reactivity of this ion, and also presented a preview of 5*f* metal ion reactivity based on comparisons of the available data on lanthanide, thorium, and uranium ions.

Cornehl *et al.* (1997a) performed a study of the activation of hydrocarbons by mono- and dioxocations MO^+ and $MO_2{}^+$ of Th, U, and their counterparts in the lanthanide series, Ce and Nd, as compared with the bare metal ions, thereby providing the first detailed study of the effects of oxo ligands in actinide ion reactivity. The monoxides and $UO_2{}^+$ proved to be rather unreactive while, in contrast, $CeO_2{}^+$ and $ThO_2{}^+$ reacted efficiently with different substrates by abstraction of a hydrogen atom or by oxygen atom transfer to unsaturated hydrocarbons.

The reactions of An^+, An^{2+}, AnO^+ (An = Th, U), and $UO_2{}^+$ with several arenes were studied by Marçalo *et al.* (1997a) which gave a new comparison of the reactivity of bare and oxo-ligated An^+ ions, again showing a decrease of reactivity as an effect of the oxo ligation. This work constituted the first examination of the reactivity of doubly charged actinide cations, An^{2+}, and revealed a significant reactivity of these ions in activation of the arene bonds, beyond the expected electron-transfer reaction channels.

FTICR/MS was also used by the group of Srzic and Klasinc to investigate the ligation of U^+ by polycyclic aromatic hydrocarbons (Srzic *et al.*, 1997a, b; Kazazic *et al.*, 2005, 2006).

Another ion trapping technique, QIT/MS, was used by Jackson *et al.* (2002) to explore the differences of the technique relative to FTICR/MS, in a study of the reactivity of Th^+, U^+, ThO^+, UO^+, and UO_2^+ with 1,2,3,4,5-pentamethylcyclopentadiene. Representative Ln^+ and LnO^+ ions were studied for comparison with the actinide ions, and with a previous FTICR/MS study of the Ln cations (Marçalo *et al.*, 1997b). Based on several experimental observations, it was concluded that the different pressure regimes of the two ion traps were responsible for the observed differences in reactivity.

Following the initial FTICR/MS studies that involved the naturally occurring and low radioactivity members of the actinide series Th and U, the special LAPRD technique came into play and was systematically employed to extend the reactivity studies of An^+ and AnO^+ ions to Pa and the transuranium actinides, Np to Es. The least radioactive isotope available in sufficient quantities for each element was employed in the LAPRD studies, as follows: ^{231}Pa, ^{237}Np, ^{242}Pu, ^{243}Am, ^{248}Cm, ^{249}Bk, ^{249}Cf, and ^{253}Es; the last being the shortest-lived isotope studied, with a half-life of 20 days.

The LAPRD setup was first tested by Gibson (1996) in reactivity studies of Ln^+ cations with cyclic hydrocarbons, which by comparison with previous FTICR/MS studies of the same systems, validated the experimental approach. Following this success, Gibson (1997b) applied the LAPRD technique to the reactions of Th and U metal and metal oxide cations with C_6 and C_8 cyclic hydrocarbons.

In the first study involving other actinides, Gibson (1998c) examined the reactions with alkenes of An^+ and AnO^+ for An = Th, U, Np, and Pu. Key findings of this work were that U^+ and Np^+ were comparably reactive whereas Pu^+ was significantly less reactive, while all the monoxide cations showed a decreased reactivity compared with metal ions.

Similar experiments for Am^+ (Gibson, 1998d) and Cm^+ and CmO^+ (Gibson and Haire, 1998) soon followed. Alkenes, benzene, and cyclic polyenes were the substrates that revealed that Am^+ had a rather low reactivity when compared with the earlier actinides in the series. Cm^+ showed a moderate reactivity with alkenes while CmO^+ was less reactive.

The remaining three transcurium actinide ions studied by the LAPRD technique in their reactions with alkenes, Bk^+ (Gibson and Haire, 2000b, 2001b), Cf^+ (Gibson and Haire, 2000a), and Es^+ (Gibson and Haire, 2003), all showed reduced reactivities, with Cf^+ and Es^+ being totally inert with the alkenes examined.

The reactions of 1,2,3,4,5-pentamethylcyclopentadiene with Np^+, Pu^+, Am^+, Cm^+, Bk^+, Cf^+, and Es^+ were also examined by LAPRD (Gibson, 2000; Gibson and Haire, 2001b, 2005). With this more reactive substrate, even the more inert actinide ions Cf^+ and Es^+ were able to induce activation, and several organometallic ions could be identified for all the actinides. These studies effectively constituted a further probing of the electronic structures of the transcurium actinides.

Protactinium completed the group of actinide ions studied for their reactions with hydrocarbons by LAPRD (Gibson and Haire, 2002). It was demonstrated, in direct comparisons with U^+, Np^+ and the corresponding monoxide ions, that Pa^+ was a very reactive actinide ion, inducing oligomerization of alkenes, PaO^+ also had an exceptional reactivity, inducing efficient dehydrogenations of the alkenes, attributed to participation of the 5*f* electrons in PaO^+ in the activation process, either directly or through promotion/hybridization.

The studies carried out with the LAPRD technique systematically probed the reactivity of An^+ ions from Th^+ to Es^+ with alkenes as substrates (with pentamethylcyclopentadiene a special case). Although reaction kinetics could not be measured with LAPRD, which would place the relative reactivity of An^+ ions on a quantitative base, all the experiments involved direct comparisons of pairs or triplets of An^+ ions (as well as comparisons with selected Ln^+ ions), thereby allowing a qualitative appraisal of the relative reactivity of An^+ from Th^+ to Es^+. Based on the LAPRD results and the previous FTICR/MS results for Th^+ and U^+, the following ordering of reactivities has been established:

$$\mathrm{Th}^+ \geq \mathrm{Pa}^+ \geq \mathrm{U}^+ \approx \mathrm{Np}^+ > \mathrm{Cm}^+ \geq \mathrm{Pu}^+ > \mathrm{Bk}^+ > \mathrm{Am}^+ \approx \mathrm{Cf}^+ \geq \mathrm{Es}^+$$

As shown by the studies summarized above, and described in detail in the two existing review papers on gas-phase actinide ion chemistry (Gibson, 2002a; Gibson and Marçalo, 2006), the reactivity of An^+ ions towards hydrocarbons can be interpreted via a bond-insertion mechanism. The reactivity generally correlates inversely with the promotion energies necessary to excite the ions from their ground states to "divalent" electronic configurations with two unpaired non-*f* electrons, of the type $[\mathrm{Rn}]5f^{\,\mathrm{n}-2}6d7s$ (where [Rn] represent the closed radon electronic core). Figure 38.6 shows a plot of the relevant promotion energies. It is immediately apparent that the An^+ reactivity correlates inversely with the promotion energy.

The addition of an oxo-ligand to an actinide ion clearly altered the reactivity with hydrocarbons. Both the FTICR/MS and QIT/MS studies with ThO^+ and UO^+ and the comparative assessments of the AnO^+ reactivities using the LAPRD technique for An = Th, Pa, U, Np, Pu, and Cm revealed a substantial reduction of the reactivity compared with the bare An^+, with the notable exception of PaO^+. These results were consistent with the involvement of chemically active valence electrons at the actinide metal centers in the An^+–O bonding, but lack of knowledge of the electronic structures of the AnO^+ ions precluded any further interpretation of the results.

Recently, FTICR/MS was used to study the reactions of An^+ and AnO^+ with alkanes and alkenes, for An from Th to Cm, in an attempt to obtain more sensitive and quantitative measurements of product distributions and reaction

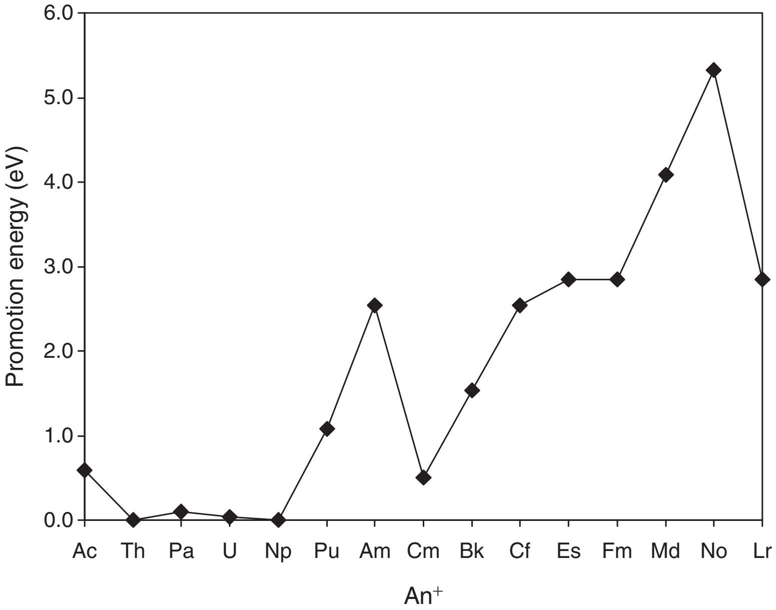

Fig. 38.6 *Promotion energies of the* An^+ *ions from the ground states to configurations with two unpaired non-f electrons* $[Rn]5f^{n-2}6d7s$. *The ground states are:* Ac^+ – $[Rn]7s^2$; Th^+ – $[Rn]6d^27s$; Pa^+ – $[Rn]5f^27s^2$; U^+ – $[Rn]5f^37s^2$; Np^+ – $[Rn]5f^46d7s$; Pu^+ – $[Rn]5f^67s$; Am^+ – $[Rn]5f^77s$; Cm^+ – $[Rn]5f^77s^2$; Bk^+ – $[Rn]5f^97s$; Cf^+ – $[Rn]5f^{10}7s$; Es^+ – $[Rn]5f^{11}7s$; Fm^+ – $[Rn]5f^{12}7s$; Md^+ – $[Rn]5f^{13}7s$; No^+ – $[Rn]5f^{14}7s$; Lr^+ – $[Rn]5f^{14}7s^2$ *(the data are from Blaise and Wyart 1992 except for* Cf^+, Md^+, No^+, *and* Lr^+ *that are estimates from Brewer 1971).*

kinetics. The objective was to provide a more detailed picture of variations in reactivity across the series (Santos *et al.*, 2006b; Gibson *et al.*, 2007b). These new studies basically confirmed the LAPRD results for both An^+ and AnO^+ ions and were able to fine-tune the relative An^+ reactivities, especially for the early An^+ ions from Th to Np. A revised ordering of reactivities from Th^+ to Cm^+ could be established:

$$Th^+ > Pa^+ > U^+ > Np^+ > Cm^+ > Pu^+ > Am^+$$

In conjunction with these experimental studies, electronic structure calculations were performed for PaO^+, which enabled an effective evaluation of the unique behavior of PaO^+.

The overall picture that emerged from this study, besides confirming the bond activation model outlined above, indicated, according to the authors, that (see Fig. 38.6): the high reactivity of Th^+ could be attributed to its quartet $6d^27s$ ground state configuration which produced a behavior typical of a *d*-block metal ion; the reactivities of Cm^+, Pu^+ and Am^+ correlated with the promotion energies to $5f^{n-2}6d7s$ states suitable for bond insertion; the markedly different reactivities of Pa^+, U^+, and Np^+, with ground states or very low-energy ($\Delta E \leq 0.1$ eV) $5f^{n-2}6d7s$ configurations, could be ascribed to a decrease in 5*f* participation from Pa^+ to U^+ to Np^+.

For the AnO^+ ions, the authors claimed that: the low to moderate reactivity of ThO^+ was indicative of radical-like behavior, as expected from its electronic structure, $Th^{3+}(7s)O^{2-}$; the low reactivity of UO^+ resulted from a ground state and low-lying states corresponding to $U^{3+}(5f^3)O^{2-}$, with a marginal participation of the 5*f* electrons in bond activation; the absence of reactivity of the transuranic AnO^+ was presumed to reflect $An^{3+}(5f^n)O^{2-}$ ground and low-lying states and inert 5*f* electrons; the high reactivity of PaO^+ resulted from a $Pa^{3+}(5f6d)O^{2-}$ ground state and, given the substantial 5*f* character of the ground and low-lying excited states (all excited states up to 1.8 eV were found to have a 5*f*-orbital occupation of $\geq$0.8 electrons), indicated significant participation of the 5*f* electrons of the oxo-ligated protactinium metal center in oxidative insertion. The authors argued that the reactivities of Pa^+ and PaO^+ constituted the first clear experimental evidence, supported by theory, of the active role of 5*f* electrons in gas-phase organoactinide chemistry, and suggested that equivalent 5*f* participation might also appear for Pa in the condensed phase, in contrast to Th and U.

The same group has used FTICR/MS to extend the reactivity studies of actinide ions to other hydrocarbon substrates, and with indene it was verified that all the An^+ and AnO^+ (An = Th, U, Np, Pu, Am) species examined were very reactive, ultimately leading to the formation of An-bis(indenyl) species (Santos *et al.*, 2003b).

In another effort to probe the involvement of the 5*f* electrons in bond activation for the early actinides, the reactions of doubly charged actinide ions, An^{2+} (An = Th, Pa, U, Np, Pu, Am, Cm), with alkanes and alkenes were studied by FTICR/MS (Gibson *et al.*, 2007a). The reaction products observed consisted of doubly charged organometallic ions and singly charged ions that resulted from electron, hydride, and methide transfers. By comparing the products of the An^{2+} reactions with those observed in reactions of Ln^{2+} (Marçalo *et al.*, 2008) and in reactions of *d*-transition metal dications (Roth and Freiser, 1991; Hill *et al.*, 1997), it was argued that Pa, here as Pa^{2+}, was again a contender for participation of the 5*f* electrons in the observed chemistry. Th^{2+} and Pa^{2+} reacted similarly to transition metal ions with d^2 or d^3 ground states, whereas U^{2+} and Np^{2+} reacted similarly to Ln^{2+} ions which have only one non-4*f* valence electron, and to dipositive group 3 transition metal ions which have d^1 ground states, equally lacking low-lying excited states with more than one valence electron. Both U^{2+} and Np^{2+} have $5f^n$ ground states, $5f^{n-1}6d$ or $5f^{n-1}7s$ states at low to moderate energies (0.03 to ~1 eV), and $5f^{n-2}6d^2$ states only at rather high energies (>2 eV) (Blaise and Wyart, 1992). Conversely, Th^{2+} has a $5f6d$ ground state and a $6d^2$ state at a very low energy (0.01 eV), while Pa^{2+} has a $5f^26d$ ground state, $5f^27s$ and $5f^3$ states at moderate energies (~0.5 eV), and a

$5f6d^2$ state at higher energy (1.2 ± 0.7 eV) (Blaise and Wyart, 1992). The authors claimed that while the low-energy $6d^2$ state most likely accounted for the observed Th^{2+} reactivity, Pa^{2+} could have a state or states with only one non-$5f$ electron determining the observed reactivity, indicating, however, that the large uncertainty in the promotion energy to the $5f6d^2$ configuration for Pa^{2+} prevented an unambiguous answer to the question.

A recent gas-phase photodissociation study of cationic uranium and uranium oxide benzene complexes (Pillai *et al.*, 2005) reported on the dissociation induced by ultraviolet laser light of $U(C_6H_6)_n{}^+$ (n = 1–3) and $UO_m(C_6H_6)^+$ (m = 1, 2) complexes produced by laser vaporization; ligand elimination and ligand decomposition channels were identified and the photodissociation trends were compared with previous reaction studies of uranium cations.

(b) Reactions with oxidants

Another group of reagents that were studied in more detail in the gas phase were oxidant molecules, which besides allowing for an assessment of the chemical properties of the actinide ions, provided information on the thermodynamics of such important species as the actinide oxides.

Early studies by Biondi and co-workers using a drift tube instrument revealed that U^+ was oxidized to UO^+ by O_2 in a exothermic process (Johnsen and Biondi, 1972), while for Th^+ exothermic oxidation to ThO^+ occurred with both O_2 and NO (Johnsen *et al.*, 1974); in this last work, the presumably endothermic oxidation of ThO^+ to $ThO_2{}^+$ by NO was also described.

In another early study, Armentrout and Beauchamp (1980a) used an ion-beam apparatus to investigate the reactions of U^+ and UO^+ with O_2, CO, CO_2, COS, and D_2O, and observed exothermic oxidations of U^+ and UO^+ with all the reagents except CO, in agreement with the currently known thermochemistry. In a complementary study, the same authors (Armentrout and Beauchamp, 1980b) examined the collision-induced dissociation (CID) of UO^+ and $UO_2{}^+$ ions colliding with argon and verified that the thresholds for dissociation agreed with the known values for $D[U^+–O]$ and $D[OU^+–O]$.

Oxidation of Th^+ and U^+ was more thoroughly examined years later by the Schwarz's group. A first report (Heinemann and Schwarz, 1995) depicted the oxidation of U^+ to UO^+ by N_2O and of UN^+ (also formed in the previous reaction) to NUO^+ by O_2. A more comprehensive study (Cornehl *et al.*, 1997a) revealed that the oxidation of Th^+ and U^+ to the monoxide ions was afforded by O_2, CO_2, N_2O, or H_2O, while the formation of the dioxide ions from ThO^+ and UO^+ occurred with all the reagents in the case of U but only with N_2O in the case of Th.

LAPRD was also used to probe the oxidation of An^+ and AnO^+ ions, this time with ethylene oxide. U^+, Np^+, Pu^+, and Am^+ all reacted to form the AnO^+ ions, which, with the exception of AmO^+ that only produced minor amounts of the dioxide ion, efficiently yielded the $AnO_2{}^+$ ions (Gibson, 2001). This study indicated that D[OPu^+–O] was substantially greater than the literature values. Pa^+ and PaO^+ were also studied, with both ions efficiently oxidizing. A comparison with uranium provided the first known estimates for D[Pa^+–O] and D[OPa^+–O] (Gibson and Haire, 2002).

Systematic studies, using FTICR/MS, of the oxidation of An^+ and AnO^+ cations (An = Th, Pa, U, Np, Pu, Am, Cm) with oxidizing reagents having a large range of thermodynamic oxidizing ability ($N_2O > C_2H_4O$ [ethylene oxide] $> H_2O > O_2 > CO_2 > NO > CH_2O$), were reported in the last few years. Besides confirming the results of previous studies summarized above, this work produced several new and revised thermodynamic data for the actinide oxides.

The initial study examined Th, U, Np, and Pu (Santos *et al.*, 2002), followed by Am (Santos *et al.*, 2003a), and more recently by Pa (Santos *et al.*, 2006c) and Cm (Gibson *et al.*, 2008). The overall picture of the reactivity of the different An^+ indicated that a correlation existed with the promotion energies from the ground states to configurations $5f^{\,n-2}6d7s$ (see Fig. 38.6), or $5f^{\,n-2}6d^2$ which follow the same general trend (Blaise and Wyart, 1992), and, based on the measured kinetics, an ordering of reactivities similar to the one found by the same authors in the case of hydrocarbons (see previous section) was established. For the monoxide cations, a general decrease in reactivity as compared with the metal cations was observed, and the ordering of reactivities corresponding to the ease of formation of the $AnO_2{}^+$ ions was as follows:

$$PaO^+ > UO^+ >> NpO^+ > PuO^+ >> ThO^+ > AmO^+ >> CmO^+ \approx 0$$

As pointed out by the authors, this trend is probably a reflection of the gas-phase thermodynamic stability of the formal oxidation state V of the different actinides, although kinetic effects may also play a role, particularly in the cases of Th and Am.

The oxidation of doubly charged actinide ions was also studied with FTICR/MS. In a ground-breaking study, Cornehl *et al.* (1996) observed the oxidation of U^{2+} by N_2O, O_2, and CO_2, and subsequently, the oxidation of UO^{2+} by N_2O and O_2 to form the ubiquitous uranyl ion $UO_2{}^{2+}$ for the first time in the gas phase.

Later, systematic studies of the reactions of An^{2+} (and the AnO^{2+} produced therein) with oxidants by FTICR/MS were performed, using the same set of seven oxidants as used before for the singly charged actinide cations. The first of these studies examined Th, U, Np, Pu, and Am (Gibson *et al.*, 2005b), followed by Pa (Santos *et al.*, 2006c) and Cm (Gibson *et al.*, 2008). Other reaction channels, like electron transfer, were observed for the reactants C_2H_4O, CH_2O, and NO, due to the fact that the second ionization energies of the actinides are higher than the ionization energies of the neutral reagents. The reactivity ordering observed for the An^{2+} was the following:

$$Th^{2+} \approx Pa^{2+} > U^{2+} >> Np^{2+} > Pu^{2+} > Am^{2+} > Cm^{2+}$$

Of note was the observation of CmO^{2+}, formally a tetravalent Cm species, formed exclusively in the reation of Cm^{2+} with N_2O. The authors did not establish any direct correlation of the oxidation efficiencies with the electronic structures and promotion energies of the An^{2+} ions, in contrast to the case of the An^+ ions (see above).

Only restricted sets of reactions of AnO^{2+} were studied due to experimental limitations and the following reactivity ordering in terms of oxidation ability of the AnO^{2+} was obtained:

$$UO^{2+} > NpO^{2+} > PuO^{2+} > PaO^{2+} > AmO^{2+} \approx ThO^{2+} \approx CmO^{2+} \approx 0$$

It was remarkable that from the reactions of AnO^{2+} with N_2O for An = Pa, Np, and Pu, and with O_2 for An = Np, it was possible to produce for the first time the bare gas-phase actinyl dipositive ions, ${AnO_2}^{2+}$; the production of bare uranyl by this approach was confirmed. The case of "protactinyl" deserves a special mention as it was the first time this species, formally of Pa(VI), was shown to exist.

An interesting observation made in these studies was that both CmO^{2+} (Gibson *et al.* 2008) and ${PaO_2}^{2+}$ (Santos *et al.*, 2006c) were active in the catalytic oxidation of CO by N_2O (Bohme and Schwarz, 2005).

Another facet of the FTICR/MS technique explored in these studies is its capability to afford quantitative information on ion and neutral thermodynamics (Ervin, 2001). If the reactant ions are properly thermalized, the reactions that are observed are either exothermic or thermoneutral, although the existence of kinetic barriers may prevent their observation. If the ion/neutral pairs are cautiously chosen, and the thermodynamic properties of some of the reactant partners are known, estimates can be obtained for the energies of bonds being formed and/or broken, and determinations can be made of other thermodynamic properties such as the ionization energies of ionic and neutral species.

In these studies, the use of oxidizing reagents with a large array of oxygen dissociation energies allowed estimates of unknown $D[An^+–O]$, $D[OAn^+–O]$, $D[An^{2+}–O]$, and $D[OAn^{2+}–O]$, and verification or correction of literature values obtained by other methods for Th (Santos *et al.*, 2002, 2004; Gibson *et al.*, 2005a), Pa (Santos *et al.*, 2006c), U (Santos *et al.*, 2002, 2004; Gibson *et al.*, 2005b), Np (Santos *et al.*, 2002, 2004; Gibson *et al.*, 2003, 2005a), Pu (Santos *et al.*, 2002, 2004; Gibson *et al.*, 2003, 2005a), Am (Santos *et al.*, 2003b, 2004; Gibson *et al.*, 2003, 2005a), and Cm (Gibson *et al.*, 2008). A particularly notable result was the conclusion that the literature values for $D[OPu^+–O]$ of 250–260 kJ mol^{-1} (Hildenbrand *et al.*, 1985; Capone *et al.*, 1999) were too low by at least ca. 250 kJ mol^{-1} (Santos *et al.*, 2002).

In the same studies, further experiments with the singly and doubly charged actinide monoxide and dioxide cations produced via the oxidation reactions provided several ionization energies of the corresponding neutral and monopositive monoxides and dioxides, IE[AnO], IE[AnO_2], IE[AnO^+], and IE [$AnO_2{}^+$].

From the study of the reactions of AnO^+ with dienes, following a model developed by Cornehl *et al.* (1997b) for the lanthanide monoxides, and using an accurate spectroscopic measurement of IE[UO] by Han *et al.* (2003) as a reference, new values for IE[NpO] (Santos *et al.* 2003a; Gibson *et al.* 2005a) and IE[PuO] (Santos *et al.*, 2003a; Gibson *et al.*, 2005a) were obtained, and values for IE[AmO] (Santos *et al.*, 2003a; Gibson *et al.*, 2005a) and IE[CmO] (Gibson *et al.*, 2008) were obtained for the first time.

In the study of reactions of $AnO_2{}^+$ ions with neutral organic compounds having well-known IE's using a "bracketing" approach (Ervin, 2001), these same authors were able to make the first determination of IE[AmO_2] (Santos *et al.*, 2003a), establish a new value for IE[NpO_2] (Gibson *et al.*, 2005a), more than 1 eV higher than the literature value (Hildenbrand *et al.*, 1985), and determine a new value for IE[PuO_2] (Santos *et al.*, 2002), lower by ca. 2.5–3 eV than the literature values (Hildenbrand *et al.*, 1985; Capone *et al.*, 1999) but consistent with the observed Pu oxidation reactions for the derived oxide bond energies (see above). One of the literature values for IE[PuO_2] (Capone *et al.*, 1999) was recently redetermined (Capone *et al.*, 2005) but this last work was the subject of debate (Gibson *et al.*, 2006); a contribution to this issue from a theoretical study was very recently added (La Macchia *et al.*, 2008).

The estimation of the ionization energies of AnO^+, unknown in all cases, was addressed by the authors mainly by elaborating on the thermodynamics of observed oxidation reactions. With this approach, the IE[AnO^+] for An = U, Np, Pu, and Am (Gibson *et al.*, 2005b) could be determined, while in the cases of Th (Gibson *et al.*, 2005b) and Pa (Santos *et al.*, 2006c) only upper limits were obtained. A different approach was used in the estimation of IE[CmO^+] (Gibson *et al.*, 2008) that involved the study of electron transfer reactions of CmO^{2+} and an adaptation of the "bracketing" technique to the particularity of two positively charged species being formed in these reactions that generate energy barriers due to the repulsive Coulombic interactions.

This last method was also used to obtain estimates of unknown IE[$AnO_2{}^+$] for An = Pa (Santos *et al.*, 2006c), U (Gibson *et al.*, 2005b), Np (Gibson *et al.*, 2005b), and Pu (Gibson *et al.*, 2005b). The IE[$AmO_2{}^+$] could also be obtained from a comparative analysis of known aqueous phase thermodynamic properties in conjunction with the estimated IE[$AnO_2{}^+$] for An = U, Np, and Pu (Gibson *et al.*, 2005b). Theoretical studies performed for $PaO_2{}^+$ and $PaO_2{}^{2+}$ provided a value for IE[$PaO_2{}^+$] in very close agreement with the experimental estimate (Santos *et al.*, 2006c).

The bond dissociation energies and ionization energies of several neutral, monopositive and dipositive AnO and AnO_2 species yielded values for their enthalpies of formation. For uranyl and plutonyl, the experimentally derived values, $\Delta_f H^o(UO_2{}^{2+}(g)) = 1524 \pm 63$ kJ mol^{-1} and $\Delta_f H^o(PuO_2{}^{2+}(g)) = 1727 \pm 66$ kJ mol^{-1} (Gibson *et al.*, 2005b), were in good agreement with recent theoretical calculations: $\Delta_f H_0°(\mathrm{UO_2}^{2+}(g)) = 1527 \pm 42$ kJ mol^{-1} (Moskaleva *et al.*, 2006b) and $\Delta_f H_0°(\mathrm{PuO_2}^{2+}(g)) = 1749 \pm 63$ kJ mol^{-1} (Moskaleva *et al.*, 2006a).

The enthalpies of formation for the bare uranyl and plutonyl ions were used in conjunction with the known aqueous thermochemistry of these species to derive "experimental" enthalpies of hydration (Gibson *et al..*, 2005b). These were found to be approximately constant for these two actinyls, $\Delta_{hyd}H°(\mathrm{AnO_2}^{2+}) = -1670$ kJ mol^{-1} or $\Delta_{hyd}G°(\mathrm{AnO_2}^{2+}) = -1790$ kJ mol^{-1}, and showed agreement with recent theoretical studies of the solvation of actinyls by water: $\Delta_{hyd}G°(\mathrm{UO_2}^{2+}) = -1795$ kJ mol^{-1} (Moskaleva *et al.*, 2004); $\Delta_{hyd}G°(\mathrm{UO_2}^{2+}) = -1773$ kJ mol^{-1} and $\Delta_{hyd}G°(\mathrm{PuO_2}^{2+}) = -1663$ kJ mol^{-1} (Cao and Balasubramanian 2005); $\Delta_{hyd}G°(\mathrm{UO_2}^{2+}) = -1730$ kJ mol^{-1}, $\Delta_{hyd}G°(\mathrm{NpO_2}^{2+}) = -1726$ kJ mol^{-1}, and $\Delta_{hyd}G°(\mathrm{PuO_2}^{2+}) = -1713$ kJ mol^{-1} (Shamov and Schreckenbach, 2005; Shamov and Schreckenbach, 2006); $\Delta_{hyd}G°(\mathrm{UO_2}^{2+}) = -1715 \pm 21$ kJ mol^{-1} (Gutowski and Dixon, 2006).

The large amount of data that was gathered from these studies of actinide oxides from thorium to curium led to a recent overall assessment of the gas-phase thermodynamics of neutral and singly and doubly charged cationic actinide monoxides and dioxides (Marçalo and Gibson, 2009). The authors evaluated the data from standard literature sources (Hildenbrand *et al.*, 1985; Lias *et al.*, 1988; Pedley and Marshall, 1983; Konings *et al.*, 2006), tested and expanded the assessment of the known bond dissociation energies of neutral and singly-charged actinide monoxides carried out by Gibson (Gibson, 2003), based on correlations with the electronic structures and energetics of the isolated metal atoms and ions, and provided correlations with condensed-phase thermochemistry. A consistent set of metal-oxygen bond dissociation enthalpies, ionization energies, and enthalpies of formation, including new or revised values, was proposed and these data are presented in Tables 38.7, 38.8, and 38.9. The authors also proposed new estimates for the second ionization energies of the actinides from Th to Cm and these are shown in Table 38.10

To complete this section on the reactions with oxidants, it should be mentioned that QIT/MS was also used to study the reactions of U^+ and U^{2+} with oxygen and water (Jackson *et al.*, 2002, 2004), with the results showing general agreement with those from FTICR/MS studies. The few differences encountered in the reactions with water have been attributed to the different pressure regimes of the two ion trap techniques.

The reactions of U^+ and U^{2+} (Michelini *et al.*, 2006), UO^+ and UO^{2+} (Michelini *et al.*, 2007), and Th^+ and Th^{2+} (Mazzone *et al.*, 2008) with water were the object of theoretical studies aimed at unraveling the corresponding mechanisms. The reactions of U^+ and U^{2+} with $\mathrm{N_2O}$ were also recently examined by the same group (Alikhani *et al.*, 2008).

Table 38.7 *Bond dissociation energies (in kJ mol*$^{-1}$*) of neutral and ionic actinide oxides from the assessment of Marçalo and Gibson*[a]

An	D[An-O]	D[An^+-O]	D[An^{2+}-O]	D[OAn-O]	D[OAn^+-O]	D[OAn^{2+}-O]
Th	872±25	843±25	829±80	684±14	462±36	0±170
Pa	801±59	800±50	781±30	780±48	780±29	317±110
U	758±13	774±13	706±45	750±14	741±14	529±31
Np	744±21	760±10	524±26	632±43	610±22	504±10
Pu	658±10	651±19	439±49	599±22	509±38	403±95
Am	582±34	560±28	367±13	509±65	410±56	256±129
Cm	709±43	670±38	342±12	405±70	202±60	0±150

[a] (Marçalo and Gibson, 2009); original references are given in the text.

Table 38.8 *First and second ionization energies (in eV) of actinide oxides from the assessment of Marçalo and Gibson*[a]

An	IE[AnO]	IE[AnO^+]	IE[AnO_2]	IE[AnO_2^+]
Th	6.6035±0.0008	11.8±0.7	8.9±0.4	16.6±1
Pa	5.9±0.2	11.8±0.7	5.9±0.2	16.6±0.4
U	6.0313±0.0006	12.4±0.6	6.128±0.003	14.6±0.4
Np	6.1±0.2	14.0±0.6	6.33±0.18	15.1±0.4
Pu	6.1±0.2	14.0±0.6	7.03±0.12	15.1±0.4
Am	6.2±0.2	14.0±0.6	7.23±0.15	15.7±0.6
Cm	6.4±0.2	15.8±0.4	8.5±1	17.9±1

[a] (Marçalo and Gibson, 2009); original references are given in the text.

(c) Reactions with assorted organic and inorganic molecules

In this section, a brief overview of the reactivity studies with molecules other than hydrocarbons and oxidants is presented; some of these studies have provided complementary information to the more extensive studies described above.

Probably the earliest reported study of gas-phase reactions of actinide ions involved the observation of endothermic formation of UH^+, UD^+, PuH^+, and PuD^+ after addition of H_2, D_2, H_2O, D_2O, or H_2O to the ion source of the mass spectrometer where isotopic analysis of U and Pu was being performed (Moreland *et al.*, 1970).

Other early work, performed by Armentrout and Beauchamp using an ion-beam instrument, consisted of a study of the endothermic reactions of U^+ with N_2 and D_2 from which D[U^+–N] and D[U^+–D] were obtained (Armentrout *et al.*, 1977b); a study of the exothermic reaction of U^+ with CS_2 to give US^+ (Armentrout and Beauchamp, 1980a); and a study of the formation of uranium halide ions in exothermic reactions of U^+ with CH_3F, CH_3Cl, and CCl_4, and in the endothermic reaction of U^+ with SiF_4, this last reaction providing a value for D[U^+–F] (Armentrout and Beauchamp, 1981).

Table 38.9 *Enthalpies of formation (in kJ mol^{-1}) of gaseous actinide oxides from the assessment of Marçalo and Gibson*[a]

An	$\Delta_f H°[AnO,g]$	$\Delta_f H°[AnO^+,g]$	$\Delta_f H°[AnO^{2+},g]$	$\Delta_f H°[AnO_2,g]$	$\Delta_f H°[AnO_2^+,g]$	$\Delta_f H°[AnO_2^{2+},g]$
Th	−21±26	617±26	1775±85	−456±19	404±38	2004±190
Pa	18±60	587±52	1726±44	−513±77	57±60	1658±119
U	24±15	606±15	1803±54	−477±21	114±21	1523±62
Np	−30±21	559±10	1909±39	−413±48	198±24	1654±40
Pu	−60±10	529±19	1879±57	−410±24	269±43	1725±111
Am	−49±34	549±28	1900±32	−309±73	389±63	1903±133
Cm	−76±44	541±39	2066±33	−232±83	588±72	2315±154

[a] (Marçalo and Gibson, 2009); original references are given in the text.

Table 38.10 *Second ionization energies (in eV) of the actinides from the assessment of Marçalo and Gibson*[a]

An	IE[An^+]
Th	11.65±0.3
Pa	11.6±0.3
U	11.7±0.3
Np	11.55±0.3
Pu	11.8±0.3
Am	12.0±0.3
Cm	12.4±0.3

[a] (Marçalo and Gibson, 2009).

Later studies by LAPRD explored the reactivities of different An^+, AnO^+, and AnO_2^+ ions with a plethora of organic reagents, probing the formation of actinide halide ions with perfluorocarbons and dihaloethanes for An = Th, U, Np, Pu, and Am (Gibson, 1999a), Cm (Gibson and Haire 1998), Bk (Gibson and Haire, 2001b), Cf (Gibson and Haire, 2000a), and Es (Gibson and Haire, 2003); or probing the effect on reactivity of the presence of functional groups in the organic reagents, with nitriles and butylamine for An = Th, U, Np, Pu, and Am (Gibson, 1999a), Cm (Gibson and Haire, 1998), Bk (Gibson and Haire, 2001b), Cf (Gibson and Haire, 2000a), and Es (Gibson and Haire, 2003), and with alcohols, ethers, and thiols for An = U, Np, Pu, and Am (Gibson, 1999b; Gibson, 2002a), Cm (Gibson and Haire, 1998), Bk (Gibson and Haire, 2001b), Cf (Gibson and Haire, 2000a), and Es (Gibson and Haire, 2003).

Additional studies by LAPRD included the fluorination reactions of Pa^+ with SF_6 (Gibson and Haire, 2002), and the reactions of An^+ and AnO^+ ions with silane, disilane, and germane for An = Th, U, Np, Pu, and Am (Gibson, 2002b) which lead to the formation of silylenes, germylenes, and in a few cases germanides.

A few studies employed ion trapping techniques to examine reactions with different inorganic, organic, and even organometallic molecules. Jackson *et al.* (2004) studied the reactions of bare and ligated uranium ions with SF_6 in a QIT/MS: U^+ produced UF_n^+ species (n = 1, 2, 3, 4) rather efficiently and the reactions of UO^+, UOH^+, and several UF_n^+ ions formed in the primary reactions were also studied.

Reactions of U^+ with a substituted phenol (Liang *et al.*, 1990) and of Th^+ and U^+ with alcohols (Carretas *et al.*, 1997), both performed by FTICR/MS, were the subject of preliminary reports.

FTICR/MS was also used to examine the reactions of Th^+, U^+, and Th and U oxide and hydroxide cations with the organometallic compounds $Fe(CO)_5$ and $Fe(C_5H_5)_2$ (Vieira *et al.*, 2001). In the case of $Fe(CO)_5$, the observed primary products of the An^+ were of the type $AnFe(CO)_x^+$ with x = 2 and 3, and evidence was obtained for the presence of direct An–Fe bonds. With ferrocene, the An^+ cations reacted by metal exchange, yielding $An(C_5H_5)_2^+$ ions.

One final point of interest for this section is the experimental observation of the unusual species UF^{3+} by charge-stripping mass spectrometry in a multisector instrument, and the associated theoretical prediction of that this is the first diatomic trication that is thermochemically stable towards Coulomb explosion due to the unusually low third IE of uranium (Schröder *et al.*, 1999).

38.6.4 Miscellaneous studies of actinide ion chemistry

In this section, brief mention is made of special cases of gas-phase reactions of actinide ions that occur in diversified systems involving mass spectrometers.

(a) Reactions in atmospheric pressure ionization mass spectrometers

Atmospheric pressure ionization in its electrospray ionization (ESI) variant is the most widely used ionization method coupled to mass spectrometry, mainly because of its ability to probe ions directly from solution. There are a growing number of studies that apply this technique to the actinides, uranium in particular, that constitute relevant contributions to actinide chemistry.

Van Stipdonk, Groenewold, and co-workers initiated a systematic study of the solvation properties of uranyl using ESI-QIT/MS. In the first study of this kind, Van Stipdonk *et al.* (2003) used CID to examine complexes composed of the uranyl ion, nitrate or hydroxide, and water or alcohol, with the dissociation pathways ultimately leading to species formally composed of uranyl and an anion – hydroxide, nitrate or alkoxide. This work was later extended to similar systems involving halide and perchlorate anions (Anbalagan *et al.*, 2004). In another CID study, Van Stipdonk *et al.* (2004b) observed the oxidation of 2-propanol in uranyl complexed by nitrate and the alcohol.

Chien *et al.* (2004) investigated the hydration of uranyl–anion complexes of the type UO_2A^+ (A = acetate, nitrate, hydroxide) and found that the relative rates for the formation of the monohydrates followed the trend acetate > nitrate >> hydroxide. In a related study, Gresham *et al.* (2003) used a sputtering ionization method (not ESI) and also a QIT/MS to produce $UO(OH)^+$, UO_2^+, and $UO_2(OH)^+$ ions from UO_3 and study the kinetics of hydration.

Van Stipdonk *et al.* (2004a) were able to produce uranyl complexes solvated only by neutral ligands, specifically acetone, and addition reactions with water or acetone were also investigated. Using nitriles in place of acetone also led to the formation of doubly charged species involving uranyl and the nitriles (Van Stipdonk *et al.*, 2006); with water as reagent, addition and charge reduction pathways were observed.

An intriguing observation reported by Groenewold *et al.* (2006a) was the coordination of molecular O_2 to complexes of UO_2^+ with two or three acetone ligands. The mode of ligation of O_2 in the complex was the object of a very recent theoretical study that described the system as a superoxo complex with O_2 in a side-on (η^2) configuration (Bryantsev *et al.*, 2008).

A recent major advance in understanding uranyl complexation has come from spectroscopic studies in which a tunable free electron laser was employed to obtain infrared vibrational spectra of gas-phase uranyl complexes. The uranyl complexes were produced by ESI and trapped in an FTICR/MS. The vibrational spectra of mass-selected complexes were obtained by variable-wavelength infrared multiphoton dissociation (IRMPD) that revealed aspects of bonding and structure for the uranyl complexes. Initial studies involved uranyl coordinated by acetone and acetonitrile (Groenewold *et al.*, 2006b). More recent studies involved complexes with general formula $[UO_2A(S)_n]^+$, where A = hydroxide, methoxide, or acetate, S = water, ammonia, acetone, or acetonitrile, and n = 0–3 (Groenewold *et al.*, 2008a); and $[UO_2(ROH)]^+$ complexes with ROH being water, methanol, ethanol, or n-propanol (Groenewold *et al.*, 2008b), and anionic nitrate complexes of UO_2^{2+} (Groenewold *et al.*, 2008c).

The solvation studies of uranyl just described bear a special importance for the field of speciation of uranium (and other actinides) in the environment, in various stages of the nuclear fuel cycle, and in radiotoxicological problems.

A preliminary study of uranyl perchlorate solutions by ESI-FTICR/MS was reported by Pires de Matos *et al.* (2000). Moulin and co-workers used ESI-MS to study the solution speciation of uranium (Moulin *et al.*, 2000) and thorium (Moulin *et al.*, 2001). Moulin and co-workers also used ESI-MS to study the interaction of uranyl with 1-hydroxyethane-1,1′-diphosphonic acid, a compound that shows promise for the decorporation of uranium (Jacopin *et al.*, 2003).

Other examples of ESI-MS studies of the complexation of uranyl, this time by compounds of significance in natural environments, comprise work by Groenewold *et al.* (2004) with desferrioxamine siderophore, and by Pemberton and co-workers (Pasilis and Pemberton, 2003; Somogyi *et al.*, 2007) with citric acid. The more recent work by Pemberton and co-workers involved the use of QIT and FTICR techniques to explore CID and reactions of uranyl-citrate cations and anions.

In a very recent, intriguing study by Hu *et al.* (2008), the reaction of an anionic uranyl species, $(CH_3UO_2OH)^-$ with water to eliminate methane was described.

(b) Reactions in elemental mass spectrometers

An area to which fundamental gas-phase actinide studies have recently contributed is the analytical chemistry of actinides using elemental mass spectrometers. The generalization of the use of collision/reaction cells in inductively coupled plasma mass spectrometers (ICP-MS), with the purpose of resolving or eliminating isobaric interferences through chemical reactions (Tanner *et al.*, 2002; Bandura *et al.*, 2006; Olesik and Jones, 2006), has led to the exploration of differences in reactivity of the An^+ ions with various substrates as described in gas-phase ion chemistry studies (Vais *et al.*, 2003; 2004a, b; Tanner *et al.*, 2004; Baranov et al., 2005). Other work in the field of actinide elemental analysis, with ICP-MS (Hattendorf and Günther, 2001) and thermal ionization mass spectrometry (TIMS) (Alamelu *et al.*, 2004), has confirmed the importance of the fundamental ion-chemistry studies to help explain reactions occurring in the ion sources. It is interesting to recall at this point that the earliest reported study of gas-phase reactions of actinide ions, referred to in a previous section, involved the observation of endothermic formation of UH^+, UD^+, PuH^+, and PuD^+ after addition of H_2, D_2, H_2O, D_2O, or H_2O to the ion source of the mass spectrometer where isotopic analysis of U and Pu was being performed (Moreland *et al.*, 1970).

(c) Reactions in laser ablation plumes

Ion/atom or ion/molecule reactions are omnipresent processes in laser ablation plumes and therefore a brief reference to the studies involving actinides in which new chemical species were produced directly and deliberately from laser ablation is justified.

Gibson (1997a) initially studied by MS the ions formed in laser ablation of dispersions of Th and U inorganic compounds in polyimide (PI) and polytetrafluoroethylene (PTFE): for PI, the products were $AnC_cH_h^+$ with c = 2 or 4 and h = 0 or 1, while for PTFE, the main products were generally AnF_n^+ with n = 1 or 2; the products formed were accounted for on the basis of their thermodynamic stabilities.

In subsequent studies, these laser ablation experiments, using PI as matrix, were extended to transuranium actinides and produced new organometallic $AnC_cH_h^+$ ions from NpO_2 and PuO_2 (Gibson, 1998b), and $AnC_xH_yN_z^+$ from AmO_2 (Gibson, 1998a), Cm_7O_{12} (Gibson and Haire, 1999), Bk_2O_3 (Gibson and Haire, 2001c), and Cf_2O_3 (Gibson and Haire, 2001c). In all cases, species incorporating oxygen were also observed and more notably small actinide oxide cluster ions could be detected. Formation of actinide oxide cluster cations from actinide oxide targets was also observed in a LAPRD study involving Th and U (Gibson, 1997b).

Other systems were studied by this approach, namely dilute mixtures of AnO_2 (An = U, Np, Pu) in selenium which yielded actinide selenide, oxide and oxide-selenide molecular and cluster cations (Gibson, 1999c).

The formation of plutonium oxide cluster ions deserved special attention and several plutonium oxide, oxide-hydroxide and hydroxide cluster ions, $Pu_xO_y(OH)_z^+$ were synthesized by laser ablation of hydrated plutonium oxalate (Gibson *et al.*, 2000; Gibson and Haire, 2001a); the diversity of compositions observed was related to the availability of several oxidation states of Pu. Gas-phase reactions with dimethylether were also investigated. In an additional study (Gibson and Haire, 2004), ternary plutonium oxide cluster ions, $M_xPu_yO_z^+$, where M was Ce, La, U, Sr, and Zr were produced and the oxidation behavior of Pu explored.

Several new actinide species were obtained in a different setup involving laser ionization coupled to FTICR/MS. In a preliminary report, formation of Th and U oxide cluster cations was described, using surface oxidized metal pieces as targets (Pires de Matos *et al*., 1995). Recently, the same setup yielded abundant mono- and polymetallic uranium oxide anions from uranium oxide samples whose structures were probed by reactivity studies with methanol and by theoretical calculations (Marçalo et al., 2009; Michelini *et al*., 2008).

As a final reference to interesting species formed in laser ablation plumes, mention is due to the formation of a series of bimetallic actinide-transition metal cations in the same experimental setup (Santos *et al*., 2006a). $AnPt^+$ ions for An = Th, Pa, U, Np, Pu, Am, and Cm where produced from dilute AnPt alloys, and also UIr^+ and UAu^+ from the corresponding U-transition metal alloy. The reactivity of the three UM^+ cations with oxidants and ethane was studied and the results discussed in the context of a theoretical prediction (Gagliardi and Pyykkö, 2004) that Ir, Pt, and Au would, respectively, behave as pseudo-pnictide, -chalcogenide, and -halide when bonded to U.

LIST OF ABBREVIATIONS

CASPT2	complete active space plus second-order perturbation theory
CASSI-SOC	complete active space state interaction – spin orbit coupling
CID	collision-induced dissociation
D	bond dissociation energy
DFT	density functional theory
EA	electron affinity
ESI	electrospray ionization
FA	flowing afterglow
FTICR	Fourier transform ion cyclotron resonance
GIB	guided ion beam
HOMO	highest occupied molecular orbital
ICP	inductively coupled plasma
ICR	ion cyclotron resonance
IE	ionization energy
IR	infrared
IRMPD	infrared multiphoton dissociation
LAPRD	laser ablation with prompt reaction and detection
LFT	ligand field theory
MATI	mass analyzed threshold ionization

MCSCF	multi-configurational self-consistent field
MRCISD	multi-reference configuration interaction with single and double excitations
MS	mass spectrometry
Nd:YAG	neodymium doped yttrium aluminium garnet
PFI-ZEKE	pulsed field ionized – zero kinetic energy
PI	polyimide
PIE	photoionization efficiency
QIT	quadrupole ion trap
REMPI	resonantly enhanced multiphoton ionization
SIFT	selected ion flow tube
TIMS	thermal ionization mass spectrometry
UV	ultraviolet

ACKNOWLEDGEMENTS

MCH gratefully acknowledges support from the Office of Basic Sciences, U. S. Department of Energy, under grant DE-FG02-01ER15153-A005.

JKG gratefully acknowledges support by the Director, Office of Science, Office of Basic Energy Sciences, Division of Chemical Sciences, Geosciences and Biosciences of the U.S. Department of Energy at Lawrence Berkeley National Laboratory, under Contract No. DE-AC02-05CH11231.

JM acknowledges the continued financial support from Fundação para a Ciência e a Tecnologia (FCT).

REFERENCES

Alamelu, D., Khodade, P. S., Shah, P. M., and Aggarwal, S. K. (2004) *Int. J. Mass Spectrom.*, **239**, 51–56.

Aldridge, J. P., Brock, E. G., Filip, H., Flicker, H., Fox, K., Galbraith, H. W., Holland, R. F., Kim, K. C., Krohn, B. J., Magnuson, D. W., Maier, W. B., McDowell, R. S., Patterson, C. W., Person, W. B., Smith, D. F., and Werner, G. K. (1985) *J. Chem. Phys.*, **83**, 34–48.

Alikhani, M. E., Michelini, M. C., Russo, N., and Silvi, B., (2008) *J. Phys. Chem. A*, **112**, 12966–74

Allen, G. C., Baerends, E. J., Vernooijs, P., Dyke, J. M., Ellis, A. M., Feher, M., and Morris, A. (1988) *J. Chem. Phys.*, **89**, 5363–72.

Anbalagan, V., Chien, W., Gresham, G. L., Groenewold, G. S., and Van Stipdonk, M. J. (2004) *Rapid Commun. Mass Spectrom.*, **18**, 3028–34.

Andrews, L., Zhou, M., Liang, B., Li, J., and Bursten, B. E. (2000) *J. Am. Chem. Soc.*, **122**, 11440–9.

Andrews, L. and Cho, H.-G. (2005) *J. Phys. Chem. A*, **109**, 6796–8.

Andrews, L. and Cho, H.-G. (2006) *Organometallics*, **25**, 4040-4053.

Andrews, L., Kushto, G. P., and Marsden, C. J. (2006) *Chem.Eur. J.*, **12**, 8324–35.

Andrews, L., Wang, X., Lindh, R., Roos, B. O., and Marsden, C. J. (2008) *Angew. Chem., Int. Ed.*, **47**, 5366–70.

Armentrout, P., Hodges, R., and Beauchamp, J. L. (1977a) *J. Am. Chem. Soc.*, **99**, 3162–3.

Armentrout, P. B., Hodges, R. V., and Beauchamp, J. L. (1977b) *J. Chem. Phys.*, **66**, 4683–8.

Armentrout, P. B. and Beauchamp, J. L. (1979) *Inorg. Chem.*, **18**, 1349–53.

Armentrout, P. B. and Beauchamp, J. L. (1980a) *Chem. Phys.*, **50**, 27–36.

Armentrout, P. B. and Beauchamp, J. L. (1980b) *Chem. Phys.*, **50**, 21–25.

Armentrout, P. B. and Beauchamp, J. L. (1981) *J. Phys. Chem.*, **85**, 4103–05.

Armentrout, P. B. (2003a) *Int. J. Mass Spectrom.*, **227**, 289–302.

Armentrout, P. B. (ed.) (2003b) *The Encyclopedia of Mass Spectrometry*, *Volume 1: Theory and Ion Chemistry*, Elsevier, New York.

Armentrout, P. B. (2004) *J. Anal. At. Spectrom.*, **19**, 571–80.

Armstrong, D. P., Harkins, D. A., Compton, R. N., and Ding, D. (1994) *J. Chem. Phys.*, **100**, 28–43.

Averin, V. G., Akhrarov, M., Baronov, G. S., Vasil'ev, B. I., Grasyuk, A. Z., Morozov, M. G., Skvortsova, E. P., and Yastrebkov, A. B. (1983) *Kvantovaya Elektron.* (*Moscow*), **10**, 346–53.

Babcock, L. M., Herd, C. R., and Streit, G. E. (1984a) *Chem. Phys. Lett.*, **112**, 169–172.

Babcock, L. M., Herd, C. R., and Streit, G. E. (1984b) *Chem. Phys. Lett.*, **112**, 173–176.

Bandura, D. R., Baranov, V. I., Litherland, A. E., and Tanner, S. D. (2006) *Int. J. Mass Spectrom.*, **255/256**, 312–327

Baranov, V. Y., Kolesnikov, Y. A., and Kotov, A. A. (1999) *Quantum Electron.* (*Moscow*), **29**, 653–666.

Baranov, V. I., Bandura, D. R., and Tanner, S. D., (2005) *Int. J. Mass Spectrom.* **247**, 40–7.

Barefield, J. E., II, Rice, W. W., Tiee, J. J., and Walters, R. T. (1983) *J. Chem. Phys.*, **79**, 2621–25.

Barefield, J. E., II, Rice, W. W., and Dye, B. A. (1985) *J. Chem. Phys.*, **83**, 567–71.

Baronov, G. S., Britov, A. D., Karavaev, S. M., Karchevskii, A. I., Kulikov, S. Y., Merzlyakov, A. V., Sivachenko, S. D., and Shcherbina, Y. I. (1981) *Kvantovaya Elektron.* (*Moscow*), **8**, 1573–6.

Beach, D. B., Bomben, K. D., Edelstein, N. M., Eisenberg, D. C., Jolly, W. L., Shinomoto, R., and Streitwieser, A., Jr. (1986) *Inorg. Chem.*, **25**, 1735–7.

Beattie, I. R., Jones, P. J., Millington, K. R., and Willson, A. D. (1988) *J. Chem. Soc., Dalton Trans.*, 2759–62.

Beauchamp, J. L. (1976a) *J. Chem. Phys.*, **64**, 718–23.

Beauchamp, J. L. (1976b) *J. Chem. Phys.*, **64**, 929–35.

Beeching, L. J., Dyke, J. M., Morris, A., and Ogden, J. S. (2001) *J. Chem. Phys.*, **114**, 9832–39.

Beitz, J. V., Williams, C. W., and Carnall, W. T. (1982) *J. Chem. Phys.*, **76**, 2756–7.

Blaise, J. and Wyart, J.-F. (1992) *Energy Levels and Atomic Spectra of Actinides*. Université Pierre et Marie Curie, Paris. http://www.lac.u-psud.fr/Database/Contents.html.

Boerrigter, P. M., Snijders, J. G., and Dyke, J. M. (1988) *J. Electron Spectrosc. Relat. Phenom.*, **46**, 43–53.

Bohme, D. K. and Schwarz, H. (2005) *Angew. Chem. Int. Ed.*, **44**, 2336–54.

Bohme, D. K. (2008) *Can. J. Chem.*, **86**, 177–98.

Boring, M. and Hecht, H. G. (1978) *J. Chem. Phys.*, **69**, 112–16.

Boring, M. and Wood, J. H. (1979) *J. Chem. Phys.*, **71**, 32–41.

Boudreaux, E. A. and Baxter, E. (2002) *Int. J. Quant. Chem.*, **90**, 629–33.

Brewer, L. (1971) *J. Opt. Soc. Am.*, **61**, 1666–82.

Brown, J. M. and Carrington, A. (2003) *Rotational Spectroscopy of Diatomic Molecules*, Cambridge University Press, Cambridge.

Bryantsev, V. S., de Jong, W. A., Cossel, K. C., Diallo, M. S., Goddard III, W. A., Groenewold, G. S., Chien, W., and Van Stipdonk, M. J. (2008) *J. Phys. Chem. A*, **112**, 5777–80.

Buchler, A., Berkowitz-Mattuck, J. B., and Dugre, D. H. (1961) *J. Chem. Phys.*, **34**, 2202–3.

Buecher, H. (1977) *Appl. Phys.*, **12**, 383–6.

Bukhmarina, V. N., Predtechenskii, Y. B., and Shklyarik, V. G. (1987) *Opt. Spektrosk.*, **62**, 1187–8.

Bukhmarina, V. N., Predtechenskii, Y. B., and Shcherba, L. D. (1990) *J. Mol. Struct.*, **218**, 33–8.

Bukhmarina, V. N., Gerasimov, A. Y., Predtechenskii, Y. B., and Shklyarik, V. G. (1992) *Opt. Spektrosk.*, **72**, 69–74.

Cao, Z. and Balasubramanian, K. (2005) *J. Chem. Phys.*, **123**, 114309.

Capone, F., Colle, Y., Hiernaut, J. P., and Ronchi, C. (1999) *J. Phys. Chem. A*, **103**, 10899–906.

Capone, F., Colle, J. Y., Hiernaut, J. P., and Ronchi, C. (2005) *J. Phys. Chem. A*, **109**, 12054–58.

Carnall, W. T. and Crosswhite, H. M. (1985) *Optical spectra and electronic structure of actinide ions in compounds and in solution*. Argonne Natl. Lab. Rpt. ANL-84-90. See also Carnall, W. T., Crosswhite, H. M. (1987) in *The Chemistry of the Actinide Elements* (eds. J. J. Katz, G. T. Seaborg, and L. R. Morss) 2nd edn, Chapman and Hall, London, pp. 1235–77.

Carretas, J. M., Marçalo, J., Pires de Matos, A., and Marshall, A. G. (1997) In *Actinides '97*, Baden-Baden, Germany.

Chang, Q. (2002) Ab Initio Calculations on UO_2. MSc. Thesis, Ohio State University, Columbus.

Chien, W., Anbalagan, V., Zandler, M., Van Stipdonk, M. J., Hanna, D., Gresham, G. L., and Groenewold, G. S. (2004) *J. Am. Soc. Mass Spectrom.*, **15**, 777–83.

Cho, H.-G., Lyon, J. T., and Andrews, L. (2008) *J. Phys. Chem. A* **112**, 6902–07.

Clavaguera-Sarrio, C., Vallet, V., Maynau, D., and Marsden, C. J. (2004) *J. Chem. Phys.*, **121**, 5312–21.

Clifton, J. R., Gruen, D. M., and Ron, A. (1969) *J. Chem. Phys.*, **51**, 224–32.

Compton, R. N. (1977) *J. Chem. Phys.*, **66**, 4478–85.

Cornehl, H. H., Heinemann, C., Schröder, D., and Schwarz, H. (1995) *Organometallics*, **14**, 992–9.

Cornehl, H. H., Heinemann, C., Marçalo, J., Pires de Matos, A., and Schwarz, H. (1996) *Angew. Chem. Int. Ed. Engl.*, **35**, 891–4.

Cornehl, H. H., Wesendrup, R., Diefenbach, M., and Schwarz, H. (1997a) *Chem. Eur. J.*, **3**, 1083–90.

Cornehl, H. H., Wesendrup, R., Harvey, J. N., and Schwarz, H. (1997b) *J. Chem. Soc. Perkin Trans. 2*, 2283–91.

David, S. J. and Kim, K. C. (1988) *J. Chem. Phys.*, **89**, 1780–6.

de Jong, W. A. and Nieuwpoort, W. C. (1996) *Int. J. Quantum Chem.*, **58**, 203–16.

Dewberry, C. T., Etchison, K. C., and Cooke, S. A. (2007a) *Phys. Chem. Chem. Phys.*, **9**, 4895–7.

Dewberry, C. T., Etchison, K. C., Grubbs, G. S., Powoski, R. A., Serafin, M. M., Peebles, S. A., and Cooke, S. A. (2007b) *Phys. Chem. Chem. Phys.*, **9**, 5897–901.

Dewey, H. J., Barefield, J. E. II, and Rice, W. W. (1986) *J. Chem. Phys.*, **84**, 684–91.

Dyall, K. G. (1999) *Mol. Phys.*, **96**, 511–8.

Dyke, J. M., Fayad, N. K., Morris, A., Trickle, I. R., and Allen, G. C. (1980) *J. Chem. Phys.*, **72**, 3822–7.

Dyke, J. M., Josland, G. D., Morris, A., Tucker, P. M., and Tyler, J. W. (1981) *J. Chem. Soc.*, *Faraday Trans. 2*, **77**, 1273–80.

Dyke, J. M., Ellis, A. M., Feher, M., and Morris, A. (1988) *Chem. Phys. Lett.*, **145**, 159–64.

Edvinsson, G. and Lagerqvist, A. (1984) *Phys. Scr.*, **30**, 309–20.

Edvinsson, G. and Lagerqvist, A. (1985a) *J. Mol. Spectrosc.*, **113**, 93–104.

Edvinsson, G. and Lagerqvist, A. (1985b) *Phys. Scr.*, **32**, 602–10.

Edvinsson, G. and Lagerqvist, A. (1987) *J. Mol. Spectrosc.*, **122**, 428–39.

Edvinsson, G. and Lagerqvist, A. (1988) *J. Mol. Spectrosc.*, **128**, 117–25.

Edvinsson, G. and Lagerqvist, A. (1990) *Phys. Scr.*, **41**, 316–20.

Eller, K. and Schwarz, H. (1991) *Chem. Rev.*, **91**, 1121–1177.

Ervin, K. M. (2001) *Chem. Rev.*, **101**, 391–444.

Ezhov, Y. S., Bazhanov, V. I., Komarov, S. A., Sevastyanov, V. G., and Yuldashev, F. (1989) *Vysokochist. Veshchestva*, **5**, 197.

Field, R. W. (1982) *Ber. Bunsenges. Phys. Chem.*, **86**, 771–9.

Fite, W. L., Lo, H. H., and Irving, P. (1974) *J. Chem. Phys.*, **60**, 1236.

Fleig, T., Jensen, H. J. A., Olsen, J., and Visscher, L. (2006) *J. Chem. Phys.*, **124**, 104106/1-104106/11.

Freiser, B. S. (1996a) *J. Mass Spectrom.*, **31**, 703–715.

Freiser, B. S. (ed.) (1996b) *Organometallic Ion Chemistry*, Kluwer, Dordrecht.

Frlec, B. and Claassen, H. H. (1967) *J. Chem. Phys.*, **46**, 4603–4.

Gabelnick, S. D., Reedy, G. T., and Chasanov, M. G. (1973a) *J. Chem. Phys.*, **58**, 4468–75.

Gabelnick, S. D., Reedy, G. T., and Chasanov, M. G. (1973b) *J. Chem. Phys.*, **59**, 6397–404.

Gabelnick, S. D., Reedy, G. T., and Chasanov, M. G. (1973c) *Chem. Phys. Lett.*, **19**, 90–3.

Gabelnick, S. D., Reedy, G. T., and Chasanov, M. G. (1974) *J. Chem. Phys.*, **60**, 1167–71.

Gagliardi, L., Skylaris, C.-K., Willetts, A., Dyke, J. M., and Barone, V. (2000) *Phys. Chem. Chem. Phys.*, **2**, 3111–3114.

Gagliardi, L., Roos, B. O., Malmqvist, P., and Dyke, J. M. (2001) *J. Phys. Chem. A*, **105**, 10602–06.

Gagliardi, L. and Pyykkö, P. (2004) *Angew. Chem. Int. Ed.*, **43**, 1573–6.

Gagliardi, L., Heaven, M. C., Krogh, J. W., and Roos, B. O. (2005) *J. Am. Chem. Soc.*, **127**, 86–91.

Gibson, J. K. (1996) *J. Phys. Chem.*, **100**, 15688–94.

Gibson, J. K. (1997a) *J. Vac. Sci. Techn. A*, **15**, 2107–118.

Gibson, J. K. (1997b) *Organometallics*, **16**, 4214–22.

Gibson, J. K. (1998a) *J. Phys. Chem. A*, **102**, 4501–08.

Gibson, J. K. (1998b) *J. Alloys Comp.*, **271**, 359–62.

Gibson, J. K. (1998c) *J. Am. Chem. Soc.*, **120**, 2633–40.

Gibson, J. K. (1998d) *Organometallics*, **17**, 2583–9.

Gibson, J. K. and Haire, R. G. (1998) *J. Phys. Chem. A*, **102**, 10746–53.

Gibson, J. K. (1999a) *Inorg. Chem.*, **38**, 165–173.

Gibson, J. K. (1999b) *J. Mass Spectrom.*, **34**, 1166–77.

Gibson, J. K. (1999c) *J. Alloys Comp.*, **290**, 52–62.

Gibson, J. K. and Haire, R. G. (1999) *Organometallics*, **18**, 4471–77.

Gibson, J. K. (2000) *Int. J. Mass Spectrom.*, **202**, 19–29.

Gibson, J. K. and Haire, R. G. (2000a) *Int. J. Mass Spectrom.*, **203**, 127–142.

Gibson, J. K. and Haire, R. G. (2000b) In *10th International Symposium on Resonance Ionization Spectroscopy and Its Applications (RIS-2000)*, American Institute of Physics, Knoxville, TN.

Gibson, J. K., Haire, R. G., and Duckworth, D. C. (2000) In *Plutonium Futures – The Science, American Institute of Physics*, Santa Fe, NM.

Gibson, J. K. (2001) *J. Mass Spectrom.*, **36**, 284–93.

Gibson, J. K. and Haire, R. G. (2001a) *J. Alloys Comp.*, **322**, 143–52.

Gibson, J. K. and Haire, R. G. (2001b) *Radiochim. Acta*, **89**, 709–19.

Gibson, J. K. and Haire, R. G. (2001c) *Radiochim. Acta*, **89**, 363–9.

Gibson, J. K. (2002a) *Int. J. Mass Spectrom.*, **214**, 1–21.

Gibson, J. K. (2002b) *Int. J. Mass Spectrom.*, **216**, 185–202.

Gibson, J. K. and Haire, R. G. (2002) *Inorg. Chem.*, **41**, 5897–906.

Gibson, J. K. (2003) *J. Phys. Chem. A*, **107** 7891–9.

Gibson, J. K. and Haire, R. G. (2003) *Radiochim. Acta*, **91**, 441–8.

Gibson, J. K. and Haire, R. G. (2004) *J. Alloys Comp.*, **363**, 112–21.

Gibson, J. K. and Haire, R. G. (2005) *Organometallics*, **24**, 119–26.

Gibson, J. K., Haire, R. G., Santos, M., Marçalo, J., and Pires de Matos, A. (2003) in *Plutonium Futures-The Science*, G. D. Jarvinen, ed., American Institute of Physics, Albuquerque, NM, USA, 30–2.

Gibson, J. K., Haire, R. G., Marçalo, J., Santos, M., Pires de Matos, A., and Leal, J. P. (2005a) *J. Nucl. Mater.*, **344**, 24–9.

Gibson, J. K., Haire, R. G., Santos, M., Marçalo, J., and Pires de Matos, A. (2005b) *J. Phys. Chem. A*, **109**, 2768–81.

Gibson, J. K. and Marçalo, J. (2006) *Coord. Chem. Rev.*, **250**, 776–83.

Gibson, J. K., Santos, M., Marçalo, J., Leal, J. P., Pires de Matos, A., and Haire, R. G. (2006) *J. Phys. Chem. A*, **110**, 4131–2.

Gibson, J. K., Haire, R. G., Marçalo, J., Santos, M., Leal, J. P., Pires de Matos, A., Tyagi, R., Mrozik, M. K., Pitzer, R. M., and Bursten, B. E. (2007a) *Eur. Phys. J. D*, **45**, 133–8.

Gibson, J. K., Haire, R. G., Marçalo, J., Santos, M., Pires de Matos, A., Mrozik, M. K., Pitzer, R. M., and Bursten, B. E. (2007b) *Organometallics*, **26**, 3947–56.

Gibson, J. K., Haire, R. G., Santos, M., Pires de Matos, A., and Marçalo, J. (2008) *J. Phys. Chem. A*, **112**, 11373–81.

Goncharov, V., Han, J., Kaledin, L. A., and Heaven, M. C. (2005) *J. Chem. Phys.*, **122**, 204311/1-204311/6.

Goncharov, V. and Heaven, M. C. (2006) *J. Chem. Phys.*, **124**, 064312/1-064312/7.

Goncharov, V., Kaledin, L. A., and Heaven, M. C. (2006) *J. Chem. Phys.*, **125**, 133202/1–133202/8.

Green, D. W., Gabelnick, S. D., and Reedy, G. T. (1976) *J. Chem. Phys.*, **64**, 1697–705.

Green, D. W. and Reedy, G. T. (1976) *J. Chem. Phys.*, **65**, 2921–2.

Green, D. W. and Reedy, G. T. (1978) *J. Chem. Phys.*, **69**, 544–51.

Green, D. W., Reedy, G. T., and Gabelnick, S. D. (1980) *J. Chem. Phys.*, **73**, 4207–16.

Gresham, G. L., Gianotto, A. K., Harrington, P. B., Cao, L., Scott, J. R., Olson, J. E., Appelhans, A. D., Van Stipdonk, M. J., and Groenewold, G. S. (2003) *J. Phys. Chem. A*, **107**, 8530–38.

Groenewold, G. S., Van Stipdonk, M. J., Gresham, G. L., Chien, W., Bulleigh, K., and Howard, A. (2004) *J. Mass Spectrom.*, **39**, 752–61.

Groenewold, G. S., Cossel, K. C., Gresham, G. L., Gianotto, A. K., Appelhans, A. D., Olson, J. E., Van Stipdonk, M. J., and Chien, W. (2006a) *J. Am. Chem. Soc.*, **128**, 3075–84.

Groenewold, G. S., Gianotto, A. K., Cossel, K. C., Van Stipdonk, M. J., Moore, D. T., Polfer, N., Oomens, J., de Jong, W. A., and Visscher, L. (2006b) *J. Am. Chem. Soc.*, **128**, 4802–13.

Groenewold, G. S., Gianotto, A. K., McIlwain, M. E., Van Stipdonk, M. J., Kullman, M., Moore, D. T., Polfer, N., Oomens, J., Infante, I., Visscher, L., Siboulet, B., and de Jong, W. A. (2008a) *J. Phys. Chem. A*, **112**, 508–21.

Groenewold, G. S., Van Stipdonk, M. J., de Jong, W. A., Oomens, J., Gresham, G. L., McIlwain, M. E., Gao, D., Siboulet, B., Visscher, L., Kullman, M., and Polfer, N. (2008b) *Chem. Phys. Chem.*, **9**, 1278–85.

Groenewold, G. S., Oomens, J., de Jong, W. A., Gresham, G. L., McIlwain, M. E., and Van Stipdonk, M. J. (2008c) *Phys. Chem. Chem. Phys.*, **10**, 1192–202.

Gruber, J. B. and Hecht, H. G. (1973) *J. Chem. Phys.*, **59**, 1713–20.

Grzybowski, J. M. and Andrews, L. (1978) *J. Chem. Phys.*, **68**, 4540–5.

Gutowski, K. E. and Dixon, D. A. (2006) *J. Phys. Chem. A*, **110**, 8840—856.

Haaland, A., Martinsen, K.-G., Swang, O., Volden, H. V., Booij, A. S., and Konings, R. J. M. (1995) *J. Chem. Soc., Dalton Trans.*, 185–90.

Han, J., Kaledin, L. A., Goncharov, V., Komissarov, A. V., and Heaven, M. C. (2003) *J. Am. Chem. Soc.*, **125**, 7176–77.

Han, J., Goncharov, V., Kaledin, L. A., Komissarov, A. V., and Heaven, M. C. (2004) *J. Chem. Phys.*, **120**, 5155–63.

Hattendorf, B. and Günther, D. (2001) *Fresenius J. Anal. Chem.*, **370**, 483–7.

Hay, P. J. (1983) *J. Chem. Phys.*, **79**, 5469–82.

Heaven, M. C., Nicolai, J. P., Riley, S. J., and Parks, E. K. (1985) *Chem. Phys. Lett.*, **119**, 229–33.

Heaven, M. C. (2006) *Phys. Chem. Chem. Phys.*, **8**, 4497–509.

Heaven, M. C., Goncharov, V., Steimle, T. C., Ma, T., and Linton, C. (2006) *J. Chem. Phys.*, **125**, 204314/1–204314/11.

Heinemann, C., Cornehl, H. H., and Schwarz, H. (1995) *J. Organomet. Chem.*, **501**, 201–09.

Heinemann, C. and Schwarz, H. (1995) *Chem. Eur. J.*, **1**, 7–11.

Hildenbrand, D. L., Gurvich, L. V., and Yungman, V. S. (1985) *The Chemical Thermodynamics of Actinide Elements and Compounds*, *Part 13*, *The Gaseous Actinide Ions*, International Atomic Energy Agency, Vienna.

Hill, Y. D., Huang, Y., Ast, T., and Freiser, B. S. (1997) *Rapid Commun. Mass Spectrom.*, **11**, 148–54.

Holland, R. F. and Maier, W. B., II (1983) *Spectrosc. Lett.*, **16**, 409–12.

Hu, B., Chen, L. H., Huan, Y. F., Zhang, X., Li, M., Liang, H. Z., and Chen, H. W. (2008) *Chem. J. Chinese Univ.* **29**, 912–15.

Huang, Y., Wise, M. B., Jacobson, D. B., and Freiser, B. S. (1987) *Organometallics*, **6**, 346–54.

Hunt, R., D., Toth, L. M., Yustein, J. T., and Andrews, L. (1994a) *Laser Ablation: Mechanisms and Applications I*, *AIP Conf. Proc.*, **288**, 148–52.

Hunt, R. D. and Andrews, L. (1993) *J. Chem. Phys.*, **98**, 3690–6.

Hunt, R. D., Yustein, J. T., and Andrews, L. (1993) *J. Chem. Phys.*, **98**, 6070–4.

Hunt, R. D., Thompson, C., Hassanzadeh, P., and Andrews, L. (1994b) *Inorg. Chem.*, **33**, 388–91.

Hurst, H. J. and Wilson, P. W. (1971) *Spectrosc. Lett.*, **5**, 275–9.

Infante, I., Gomes A. S. P., and Visscher, L. (2006) *J. Chem. Phys.*, **125**, 074301/1–074301/9.

Infante, I., Eliav, E., Vikas, M. J., Ishikawa, Y., Kaldor, U., and Visscher, L. (2007a) *J. Chem. Phys.*, **127**, 124308.

Infante, I., Raab, J., Lyon, J. T., Liang, B., Andrews, L., and Gagliardi, L. (2007b) *J. Phys. Chem. A* **111**, 11996–12000.

Jackson, G. P., Gibson, J. K., and Duckworth, D. C. (2002) *Int. J. Mass Spectrom.*, **220**, 419–41.

Jackson, G. P., Gibson, J. K., and Duckworth, D. C. (2004) *J. Phys. Chem. A*, **108**, 1042–51.

Jacopin, C., Sawicki, M., Plancque, G., Doizi, D., Taran, F., Ansoborlo, E., Amekraz, B., and Moulin, C. (2003) *Inorg. Chem.*, **42**, 5015–22.

Johnsen, R. and Biondi, M. A. (1972) *J. Chem. Phys.*, **57**, 1975–1979.

Johnsen, R., Castell, F. R., and Biondi, M. A. (1974) *J. Chem. Phys.*, **61**, 5404–07.

Jones, L. H. and Ekberg, S. (1977) *J. Chem. Phys.*, **67**, 2591–5.

Kaledin, L. A., Shenyavskaya, E. A., and Gurvich, L. V. (1986) *Zh. Fiz. Khim.*, **60**, 1049–50.

Kaledin, L. A. and Kulikov, A. N. (1989) *Zh. Fiz. Khim.*, **63**, 1697–700.

Kaledin, L. A., Kulikov, A. N., and Gurvich, L. V. (1989) *Zh. Fiz. Khim.*, **63**, 801–3.

Kaledin, L. A., Linton, C., Clarke, T. E., and Field, R. W. (1992) *J. Mol. Spec.*, **154**, 417–26.

Kaledin, L. A., McCord, J. E., and Heaven, M. C. (1994) *J. Mol. Spec.*, **164**, 27–65.

Kaledin, L. A. and Heaven, M. C. (1997) *J. Mol. Spec.*, **185**, 1–7.

Kaltsoyannis, N., Hay, P. J., Li, J., Blaudeau, J.-P., and Bursten, B. E. (2006) In *The Chemistry of the Actinide and Transactinide Elements* (eds. L. R. Morss, N. M. Edelstein, and J. Fuger), 3rd edn, Springer, Dordrecht, pp. 1893–2012.

Kaufman, M., Muenter, J., and Klemperer, W. (1967) *J. Chem. Phys.*, **47**, 3365–6.

Kazazic, S., Kazazic, S. P., Klasinc, L., Rozman, M., and Srzic, D. (2005) *Croatica Chem. Acta*, **78**, 269–74.

Kazazic, S., Kazazic, S. P., Klasinc, L., Rozman, M., and Srzic, D. (2006) *Croatica Chem. Acta*, **79**, 125–8.

Kim, K. C., Krohn, B. J., Briesmeister, R. A., and Rabideau, S. (1987) *J. Chem. Phys.*, **87**, 1538–9.

Kim, K. C., Krohn, B. J., Briesmeister, R. A., and David, S. J. (1988) *J. Mol. Spectrosc.* 132, 207–15.

Kim, K. C. and Mulford, R. N. (1989) *Chem. Phys. Lett.*, **159**, 327–30.

Kim, K. C. and Mulford, R. N. (1990) *THEOCHEM*, **207**, 293–9.

Koelling, D. D., Ellis, D. E., and Bartlett, R. J. (1976) *J. Chem. Phys.*, **65**, 3331–40.

Konings, R. J. M. (1996) *J. Chem. Phys.*, **105**, 9379–80.

Konings, R. J. M., Booij, A. S., Kovacs, A., Girichev, G. V., Giricheva, N. I., and Krasnova, O. G. (1996) *J. Mol. Struct.*, **378**, 121–131.

Konings, R. J. M. and Hildenbrand, D. L. (1998) *J. Alloys Compd.*, **271–273**, 583–6.

Konings, R. J. M., Morss, L. R., and Fuger, J. (2006). In *The Chemistry of the Actinide and Transactinide Elements* (eds. L. R. Morss, N. M. Edelstein and J. Fuger), 3rd edn, Springer, Dordrecht, **4,** pp. 2113–224.

Koren, G., Gertner, Y., and Shreter, U. (1982) *Appl. Phys. Lett.*, **41**, 397–9.

Krauss, M. and Stevens, W. J. (1983) *Chem. Phys. Lett.*, **99**, 417–421.

Krauss, M. and Stevens, W. J. (2003) *Mol. Phys.*, **101**, 125–30

Kroger, P. M., Riley, S. J., and Kwei, G. H. (1978) *J. Chem. Phys.*, **68**, 4195–201.

Krohn, B. J., McDowell, R. S., Patterson, C. W., Nereson, N. G., Reisfeld, M. J., and Kim, K. C. (1988) *J. Mol. Spectrosc.*, **132**, 285–309.

Kuchle, W., Dolg, M., Stoll, H., and Preuss, H. (1994) *J. Chem. Phys.*, **100**, 7535.

Kugel, R., Williams, C., Fred, M., Malm, J. G., Carnall, W. T., Hindman, J. C., Childs, W. J., and Goodman, L. S. (1976) *J. Chem. Phys.*, **65**, 3486–92.

Kunze, K. R., Hauge, R. H., Hamill, D., and Margrave, J. L. (1976) *J. Chem. Phys.*, **65**, 2026–7.

Kunze, K. R., Hauge, R. H., Hamill, D., and Margrave, J. L. (1977) *J. Phys. Chem.*, **81**, 1664–7.

Kunze, K. R., Hauge, R. H., Hamill, D., and Margrave, J. L. (1978) *J. Chem. Soc., Dalton Trans.*, 433–40.

Kushto, G. P., Souter, P. F., and Andrews, L. (1997) *J. Chem. Phys.*, **106**, 5894–903.

Kushto, G. P., Souter, P. F., and Andrews, L. (1998) *J. Chem. Phys.*, **108**, 7121–30.

Kushto, G. P., and Andrews, L. (1999) *J. Phys. Chem. A* **103**, 4836–44.

La Macchia, G., Infante, I., Raab, J., Gibson, J. K., and Gagliardi, L. (2008) *Phys. Chem. Chem. Phys.*, **10**, 7278–83.

Lang, N. C., Stern, R. C., and Finley, M. G. (1980) *Chem. Phys. Lett.*, **69**, 301–04.

Leal, J. P., Marçalo, J., Pires de Matos, A., Marshall, A. G., Yin, W. W., and Spirlet, J.-C. (1993) In *2nd European FTMS Workshop*, University of Antwerp (UIA), Antwerp, Belgium.

Lewis, W. B., Asprey, L. B., Jones, L. H., McDowell, R. S., Rabideau, S. W., Zeltmann, A. H., and Paine, R. T. (1976) *J. Chem. Phys.*, **65**, 2707–14.

Li, J., Bursten, B. E., Zhou, M., and Andrews, L. (2001) *Inorg. Chem.*, **40**, 5448–60.

Li, J., Bursten, B. E., Andrews, L., and Marsden, C. J. (2004) *J. Am. Chem. Soc.*, **126**, 3424–5.

Li, J., Hu, H.-S., Lyon Jonathan, T., and Andrews, L. (2007) *Angew. Chem. Int. Ed.*, **46**, 9045–9.

Liang, B., Andrews, L., Li, J., and Bursten Bruce, E. (2002) *J. Am. Chem. Soc.*, **124**, 6723–33.

Liang, B., Hunt Rodney, D., Kushto Gary, P., Andrews, L., Li, J., and Bursten Bruce, E. (2005) *Inorg. Chem.*, **44**, 2159–68.

Liang, Z., Marshall, A. G., Pires de Matos, A., and Spirlet, J. C. (1990) In *ACS Symposium Transuranium Elements: A Half Century*, American Chemical Society, Washington, DC.

Lias, S. G., Bartmess, J. E., Liebman, J. F., Holmes, J. L., Levin, R. D., and Mallard, W. G. (1988) *Gas-Phase Ion and Neutral Thermochemistry*, American Chemical Society, Washington DC.

Linton, C., Ma, T., Wang, H., and Steimle, T. C. (2008) *J. Chem. Phys.*, **129**, 124310/1–124310/5.

Lue, C. J., Jin, J., Ortiz, M. J., Rienstra-Kiracofe, J. C., and Heaven, M. C. (2004) *J. Am. Chem. Soc.*, **126**, 1812–5.

Lyon J. T., Andrews, L., Hu, H.-S., and Li, J. (2008) *Inorg. Chem.*, **47**, 1435–42.

Lyon, J. T. and Andrews, L. (2005) *Inorg. Chem.*, **44**, 8610–6.

Lyon, J. T. and Andrews, L. (2006) *Inorg. Chem.*, **45**, 1847–52.

Lyon, J. T., Andrews, L., Malmqvist, P.-A., Roos, B. O., Yang, T., and Bursten, B. E. (2007a) *Inorg. Chem.*, **46**, 4917–25.

Lyon, J. T., Hu, H.-S., Andrews, L., and Li, J. (2007b) *Proc. Natl. Acad. Sci.*, **104**, 18919–24.

Lyon, J. T. and Andrews, L. (2008) *Eur. J. Inorg. Chem.*, 1047–58.

Maartensson, N., Malmquist, P. A., Svensson, S., and Johansson, B. (1984) *J. Chem. Phys.*, **80**, 5458–64.

Majumdar, D., Balasubramanian, K., and Nitsche, H. (2002) *Chem. Phys. Lett.*, **361**, 143–151.

Malli, G. L. (1989) in *The Challenge of d and f Electrons, Theory and Computations* (eds. D. R. Salahub and M. C. Zerner), ACS Symposium series, American Chemical Society, Washington, DC, pp. 291–308.

Marçalo, J., Gibson, J. K. (2009) *J. Phys. Chem. A*, **113**, 12599–606.

Marçalo, J., Leal, J. P., and Pires de Matos, A. (1995) In *43rd ASMS Conference on Mass Spectrometry and Allied Topics*, American Society for Mass Spectrometry, Atlanta, GA.

Marçalo, J., Leal, J. P., and Pires de Matos, A. (1996) *Int. J. Mass Spectrom. Ion Processes*, **157/158**, 265–74.

Marçalo, J., Leal, J. P., Pires de Matos, A., and Marshall, A. G. (1997a) *Organometallics*, **16**, 4581–8.

Marçalo, J., Pires de Matos, A., and Evans, W. J. (1997b) *Organometallics*, **16**, 3845–50.

Marçalo, J., Santos, M., Pires de Matos, A., Gibson, J. K., and Haire, R. G. (2008) *J. Phys. Chem. A*, **112**, 12647–56.

Marçalo, J., Santos, M., Pires de Matos, A., Gibson, J. K. (2009) *Inorg. Chem.*, **48**, 5055–7.

Marian, C. M., Wahlgren, U., Gropen, O., and Pyykko, P. (1988) *THEOCHEM*, **46**, 339–54.

Maron, L., Leininger, T., Schimmelpfennig, B., Vallet, V., Heully, J.-L., Teichteil, C., Gropen, O., and Wahlgren, U. (1999) *Chem. Phys.*, **244**, 195–201.

Mathur, B. P., Rothe, E. W., and Reck, G. P. (1977) *J. Chem. Phys.*, **67**, 377–81.

Matsika, S. and Pitzer, R. M. (2000) *J. Phys. Chem. A*, **104**, 4064–8.

Mazzone, G., Michelini, M. C., Russo, N., and Sicilia, E. (2008) *Inorg. Chem.*, **47**, 2083–8.

McAskill, N. A. (1975) *Aust. J. Chem.*, **28**, 1879–91.

McDiarmid, R. (1976) *J. Chem. Phys.*, **65**, 168–73.

McDowell, R. S., Asprey, L. B., and Paine, R. T. (1974) *J. Chem. Phys.*, **61**, 3571–80.

McDowell, R. S., Reisfeld, M. J., Nereson, N. G., Krohn, B. J., and Patterson, C. W. (1985) *J. Mol. Spectrosc.*, **113**, 243–9.

McLuckey, S. A. and Goeringer, D. E. (1997) *J. Mass Spectrom.*, **32**, 461–74.

McLuckey, S. A. and Wells, J. M. (2001) *Chem. Rev.*, **101**, 571–606.

Mercero, J. M., Matxain, J. M., Lopez, X., York, D. M., Largo, A., Eriksson, L. A., and Ugalde, J. M. (2005) *Int. J. Mass Spectrom.*, **240**, 37–99.

Merritt, J. M., Han, J., and Heaven, M. C. (2008) *J. Chem. Phys.*, **128**, 084304/1–084304/8.

Merritt, J. M., Bondybey, V. E., and Heaven, M. C. (2009) *J. Chem. Phys.* **130**, 144503

Meyer, E. R. and Bohn, J. L. (2008) *Phys. Rev. A: At., Mol., Opt. Phys.*, **78**, 010502/1–010502/4.

Michelini, M. C., Russo, N., and Sicilia, E. (2006) *Angew. Chem. Int. Ed.*, **45**, 1095–9.

Michelini, M. C., Russo, N., and Sicilia, E. (2007) *J. Am. Chem. Soc.*, **129**, 4229–39.

Michelini, M. C., Gibson, J. K., Marçalo, J., and Russo, N. (2008) In *NATO Advanced Research Workshop – Molecular Self-Organization in Micro-, Nano-, and Macro-Dimensions: From Molecules to Water, to Nanoparticles, DNA and Proteins*, Kiev, Ukraine.

Michels, H. H. and Hobbs, R. H. (1983) *Theoretical Study of the Radiative and Kinetic Properties of Selected Metal Oxides and Air Molecules*, United Technol. Research Centre,East Hartford,CT, 91 pp.

Michels, H. H. (1989) *Radiative Properties of Uranium Oxide Positive Ion* (UO^+), United Technol. Research Centre, East Hartford,CT, 25 pp.

Miller, J. C., Allison, S. W., and Andrews, L. (1979) *J. Chem. Phys.*, **70**, 3524–30.

Moreland, P. E., Rokop, D. J., and Stevens, C. M. (1970) *Int. J. Mass Spectrom. Ion Phys.*, **5**, 127–36.

Morrey, J. R., Carter, D. G., and Gruber, J. B. (1967) *J. Chem. Phys.*, **46**, 804–9.

Moskaleva, L. V., Krüger, S., Spörl, A., and Rösch, N. (2004) *Inorg. Chem.*, **43**, 4080–90.

Moskaleva, L. V., Matveev, A. V., Dengler, J., and Rösch, N. (2006a) *Phys. Chem. Chem. Phys.*, **8**, 3767–73.

Moskaleva, L. V., Matveev, A. V., Krüger, S., and Rösch, N. (2006b) *Chem. Eur. J.*, **12**, 629–34.

Moulin, C., Charron, N., Plancque, G., and Virelizier, H. (2000) *App. Spectrosc.*, **54**, 843–8.

Moulin, C., Amekraz, B., Hubert, S., and Moulin, V. (2001) *Anal. Chim. Acta*, **441**, 269–79.

Mulford, R. N., Dewey, H. J., and Barefield, J. E., II (1991) *J. Chem. Phys.*, **94**, 4790–6.

Mulford, R. N. and Kim, K. C. (1996) *J. Mol. Spectrosc.*, **176**, 369–74.

Nibbering, N. (ed.) (2004) *The Encyclopedia of Mass Spectrometry, Volume* 4*: Fundamentals of and Applications to Organic* (*and Organometallic*) *Compounds*, Elsevier, New York.

Okada, Y., Kato, S., Satooka, S., Tashiro, H., and Takeuchi, K. (1995) *J. Nucl. Sci. Technol.*, **32**, 1174–80.

Oldenborg, R. C., Rice, W. W., and Wampler, F. B. (1978) *J. Chem. Phys.*, **69**, 2181–7.

Olesik, J. W. and Jones, D. R. (2006) *J. Anal. At. Spectrom.* **21**, 141–159.

Onoe, J., Nakamatsu, H., Sekine, R., Mykoyama, T., Adachi, H., and Takeuchi, K. (1994) *J. Electron Spectrosc. Relat. Phenom.*, **70**, 89–93.

Operti, L. and Rabezzana, R. (2003) *Mass Spectrom. Rev.*, **22**, 407–28.

Operti, L. and Rabezzana, R. (2006) *Mass Spectrom. Rev.*, **25**, 483–513.

Oyama, T., Watanabe, T., Midorikawa, K., Tashiro, H., Takami, M., Namba, S., and Nakane, R. (1986) *J. Nucl. Sci. Technol.*, **23**, 522–8.

Pack, R. T., Rice, W. W., and Barefield, J. E. (1986) *J. Chem. Phys.*, **85**, 2054–68.

Paine, R. T., McDowell, R. S., Asprey, L. B., and Jones, L. H. (1976) *J. Chem. Phys.*, **64**, 3081–3.

Pasilis, S. P. and Pemberton, J. E. (2003) *Inorg. Chem.*, **42**, 6793–800.

Paulovic, J., Nakajima, T., Hirao, K., Lindh, R., and Malmqvist, P. A. (2003) *J. Chem. Phys.*, **119**, 798–805.

Paulovic, J., Gagliardi, L., Dyke, J. M., and Hirao, K. (2005) *J. Chem. Phys.*, **122**, 144317/1–144317/6.

Pedley, J. B. and Marshall, E. M. (1983). *J. Phys. Chem. Ref. Data*, **12**, 967–1031.

Pepper, M. and Bursten, B. E. (1991) *Chem. Rev.*, **91**, 719–41.

Peralta, J. E., Batista, E. R., Scuseria, G. E., and Martin, R. L. (2005) *J. Chem. Theory Comput.*, **1**, 612–16.

Person, W. B., Kim, K. C., Campbell, G. M., and Dewey, H. J. (1986) *J. Chem. Phys.*, **85**, 5524–8.

Pierloot, K., Renders, A., Goodman, G. L., Devoghel, D., Gorller-Walrand, C., and Vanquickenborne, L. G. (1991) *J. Chem. Phys.*, **94**, 2928–39.

Pillai, E. D., Molek, K. S., and Duncan, M. A. (2005) *Chem. Phys. Lett.*, **405**, 247–51.

Pires de Matos, A., Marçalo, J., and Leal, J. P. (1995) In *43rd ASMS Conference on Mass Spectrometry and Allied Topics*, American Society for Mass Spectrometry, Atlanta, GA.

Pires de Matos, A., Marçalo, J., Freitas, M. A., Marshall, A. G., and Choppin, G. R. (2000) In *15th International Mass Spectrometry Conference*, Barcelona, Spain.

Raab, J., Lindh Roland, H., Wang, X., Andrews, L., and Gagliardi, L. (2007) *J. Phys. Chem. A*, **111**, 6383–7.

Rabinowitz, P., Stein, A., and Kaldor, A. (1978) *Opt. Commun.*, **27**, 381–5.

Rauh, E. G. and Ackerman, R. J. (1974) *J. Chem. Phys.*, **60**, 1396–1400.

Rice, W. W., Wampler, F. B., Oldenborg, R. C., Lewis, W. B., Tiee, J. J., and Pack, R. T. (1980) *J. Chem. Phys.*, **72**, 2948–58.

Rice, W. W. and Barefield, J. E., II (1985a) *J. Chem. Phys.*, **83**, 6128–9.

Rice, W. W. and Barefield, J. E., II (1985b) *J. Chem. Phys.*, **82**, 2553–4.

Rice, W. W., Barefield, J. E., II, Pack, R. T., and Dye, B. A. (1985) *J. Chem. Phys.*, **82**, 58–64.

Rice, W. W., Barefield, J. E. II, and Pack, R. T. (1986) *J. Chem. Phys.*, **85**, 255–61.

Roithová, J. and Schröder, D. (2007) *Phys. Chem. Chem. Phys.*, **9**, 2341–9.

Roos, B. O., Lindh, R., Cho, H.-G., and Andrews, L. (2007) *J. Phys. Chem. A* **111**, 6420–4.

Roth, L. M. and Freiser, B. S. (1991) *Mass Spectrom. Rev.*, **10**, 303–28.

Russell, D. H. (ed.) (1989) *Gas Phase Inorganic Chemistry*, Plenum Press, New York.

Santos, M., Marçalo, J., Pires de Matos, A., Gibson, J. K., and Haire, R. G. (2002)

J. Phys. Chem. A, **106**, 7190–4.

Santos, M., Marçalo, J., Leal, J. P., Pires de Matos, A., Gibson, J. K., and Haire, R. G. (2003a) *Int. J. Mass Spectrom.*, **228**, 457–65.

Santos, M., Marçalo, J., Pires de Matos, A., Gibson, J. K., and Haire, R. G. (2003b) In *16th International Mass Spectrometry Conference*, Edinburgh, Scotland.

Santos, M., Marçalo, J., Leal, J. P., Pires de Matos, A., Gibson, J. K., and Haire, R. G. (2004) In *6th International Conference on Nuclear and Radiochemistry*, Forchungszentrum Jülich, Aachen, Germany.

Santos, M., Marçalo, J., Pires de Matos, A., Gibson, J. K., and Haire, R. G. (2006a) *Eur. J. Inorg. Chem.*, 3346–9.

Santos, M., Marçalo, J., Pires de Matos, A., Gibson, J. K. and Haire, R. G. (2006b) In *54th ASMS Conference on Mass Spectrometry and Allied Topics*, American Society for Mass Spectrometry, Seattle, WA.

Santos, M., Pires de Matos, A., Marçalo, J., Gibson, J. K., Haire, R. G., Tyagi, R., and Pitzer, R. M. (2006c) *J. Phys. Chem. A*, **110**, 5751–9.

Schilling, J. B. and Beauchamp, J. L. (1988) *J. Am. Chem. Soc.*, **110**, 15–24.

Schröder, D. and Schwarz, H. (1995) *Angew. Chem. Int. Ed. Engl.*, **34**, 1973–95.

Schröder, D., Diefenbach, M., Klapotke, T. M., and Schwarz, H. (1999) *Angew. Chem. Int. Ed. Engl.*, **38**, 137–140.

Schröder, D. and Schwarz, H. (1999) *J. Phys. Chem. A*, **103**, 7385–94.

Schröder, D., Schwarz, H., and Shaik, S. (2000) *Struct. Bond.*, **97**, 91–123.

Schwarz, H. (2003) *Angew. Chem. Int. Ed.*, **42**, 4442–54.

Shamov, G. A. and Schreckenbach, G. (2005) *J. Phys. Chem. A*, **109**, 10961–74.

Shamov, G. A. and Schreckenbach, G. (2006) *J. Phys. Chem. A*, **110**, 12072.

Sherrow, S. A. and Hunt, R. D. (1992) *J. Phys. Chem.*, **96**, 1095–9.

Sleno, L. and Volmer, D. A. (2004) *J. Mass Spectrom.*, **39**, 1091–112.

Somogyi, A., Pasilis, S. P., and Pemberton, J. E. (2007) *Int. J. Mass Spectrom.*, **265**, 281–94.

Souter, P. F., Kushto, G. P., and Andrews, L. (1996) *Chem. Commun.*, 2401–2.

Souter, P. F. and Andrews, L. (1997) *J. Mol. Struct.*, **412**, 161–7.

Souter, P. F., Kushto, G. P., Andrews, L., and Neurock, M. (1997a) *J. Am. Chem. Soc.*, **119**, 1682–7.

Souter, P. F., Kushto, G. P., Andrews, L., and Neurock, M. (1997b) *J. Phys. Chem. A* **101**, 1287–91.

Srivastava, S. K., Cartwright, D. C., Trajmar, S., Chutjian, A., and Williams, W. X. (1976) *J. Chem. Phys.*, **65**, 208–11.

Srzic, D., Kazazic, S., Klasinc, L., Gusten, H., and McGlynn, S. P. (1997a) *Croatica Chem. Acta*, **70**, 223–8.

Srzic, D., Kazazic, S., Klasinc, L., and Budzikiewicz, H. (1997b) *Rapid Commun. Mass Spectrom.*, **11**, 1131–3.

Stace, A. J. (2002) *J. Phys. Chem. A*, **106**, 7993–8005.

Steindler, M. J. and Gunther, W. H. (1964) *Spectrochim. Acta*, **20**, 1319–22.

Steindler, M. J. and Gerding, T. J. (1966) *Spectrochim. Acta*, **22**, 1197–1200.

Stockdale, J. A. D., Compton, R. N., and Schweinler, H. C. (1970) *J. Chem. Phys.*, **53**, 1502–07.

Streit, G. E. and Newton, T. W. (1980) *J. Chem. Phys.*, **73**, 3178–82.

Streit, G. E. and Babcock, L. M. (1987) *Int. J. Mass Spectrom. Ion Process.*, **75**, 221–232.

Sunderlin, L. S. and Armentrout, P. B. (1989) *J. Am. Chem. Soc.*, **111**, 3845–55.

Tague, T. J. Jr., Andrews, L., and Hunt, R. D. (1993) *J. Phys. Chem.*, **97**, 10920–4.

Takeuchi, K., Tashiro, H., Kato, S., Midorikawa, K., Oyama, T., Satooka, S., and Namba, S. (1989) *J. Nucl. Sci. Technol.*, **26**, 301–3.

Tanner, S. D., Baranov, V. I., and Bandura, D. R. (2002) *Spectrochim. Acta B*, **57**, 1361–1452.

Tanner, S. D., Li, C., Vais, V., Baranov, V. I., and Bandura, D. R. (2004) *Anal. Chem.*, **76**, 3042–8.

Thornton, G., Edelstein, N., Roesch, N., Egdell, R. G., and Woodwark, D. R. (1979) *J. Chem. Phys.*, **70**, 5218–21.

Tiee, J. J. and Wittig, C. (1978) *Opt. Commun.*, **27**, 377–80.

Tyagi, R. (2005) Ph.D. Thesis, Department of Chemistry, Ohio State University, Columbus.

Vais, V., Li, C., and Cornett, J. (2003) *Anal. Bioanal. Chem.*, **377**, 85–8.

Vais, V., Li, C., and Cornett, J. (2004a) *Anal. Bioanal. Chem.*, **380**, 235–9.

Vais, V., Li, C., and Cornett, J. (2004b) *J. Anal. Atom. Spectrom.*, **19**, 1281–3.

Van Stipdonk, M. J., Anbalagan, V., Chien, W., Gresham, G. L., Groenewold, G. S., and Hanna, D. (2003) *J. Am. Soc. Mass Spectrom.*, **14**, 1205–14.

Van Stipdonk, M. J., Chien, W., Anbalagan, V., Bulleigh, K., Hanna, D., and Groenewold, G. S. (2004a) *J. Phys. Chem. A*, **108**, 10448–57.

Van Stipdonk, M. J., Chien, W., Anbalagan, V., Gresham, G. L., and Groenewold, G. S. (2004b) *Int. J. Mass Spectrom.*, **237**, 175–83.

Van Stipdonk, M. J., Chien, W., Bulleigh, K., Wu, Q., and Groenewold, G. S. (2006) *J. Phys. Chem. A*, **110**, 959–70.

Vestal, M. L. (2001) *Chem. Rev.*, **101**, 361–75.

Vieira, M. C., Marçalo, J., and Pires de Matos, A. (2001) *J. Organomet. Chem.*, **632**, 126–32.

Von Bornstedt, A., Edvinsson, G., Lagerqvist, A., and Renhorn, I. (1979) *Phys Scr*, **20**, 599–602.

Walters, R. T. and Briesmeister, R. A. (1984) *Spectrochim. Acta*, **40A**, 587–9.

Wampler, F. B., Oldenborg, R. C., and Rice, W. W. (1978a) *Chem. Phys. Lett.*, **54**, 560–1.

Wampler, F. B., Oldenborg, R. C., and Rice, W. W. (1978b) *Chem. Phys. Lett.*, **54**, 557–9.

Wampler, F. B., Oldenborg, R. C., and Rice, W. W. (1978c) *J. Photochem.*, **9**, 473–9.

Wampler, F. B., Oldenborg, R. C., and Rice, W. W. (1978d) *Chem. Phys. Lett.*, **54**, 554–6.

Wampler, F. B., Oldenborg, R. C., and Rice, W. W. (1979a) *J. Photochem.*, **11**, 369–74.

Wampler, F. B., Rice, W. W., and Oldenborg, R. C. (1979b) *Int. J. Chem. Kinet.*, **11**, 275–83.

Wampler, F. B., Rice, W. W., Oldenborg, R. C., Akerman, M. A., Magnuson, D. W., Smith, D. F., and Werner, G. K. (1979c) *Opt. Lett.*, **4**, 143–5.

Wang, X., Andrews, L., Li, J., and Bursten, B. E. (2004) *Angew. Chem. Int. Ed.*, **43**, 2554–7.

Wang, X. and Andrews, L. (2005) *Phys. Chem. Chem. Phys.*, **7**, 3834–8.

Wang, X., Andrews, L., and Li, J. (2006) *Inorg. Chem.*, **45**, 4157–4166.

Wang, X., Andrews, L., and Marsden, C. J. (2007) *Chem. Eur. J.*, **13**, 5601–06.

Wang, X., Andrews, L., and Gagliardi, L. (2008a) *J. Phys. Chem. A* **112**, 1754–61.

Wang, X., Andrews, L., and Marsden, C. J. (2008b) *Chem. Eur. J.*, **14**, 9192–9201.

Weisshaar, J. C. (1993) *Acc. Chem. Res.*, **26**, 213–19.

Wood, J. H., Boring, M., and Woodruff, S. B. (1981) *J. Chem. Phys.*, **74**, 5225–33.
Yato, Y. and Yamaguchi, H. (1992) *J. Nucl. Sci. Technol.*, **29**, 179–83.
Zhang, J., Zhong, Q. H., Wu, N. L., Wang, J. W., Zhao, J., Guo, S. T., and Ying, C. T. (1996) *Infrared Phys. Technol.*, **37**, 741–6.
Zhou, M. and Andrews, L. (1999) *J. Chem. Phys.*, **111**, 11044–9.
Zhou, M., Andrews, L., Li, J., and Bursten, B. E. (1999a) *J. Am. Chem. Soc.*, **121**, 12188–9.
Zhou, M., Andrews, L., Li, J., and Bursten, B. E. (1999b) *J. Am. Chem. Soc.*, **121**, 9712–21.
Zhou, M., Andrews, L., Ismail, N., and Marsden, C. (2000) *J. Phys. Chem. A* **104**, 5495–502.